TECHNISCHE UNIVERSITÄT MÜNCHEN

Lehrstuhl für Technische Chemie II

Activation and Transformation of *n*-Alkanes and *n*-Alkene in Zeolites

Lin Lin

Vollständiger Abdruck der von der Fakultät für Chemie der Technischen Universität München zur Erlangung des akademischen Grades eines

Doktors der Naturwissenschaften (Dr. rer. nat.)

genehmigten Dissertation.

Vorsitzender: Univ.-Prof. Dr.-Ing. K.-O. Hinrichsen

Prüfer der Dissertation:

      1.   Univ.-Prof. Dr. J. A. Lercher

      2.   Univ.-Prof. Dr. K. Köhler

Die Dissertation wurde am 14.08.2012 bei der Technischen Universität München eingereicht und durch die Fakultät für Chemie am 03.12.2012 angenommen.

"士不可不弘毅，任重而道远"

"An intellectual cannot but be resolute and broad-minded, for one has taken up a heavy responsibility and a long course."

Confucius (551BC-479BC)

Acknowledgements

Great thanks have to go to my colleagues Hui Shi and Baoxiang, who spare no effort in scientific discussion and sharing valuable experiences in laboratory work. Without your help and encouragement I would not have been able to get a better chance to leave Munich.

Last but not least, I am deeply indebted to my family, for their love and never-ending support under any circumstances. I cannot find any words to express the full measure of my gratitude to you!

<div style="text-align: right">

Lin

July 2012

</div>

Activation and Transformation of *n*-Alkanes and *n*-Alkene in Zeolites

High temperature activation and transformation of light *n*-alkanes and pentene on parent and post-synthesis-modified ZSM-5 were systematically investigated to seek insight into reaction mechanism and structures of transition states and intermediates involved. The transition state in monomolecular cracking of alkanes is carboniumion-like with the configuration resembling the products. The cleavage of C-C bonds closer to the center of the molecules leads to lower activation entropies compared to the cleavage of terminal bonds. Changes in the catalytic activity by steamed ZSM-5 samples are dominated by the stability of transition state species, which interact with framework oxygen via electrostatic forces. The formation of energetically favored intermediate is shown for the monomolecular scission of C=C bonds in acid-catalyzed transformation of pentene.

Aktivierung und Umsetzung von *n*-Alkanen und *n*-Alken in Zeolithen

Die Aktivierung und Umsetzung von leichten *n*-Alkanen und Penten bei hoher Temperatur durch modifizierter und nichtmodifizierter ZSM-5 wurde systematisch untersucht, um Einblicke in den Reaktionsmechanismus und die Strukturen der Übergangszustände und Zwischenprodukten zu ermöglichen. Der Übergangszustand in monomolekularem Kracken von Alkanen bezieht sich auf produktenahen Oberflächenprodukten, die Carbonium Ionen ähneln. Die Spaltung von C-C-Bindungen in der Kettenmitte hat eine niedrigere Aktivierungsentropie als die Spaltung der terminalen Bindungen. Die Änderungen in der katalytischen Aktivität von Wasserdampf behandelten ZSM-5 sind durch die Stabilität der Übergangsspezies bestimmt, der mit Gerüstsauerstoffen durch elektrostatische Kräfte wechselwirkt. Die Bildung von energetisch bevorzugtem Zwischenprodukt ist für die monomolekulare Spaltung der C=C-Bindung in Säure-katalysierte Umsetzung von Penten nachgewiesen worden.

Table of contents

Chapter 3

3. Transition state consideration in protolytic cracking on steamed

Chapter 4

4. Mechanistic consequence of reaction intermediates in acid-catalysis by zeolites: kinetic studies of 1-pentene cracking 78

Chapter 1

Introduction

1.1 General introduction

As an essential feedstock for the petrochemical industry and dominant energy source, crude oil exploitation and further refining attract great attention in recent decades. However, the world crude oil reserves at most can only cover energy demand for 50 years at current consumption rate due to the global economic expansion [1]. Consequently, efficient conversion of crude oil into desirable petrochemical products and fuel feedstock becomes hot topics in petrochemical industry. At present, refinery or petrochemical processes rely mainly on the application of catalysts, especially zeolites. For example, as one of the most important zeolite based catalytic process fluid catalytic cracking (FCC) accounts for over 95 % of the zeolite market [2, 3]. Improvement in catalytic properties of these catalysts can have a promoting effect on the product quality and lead to enhancement of efficiency. Figure 1-1 shows the major operations widely applied in modern oil refinery industries. Zeolites are utilized in the partially or fully in green colored processes as adsorbents or catalyst.

Zeolites are naturally or artificially created crystalline allumiosilicates consisting of tetrahedral SiO_4 units linked to frameworks. The substitution of a Si atom by an Al atom creates a negative charge for the AlO_4 unit, which are compensated by additional cations. If the cation is a proton, a Brønsted acid site is created. In addition, framework aluminum in zeolites can be dislocated from the crystalline lattice structure to form extra-framework aluminum (EFAL) species, which are regarded as the origin of Lewis acidity of the zeolites. In general, dehydroxylation, dealumination of zeolites by post-synthesis treatment can lead to the formation of EFAL species [4-6]. The coexistence of both Brønsted and Lewis acid sites is ubiquitous in a large amount of zeolites. For example, dealumination by mild steaming of H-ZSM-5 leads to the formation of EFAL, which is supposed to account for the dramatic increase of catalytic activity for cracking of *n*-hexane [7-10]. Three mechanisms have been proposed to interpret the role of EFAL in the catalytic activity: (i) some EFAL species themselves can serve as catalytic active

sites [11]; (ii) the negative charge in absence of acidic proton in the lattice can be stabilized by those EFAL species [12]; (iii) EFAL species and Brønsted acid sites in the nearby position may take part in the catalytic mechanism synergistically [13-16].
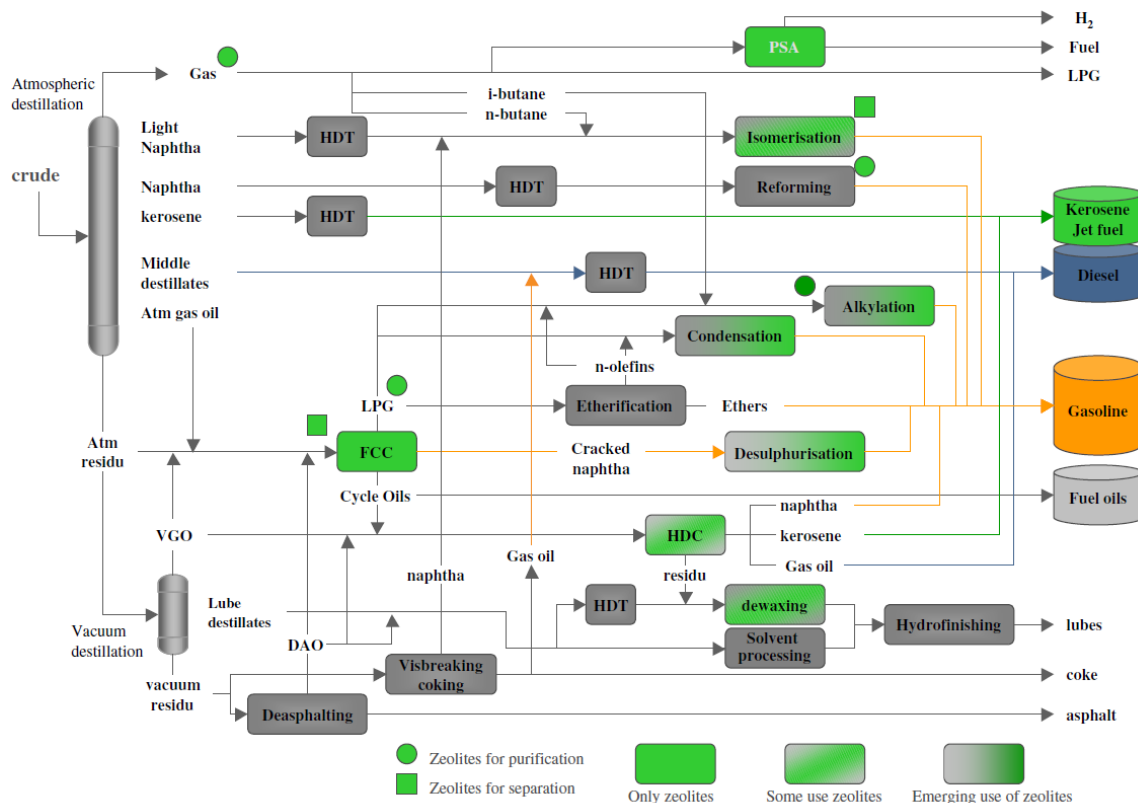
Figure 1-1 Operation units applied in oil refinery industry [17]

From the view of catalyst design, knowledge of acid sites number, distribution and acid strength is vital, since the acid properties are directly related to the catalytic behavior. A large number of physicochemical techniques assess both acid site densities and strength. For instance, determination of concentration of the acid sites (acid site density) is extensively implemented by infrared spectroscopy, ^{27}Al NMR; by using X ray diffraction [18] and ^{29}Si NMR [19] one can determine the lattice parameter to quantify the framework Al content in some zeolites. Furthermore, acid strength and distribution are approached by various methods such as stoichiometric adsorption of some complexes [20-22], calorimetric measurements [23-24], NMR measurement [25, 26]. Applying ab initio calculation and modeling of zeolites one can also theoretically

quantify acid strength based on simulation of different zeolite structures with the lattice increasing interaction from short via medium to long range [27-29].

1.2   Adsorption of aliphatic hydrocarbon in zeolites

The heat released from the sorption of alkanes in the acidic zeolites is generated from the diverse interaction between the sorbate and the pore structure of zeolitic sorbent. In general, the interaction could be that between: (i) sorbates and zeolite lattice (pore and channels) (ii) sorbates and acid sites (iii) different sorbed molecules. Among these three interactions it was reported that the major contribution results from the first one [30]. Moreover, Eder et al. [23] investigated the individual contributions of these interactions by employing gravimeter, calorimeter and infrared spectroscopy. From the comparison of acidic and nonacidic zeolites, the interaction with acid sites leads to constant difference independent of absorbed molecules, 10 kJ·mol^{-1} for MFI and 6 kJ·mol^{-1} for FAU (Figure 1-2). The increase in the heat of adsorption with the increase in chain length of adsorbed alkanes is attributed to the stronger strength of interaction with zeolite lattice. The lower adsorption heat for FAU could be owing to partial compensation of the stronger interaction between alkane and acid sites by weaker interaction of zeolites with other molecules. Besides, intermolecular interactions can be induced by the formation of energetically more favored sorption sites upon absorbing gaseous molecules. Accordingly, a compensation effect between enthalpy and entropy can be observed from the adsorption on both acidic and nonacidic samples (Figure 1-3).
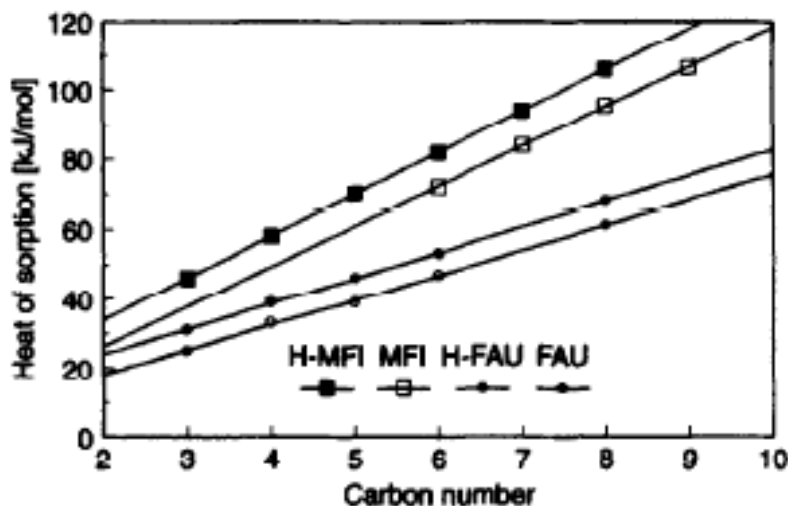
Figure 1-2 Heat of different *n*-alkane sorption on acidic and neutral MFI and FAU type zeolites [23]
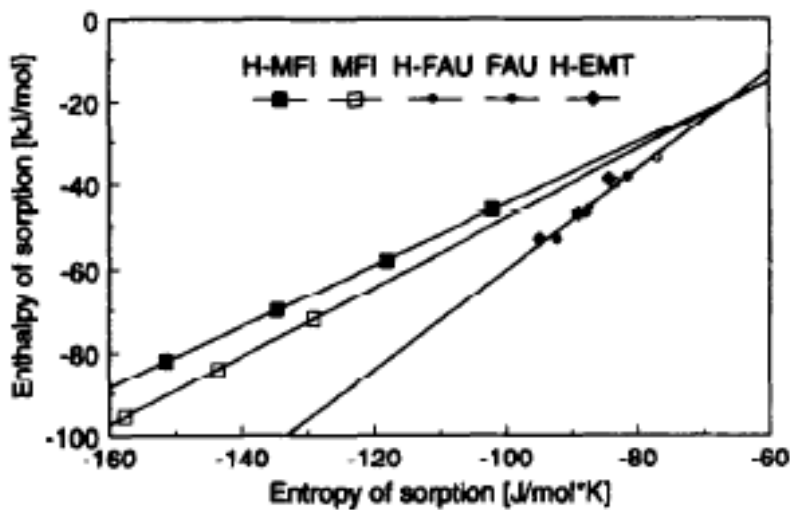
Figure 1-3 Dependence of enthalpy and entropy of *n*-alkanes sorption on different zeolites [23]

From energy minimization techniques [31], molecular dynamics studies [32], and Monte Carlo simulations [33, 34], it can be concluded that the strength of interaction between alkane molecules and zeolites increases with the decrease of pore size, which consequently results in the increase of adsorption heat. This idea is further substantiated by Lercher et al. [30]. They compared the sorption of *n*-alkanes in

different molecular sieves with varying pore size. As shown in Figure 1-4, the heat of alkane sorption decreases consistently with the pore diameter. As the sorption heat from the contribution of acid sites is similar (4 kJ·mol^{-1} for H-MFI and H-FAU [30]), it was addressed that the trend depends predominantly on the structure parameters. For the framework density increases usually with decreasing pore size, they proposed that the higher framework density results in an increase in the strength of interaction between the zeolite lattice structure and the absorbed alkane molecules.

Beside the influence of Brønsted acid sites, Van Bokhoven found that the presence of Lewis acid sites can increase the adsorption heat, which may account for the enhanced activity for light alkane conversion in mildly steamed dealuminated mordenite [35, 38]. Figure 1-5 illustrates the heat of adsorption as a function of coverage for parent H-MOR, steamed H-MOR and H-MOR free of Lewis acid sites. The sample without Lewis acid sites exhibits an invariable heat of adsorption for all coverage, while adsorption on H-MOR and steamed H-MOR samples release higher heats at low coverage. The enhancement of adsorption heats at initial stage could indicate that the interaction with Lewis acid sites is larger than that with zeolite lattice or Brønsted acid sites.
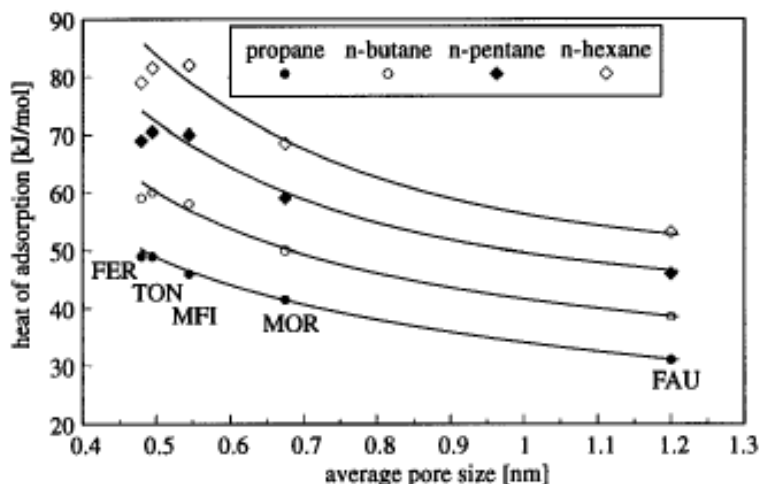
Figure 1-4 Differential heat of adsorption of different alkanes on acidic zeolites with varying pore diameter [24]
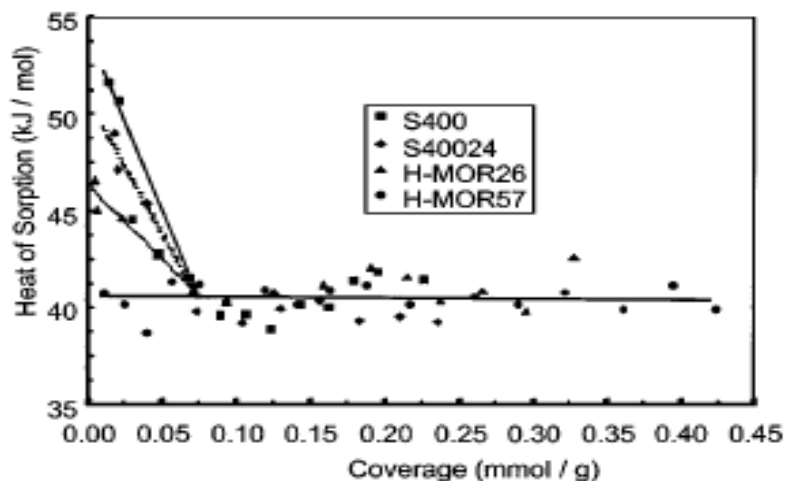
Figure 1-5 Enthalpy of propane adsorption on parent and steamed H-MOR at 323K as a function of the surface coverage [36]

1.3 Mechanism of alkane and alkene cracking

1.3.1 Protolytic cracking of alkane

The establishment of Haag-Dessau mechanism in 1984 is regarded as landmark since it relates the Olah´s hydrocarbon chemistry in super acids to the industrial petroleum refining. In their work [37, 38] penta-coordinated carbonium ions are proposed to be involved in transition state, based on product distribution of 3-methylpentane or *n*-hexane cracking over zeolites (H-ZSM-5, H-Y or silica-alumina). In contrast to the classical cracking, which will be discussed in detail in the mechanism of alkene cracking in the following, alkane molecules can be directly protonated by Brønsted acid sites in solid acids to form carbonium ions. If the proton attacks the C-C bond of the molecule, a non-classical three-centered C-C-H bond contained carbonium ion can be formed, which then collapse into a smaller paraffin and alkoxy species on the surface of catalyst (Figure 1-6 B). If the C-H bond is protonated by the acid sites, the formed non-classical three-centered C-H-H carbonium ions can be cleaved into dihydrogen molecule with the

hydrocarbon residue bound to a zeolite proton (Figure 1-6 C). The first pathway is named as protolytic cracking or monomolecular cracking .The absorbed alkoxy species can further desorb from the catalyst surface leading to the corresponding olefins and free the Brønsted acid sites. A typical cycle of monomolecular cracking is depicted in Figure 1-7.
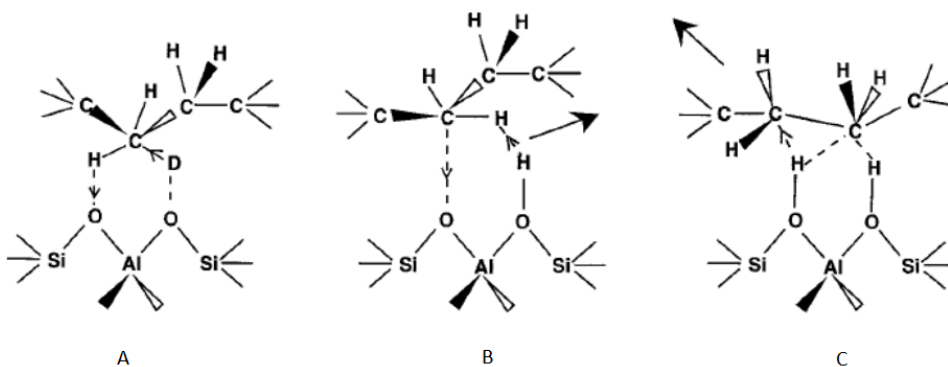
Figure 1-6 Proposed transtion states for (A) H/D exchange (B) butane dehydrogenation (C) cracking [39]
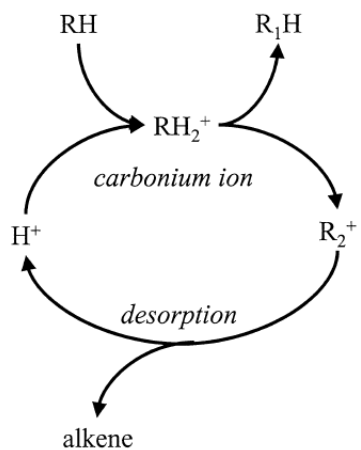
Figure 1-7 Haag-Dessau mechanism for an alkane molecule (RH) [37]

Extensive studies have been done on protolytic cracking of small paraffin molecules. For example, Narbeschuber and his co-workers reported an exponential increase in

reaction rate as a function of carbon atoms in the reactant from the experimental results of monomolecular cracking of various light *n*-alkanes [40]. The enhancement of catalytic activity with increasing carbon chain length is directly related to the contribution of adsorption heat. The apparent activation energies decrease with increasing chain length of the hydrocarbons, while the heat of adsorption shows an opposite trend of changes. It was concluded the intrinsic activation energy for C-C bond cleavage of saturated hydrocarbon is independent of the chain length of molecules. Furthermore, steady-state and transient isotope tracing experiments for *n*-butane conversion over H-MFI samples [41] showed an isotopic effect for reaction rate of *n*-(H_{10}) butane cracking and *n*-(D_{10}) butane cracking. The rate of cracking decreased with decreasing of proton concentration on the surface of catalysts, indicating that the protonation of alkane by zeolites is the rate determining step for the reaction regime. The authors proposed the transition state for monomolecular cracking involving carbonium ions, which interacts with framework oxygen atom as depicted in Figure 1-6C [41].

1.3.2 Cracking of alkenes

The classical cracking mechanism (or bimolecular cracking) has been established for years to predict products distribution of hydrocarbon conversion in petrochemistry. In this mechanism (Figure 1-8), the reaction cycle is initiated by a carbenium ion which is formed by protonation of an olefin molecule by the acidic proton or by the abstraction of a hydride from a Lewis acid site [42, 43]. Once the carbenium species are formed, the reaction chain could propagate in different pathways. In the first case, the carbenium ion abstracts a hydride from one reactant alkane to form an alkane molecule, while the reactant molecule converts to another carbenium ion. Furthermore, the newly formed carbenium ions from hydride transfer can undergo β-scission to form a small olefin leaving a carbenium ion on the active sites in zeolites. The generation of a primary

carbenium ion in the β-scission is less favored because of the involved high energy barrier, which accounts for the trace amount of methane and ethane in the products from β-scission. Nevertheless, during the hydride transfer process sometimes it is inevitable to form a primary carbenium ion in the routine pathway. Therefore, a new mechanism was proposed which involves isomerization of a protonated cyclopropane structure (PCP) in advance of β-scission step (Figure 1-9) [44, 45]. The mechanism could exclude the formation of a primary carbenium ion and thus account for the high yield of isoparaffins during the cracking of *n*-paraffins.
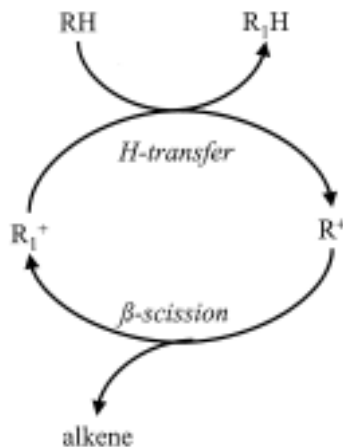
Figure 1-8 Classical cracking mechnism for an alkane molecule (RH) [37]

Monomolecular cracking occurs preferentially at high temperature and low conversion, while the bimolecular pathway dominates at relative low temperature and high conversion. Apparently, the product distribution of paraffin cracking is dependent of the weighing of protolytic and β-scission mechanism under certain reaction condition. High yield of branched products in the conversion of paraffin implies that the bimolecular mechanism is prevalent. However, if more lineal paraffins, H_2, methane and ethane are produced, monomolecular cracking becomes the dominant pathway.
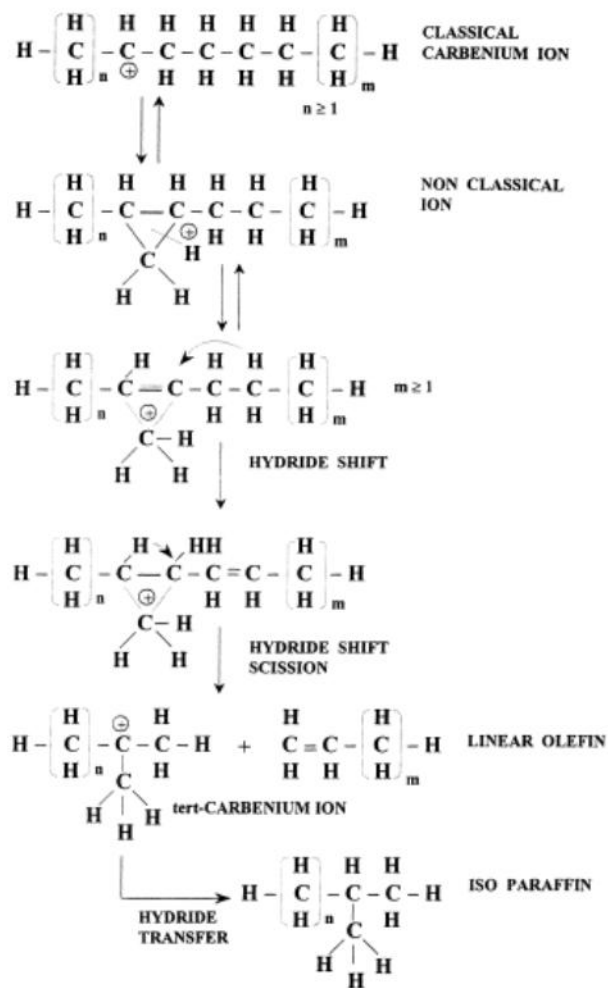
Figure 1-9 Isomerization-cracking mechanism of paraffins [46]

By means of quantum-chemical methods, Rigby et al. investigated plenty of elementary reactions in the conversion of hydrocarbons, including chemisorption of olefins, protolytic cracking of paraffins, protolytic dehydrogenation of paraffins, skeletal isomerization, β-scission, alkylation and hydride transfer reaction [46]. The calculation results showed that alkoxy groups covalently attached to one of the bridging oxygen atoms of the acid sites in zeolites are stable intermediates, while the transition states are similar with carboncations species. The finding is consistent with Kazansky' results, that the primary, secondary and tertiary surface alkoxy species are almost energetically equal [47, 48]. Hence they suggested that the distribution of reaction products depends

11

mainly on the reaction barriers for the formation of initial and/or final alkoxy species. ONIOM studies showed the influence of hydrocarbon nature and active site structure on the formation of intermediates and transition state in acid catalysis [49]. It was concluded that the stability of alkoxide species increases with the length of the olefin. Besides, the angle of AlO_bSi involved in the complex, which is determined by the deprotonation ability of zeolite, increase linearly with the stability of alkoxide. Consequently, the activation energies are less related to the local geometry of the active site, but more to the positive charge stabilized by the carbon atom of Brønsted acid sites and to the ionic character of the transition state.

1.3.3 Alkane dehydrogenation

As discussed above in the protolytic mechanism, protonation of C-H bond of an alkane molecule leads to the formation of a carbonium ion, which collapses into a hydrogen molecule and carbenium ion/alkoxy group. Mc Vicker et al. [50] firstly proposed that a radical can be initiated over electron acceptor sites and the decomposition of such a surface-bound radical results in the formation of olefins. This proposal was later supported by some authors [44, 45, 51, 52], they claimed Lewis acid or electron acceptor sites in a lot of solid acid catalysts can promote the dehydrogenation rate of paraffins. To elucidate dehydrogenation mechanism at high temperature, Narbeshuber et al. [53] performed steady state study and [13]C-, D- tracing experiment. They found that two mechanisms of dehydrogenation coexist in the catalytic conversion of light hydrocarbon on the zeolites containing EFAL species. The high initial dehydrogenation rate is likely attributed to the activity of these EFAL with desorption as the rate determining step. At steady state this pathway is disfavored due to formation of hydrogen, whereas the protolytic dehydrogenation is responsible at this stage. In contrast to the second dehydrogenation pathway, experiment results

supported that olefin desorption from active sites is the rate determining step for monomolecular dehydrogenation.

1.4 Catalytic activity of protolytic cracking

Protolytic cracking of alkane is a model reaction, which is often used to study the catalytic activity and to characterize the acid properties of zeolites. Catalytic activity of the reaction is influenced by multifactor such as nature of the reactants, properties of the acid sites, pore structure and topology of the zeolites.

Zeolites are composed of channels and pores in molecular dimensions that provide a thermodynamically non-ideal environment for chemical reactions. Molecules can be "solved" in the channels; therefore, equilibrium between intrachannel and external fluid phases is established. In general, transition state treatments can be used to describe the thermodynamic factors controlling reaction rates, which can be formulized in following expression:

$$r = A exp\left(\frac{-\Delta H^{\circ\dagger}}{R_g T}\right) C_{P_z} = k C_{P_z} \qquad (1\text{-}1)$$

The pre-exponential factor A includes the equilibrium constant (K_r) and the ratio of activity coefficients $\gamma_{H^+{}_Z}\gamma_{P_z}/\gamma^\dagger$, which are relevant to the nature of acid sites and physiochemical properties of the zeolites. $\Delta H^{\circ\dagger}$ denotes the enthalpy of activation.

Under the reaction condition for monomolecular cracking, which occurs exclusively at high temperature, almost all of H^+ sites in the zeolites remain unoccupied. Thus, C_{pz} becomes directly proportional to the partial pressure of alkane (p) based on Langmuir adsorption:

$$r = k \cdot K \cdot P \qquad (1\text{-}2)$$

In equation (1-2) k is the intrinsic cracking rate constant, while K is the adsorption equilibrium constant for the reactant, which can be obtained from adsorption isotherm of the reactants. These two parameters can be further expressed as:

$$K = e^{(-\frac{\Delta G_{ads}}{RT})} = e^{(-\Delta H_{ads}/RT)} e^{(\frac{\Delta S_{ads}}{R})} \tag{1-3}$$

$$k = A e^{(-\frac{E_a}{RT})} \tag{1-4}$$

Based on (1-2), (1-3) and (1-4) the apparent activation energies (E_{app}), rate constant (k_{app}) and pre-exponential factors (A_{app}) can be derived:

$$E_{app} = E_{int} + \Delta H_{ads} \tag{1-5}$$

$$k_{app} = k \cdot K \tag{1-6}$$

$$\ln(A_{app}) = \ln(A_{int}) + (\frac{\Delta S_{ads}}{R}) \tag{1-7}$$

In this section we focus on the influence of thermodynamic properties of adsorbed reactant and physiochemical properties of the zeolites on catalytic activity of the protolytic cracking.

1.4.1 Concentrating the reactants

Previous studies showed the reaction rates for protolytic cracking and dehydrogenation increase exponentially with carbon number of the paraffins [41]. The difference in catalytic activity for various *n*-alkanes is mainly determined by varying adsorption heat of the reactant, since the intrinsic activation energies are independent of the chain length of the hydrocarbon. Thus, compensation between pre-exponential factor and activation enthalpies can be established for monomolecular cracking of *n*-alkane in a series of zeolites [35]. As depicted in Figure 1-10 one can observe an isokinetic point by extrapolation of the Arrhenius plots for monomolecular cracking of various *n*-alkanes over H-ZSM-5. It is further suggested that the isokinetic point could imply true compensation, revealing intrinsic kinetic parameters are similar for different

reactant and zeolites [54]. Therefore, the differences in observed reaction rates are governed preferentially by the surface coverage of alkane. The proposal is supported by adsorption measurement of *n*-hexane in different zeolites, some of which are post treated [55]. In spite of diversity in structure and composition of the zeolites, compensation between the entropy and enthalpy of adsorption is found for all of the zeolites, implying the adsorption of reactants on the zeolites account for the difference in catalytic activity of monomolecular cracking of *n*-hexane over various zeolites, and intrinsic acid strengths in zeolites of different structures are similar.
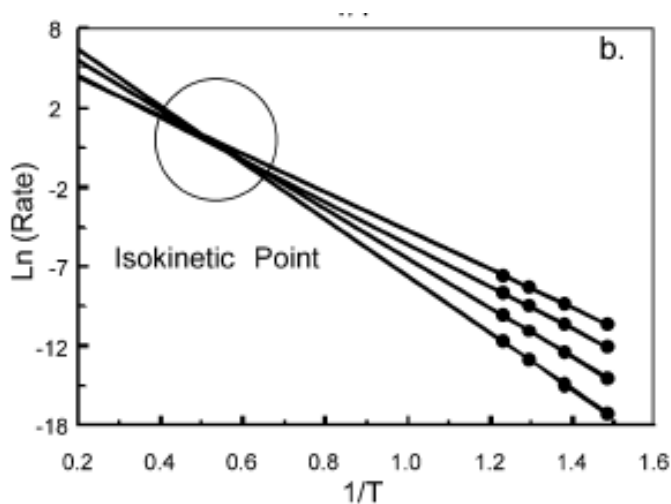
Figure 1-10 Isokinetic point by extrapolation of the Arrhenius plots for protolytic cracking of *n*-alkane on H-ZSM-5 [35]

1.4.2 Role of pore structure

Nevertheless, entropic effects on catalytic activity were emphasized recently [56]. It was argued that the significant difference in monomolecular cracking rates of different alkanes in various zeolites cannot be merely attributed to adsorption properties of the reactants. According to the calculation compensation between adsorption entropies and enthalpies leads to less than a two-fold variation in adsorption equilibrium constants.

Thus, it was addressed the pronounced increase in turnover rates of protolytic cracking with increasing chain length of the reactants is due to the increase in the activation entropies, which is in turn influenced by the structure of zeolite and solvating properties of channels. Furthermore, a confinement effect in monomolecular activation of alkane was observed [57, 58]. Monomolecular cracking and dehydrogenation of alkane occur preferentially within small 8-MR side pockets in H-MOR, which provide a spatially more constrained environment than 12-MR. It was concluded that the activity is mainly influenced by the location of Brønsted acid sites within zeolite channels because of stabilization effects of narrow channels for cationic transition states. The strong specificity with 8-MR pockets (Figure 1-11) reflects that the incomplete containment within these small 8-MR side pockets results in a lower free energy for transition states, leading to gains in the activation entropies, which compensate the penalties in activation enthalpies. Channel environment in zeolites influences the catalytic activity mainly through their solvation of transition states in the framework and mediation of trade-off in enthalpy and entropy parameters.
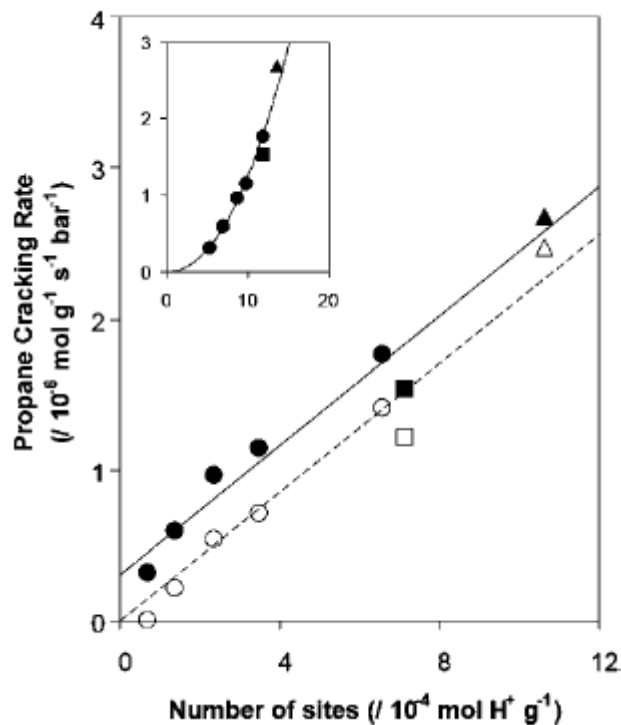
Figure 1-11 Dependence of total cracking rates (closed symbols) and cracking rates in 12-MR (open symbols) of propane on the density of Brønsted acid sites in 8-MR pockets [62]

1.4.3 Role of acid properties

In addition to adsorption of reactants and topology effects of zeolites, some authors emphasized the influence of acid sites strength and density on the catalytic activity of monomolecular cracking. By applying ammonia IRMS-TPD Niwa [59] studied the distribution of acid sites in mordenite, revealing the strength of Brønsted acid sites measured by adsorption heat of ammonia ΔH is larger on 8-MR than on the 12-MR. Since the catalytic activity of octane cracking on 8-MR decreased shortly after the initiation stage in contrast to stable activity on 12-MR, it was concluded that stronger acid sites in 8-MR leads to higher concentration of octane which accounts for the coking formation during deactivation. Moreover, these authors found a strong dependence of the TOF on the acid strength ΔH by comparing various zeolites [60, 61]. Except for the

zeolites with small pore size like FER and MOR, a single relation between acid strength and TOF of octane cracking indicated that the equilibrium constant of the reaction intermediate formation depends strongly on the strength of Brønsted acid sites as active sites for cracking of octane.
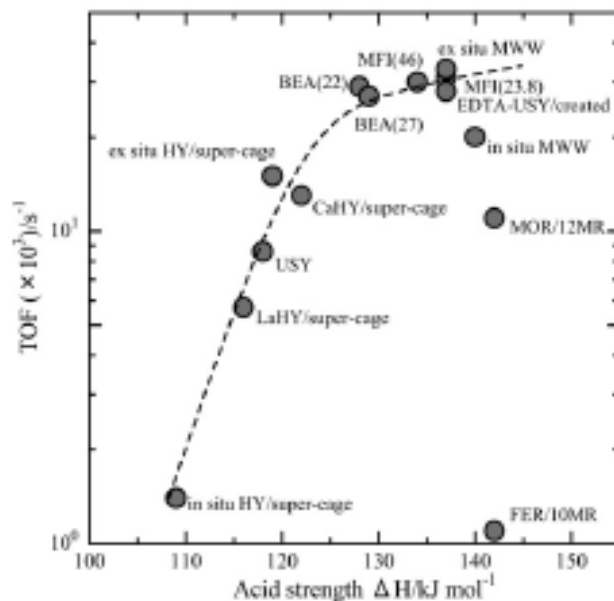
Figure 1-12 Turnover frequency for octane cracking plotted against acid strength ΔH from ammonia IRMS-TPD [63]

Nevertheless, Xu et al. proposed that the protonation ability of the Brønsted acid sites is similar among amorphous silica-aluminas (ASA) and H-ZSM-5, since the intrinsic activation energies for monomolecular propane cracking after correction of adsorption heat were comparable among those zeolites [62]. The lower cracking activity on ASA is attributed to the smaller heat of adsorption and less number of active sites in the samples. The argument was further supported by the latter work [63], which showed the reaction rate of propane cracking normalized to the sample weight increases with Si/Al ratio of H-Y zeolites, whereas the intrinsic activation energy keeps constant on both samples with and without EFAL species. Thus, the intrinsic activities of the active sites remain identical for all the samples.

1.5 Scope of the thesis

In this work activation and transformation of *n*-alkanes and *n*-alkenes are systematically investigated over a series of ZSM-5 samples. On one hand, the measured kinetic parameter reflects catalytic consequences of the acid properties, such as density, distribution, strength of acid sites. On the other hand, the assessment of those kinetic parameters provides substantive information about mechanistic aspects of reactions, which are mainly envisioned by theoretical investigation. By means of infrared spectroscopy, nuclear magnetic resonance and temperature programmed desorption one can quantify the acid sites in the zeolites in terms of density and strength. Moreover, diverse interactions between sorbates and porous sorbent of zeolites, which are essential for catalytic activities of reactions, can be studied upon adsorption of reactants by gravimeter, calorimeter and infrared spectroscopy.

While substantial research has been devoted to study the reaction mechanism of protolytic cracking, the geometry of transition state and its role for the product selectivity are only accessible via theory. To address this question the first part of the work focuses on monomolecular cracking of C_3-C_6 alkanes over H-ZSM-5 samples with different Si/Al ratio. Transition state theory and thermochemical cycles are used to assess kinetic parameters regarding activation energy and entropy of different cracking pathways.

It is widely recognized that mild steaming of H-ZSM-5 results in enhancement of catalytic activities for various reactions such as paraffin cracking, isomerization and disproportionation. Nevertheless, promotion mechanism of steaming remains still controversial. In this context we chose H-ZSM-5 zeolites with Si/Al of 45 as the parent material and finely tuned the framework Al concentration by mild steaming to varying dealumination severity. *n*-Pentane cracking at elevated temperature was chosen as model reaction to study the catalytic activity. In combination with several characterization methods like Infrared spectroscopy, ^{27}Al MAS NMR, XRD and

calorimetric study, kinetic assessment applying transition state treatment and thermochemical cycles provides the experimental proof on the decisive role of transition state species in the promotion effect of mild steaming.

In contrast to monomolecular cracking of alkane, quantification of the elementary reactions is difficult for cracking of pure olefins over zeolite samples. Owning to the complicated reaction network it becomes an arduous task to determine the rate-determining step and assign measured activation enthalpies to one of the kinetically relevant steps. Furthermore, assessment of the kinetic data is confounded by experimental acquisition of adsorption enthalpies for olefin in zeolites due to inevitable side reactions at nearly room temperature. In the third part we focus on cracking of 1-pentene over H-ZSM-5 samples at elevated temperature, which preferentially favors cracking rather than the side reactions such as polymerization and coke formation. The work aims to provide a fundamental understanding of carbenium-ions cracking mechanism in terms of the possible elementary steps, which are based on the zero-conversion extrapolation of the kinetic data to exclude implication of secondary reactions.

1.6 References

1. Marcilly, C. *Stud. Surf. Sci.Catal.* **2001**,135, 37.

2. *The intelligence report: Business Shift in the Global Catalytic Process Industries 2005–2011;* The Catalyst Group Resources, Inc.: Spring House, **2006.**

3. *World Catalysts;* The Freedonia Group, Inc.: Cleveland, **2007.**

4. Coster, D.; Biumenfeld, A. L.; Fripiat, J. J. *J. Phys. Chem.* **1994,** 98, 6201.

5. Pellet, R. J.; Scott-Blackwell, C.; Rabo, J. A. *J. Catal.* **1988**, 114, 71.

6. Sam, J.; Fornes, V.; Corma, A. *J. Chem., Soc., Faraday Trans. I.* **1988**, 84, 3113.

7. Narbeshuber, T. F.; Brait, A.; Seshan, K.; Lercher, J. A. *Appl. Catal. A.* **1996**, 146, 119.

8. Lago, R. M.; Haag, W. O.; Mikovsky, R. J.; Olson, D. H.; Hellring, S. D.; Schmitt, K. D.; Kerr, G. T. *Stud. Surf. Sci. Catal.* **1986**, 28, 677.

9. Sohn, J. R.; DeCanio, S. J.; Fritz, P. O.; Lunsford, J. H. *J. Phys. Chem.* **1986**, 90, 4847.

10. Lonyi, F.; Lunsford, J. H. *J. Catal.* **1992**, 136, 566.

11. Carvajal, R.; Chu, P.; Lunsford, J. H. *J. Catal.* **1990**, 125, 123.

12. Lunsford, J. H.; *J. Phys. Chem.* **1968**, 72, 4163.

13. Mirodatos, C.; Barthomeuf, D. *J. Chem. Soc., Chem. Commun.* **1981**, 2, 39.

14. Wang, Q. L.; Giannetto, G.; Guisnet, M. *J. Catal.* **1991**, 130, 471.

15. Corma, A.; Forne´s, V.; Rey, F. *Appl. Catal.* **1990**, 59, 267.

16. Batamack, P.; Morin, C. D.; Vincent, R.; Fraissard, J. *Micropor. Mater.* **1994**, 2, 525.

17. Vermeiren, W.; Gilson, J. P. *Top. Catal.* **2009***, 52, 1131.

18. Sohn, J. R.; Decanio, S. J.; Lunsford, J. H.; O'Donnell, D. J. *Zeolites.* **1986**, 6, 225.

19. Klinowski, J.; Ramdas, S.; Thomas, J.; Fyfe, C. A.; Hartman, J. S. *J. Chem. Soc. Faraday Trans. II.* 1982, 78, 1025.

20. Parrillo, D. J.; Adamo, A. T.; Kokotailo, G. T.; Gorte, R. J. *Appl.Catal.* **1990**, 67, 107.

21. Ison, A.; Gorte, R. J. *J. Catal.* **1984**, 89, 150.

22. Lee, C. C.; Gorte, R. J.; Farneth, W. E. *J. Phys. Chem. B.* **1997**, 101, 3811.

23. Eder, F.; Lercher, J. A. *Zeolites.* **1997**, 18, 75.

24. Eder, F.; Lercher, J. A. *J. Phys. Chem. B.* **1997**, 101, 1273.

25. Sepa, J.; Lee, C.; Gorte, R. J.; White, D.; Kassab, H.; Evleth, E.; Allavena, M. *J. Phys. Chem.* **1996**, 100, 18515.

26. Biaglow, A. I.; Gorte, R. J.; White, D. *J. Catal.* **1994**, 148, 779.

27. Sauer, J. *Chem. Rev.* **1989**, 89, 199.

28. Van Santen, R. A.; Kramer, G. J. *Chem. Rev.* **1995**, 95, 637.

29. Rozanska, X.; Van Santen, R. A.; Hutschka, F. *Prog. Theor. Chem.Phys.* **2001**, 8, 1.

30. Eder, F.; Stockenhuber, M.; Lercher, J. A. *J. Phys. Chem.B.* **1997**, 101, 5414.

31. Titiloye, J. O.; Parker, S. C.; Stone, F. S.; Catlow, C. R. A. *J. Phys.Chem.* **1991**, 95, 4038.

32. June, R. L.; Bell, A. T.; Theodorou, D. N. *J. Phys. Chem.* **1992**, 96, 1051.

33. Smit, B.; Siepmann, J. I. *J. Phys. Chem.* **1994**, 98, 8443.

34. Bigot, B.; Peuch, V. H. *J. Phys. Chem.* **1995**, 99, 8206.

35. Van Bokhoven, J. A.; Williams, B. A.; Ji, W.; Koningsberger, D. C.; Kung, H. H.; Miller, J. T. *J.Catal.* **2004**, 224, 50.

36. Van Bokhoven, J. A.; Tromp, M.; Koningsberger, D. C.; Miller, J. T.; Pieterse, J. A. Z.; Lercher, J. A.; Williams, B. A.; Kung, H. H. *J.Catal.* **2001**, 202, 129.

37. Haag, W. O.; Dessau, R. M. *Proceedings of The Eighth International Congress On Catalysis*, **1984,** 305.

38. Krannila, H.; Haag, W. O.; Gates, B. C. *J. Catal.* **1992**, 135, 115.

39. Lercher, J. A.; van Santen, R. A.; Vinek, H. *Catal. Lett.* **1994**, 27, 91.

40. Narbeshuber, T. F.; Vinek, H.; Lercher, J. A. *J. catal.* **1995,**157, 388.

41. Narbeshuber, T. F.; Stockenhuber, M.; Brait, A.; Seshan, K.; Lercher, J. A. *J. Catal.* **1996**, 160, 183.

42. Brait, A.; Koopmans, A.; Weinstabe, H.; Ecker, A.; Seshan, K.; Lercher, J. A. *Ind. Eng. Chem. Res.* **1998**, 37, 873.

43. Tung, S. E.; McIninch, E. J. *J. Catal.* **1968**, 10, 166.

44. Sie, S. T. *Ind. Eng. Chem. Res.* **1992**, 31, 1881.

45. Sie, S. T. *Ind. Eng. Chem. Res.* **1993**, 32, 397.

46. Rigby, A. M.; Kramer, G. J.; van Santen, R. A. *J. Catal.* **1997**, 170, 1.

47. Kazansky, V. B. *Acc. Chem. Res.* **1991**, 24, 379.

48. Kazansky, V. B. *Stud. Surf. Sci. Catal.* **1994**, 85, 251.

49. Boronat, M.; Viruela, P. M.; Corma, A. *J. Am. Chem. Soc.* **2004**, 126, 3300.

50. McVicker, G. B.; Kramer, G. M.; Ziemiak, J. J. *J. Catal.* **1983**, 83, 286.

51. Bizreh, Y. W.; Gates, B. C. *J. Catal.* **1984**, 88, 240.

52. Marczewski, M. *J. Chem. Soc. Faraday Trans.* **1986**, 182, 1687.

53. Narbeshuber T. F.; Brait, A.; Seshan, K.; Lercher, J. A. *J. Catal.* **1997**, 172, 127.

54. Bond, G. C.; Keane, M. A.; Lercher, J. A. *Catal. Rev.-Sci. Eng.* **2000**, 42, 323.

55. Ramachandran, C. E.; Williams, B. A.; van Bokhoven, J. A.; Miller, J. T. *J. Catal.* **2005**, 233, 100.

56. Bhan, A.; Gounder, R.; Macht, J.; Iglesia, E. *J. Catal.* **2008**, 253, 221-224.

57. Gounder, R.; Iglesia, E. *J. Am. Chem. Soc.* **2009**, 131, 1958.

58. Gounder, R.; Iglesia, E. *Angew. Chem. Int. Ed.* **2010**, 49, 808.

59. Niwa, M.; Suzuki, K.; Katada, N.; Kanougi, T.; Atoguchi, T. *J. Phys. Chem. B.* **2005**, 109, 18749.

60. Suzuki, K.; Noda, T.; Katada, N.; Niwa, M. *J. Catal.* **2007**, 250, 151.

61. Katada, N.; Suzuki, K.; Noda, T.; Miyatani, W,; Taniguchi, F.; Niwa, M. *Appl. Catal. A.* **2010**, 373, 208.

62. Xu, B.; Sievers, C.; Lercher, J. A.; Rob van Veen, J. A.; Giltay, P.; Prins, R.; van Bokhoven, J. A. *J. Phys. Chem. C.* **2007**, 111, 12075.

63. Xu, B.; Bordiga, S.; Prins, R.; van Bokhoven, J. A. *Appl. Catal. A.* **2007**, 333, 245.

Chapter 2

Influence of transition enthalpy and entropy on the protolytic cracking of alkane

The rates and selectivities for individual reaction paths of alkane monomolecular cracking on MFI zeolites with varying Si/Al ratios are shown to be governed by subtle changes in transition enthalpy and entropy. The stability of the transition states involved appears to be controlled by the polarizability of the individual C-H bonds, the configurational space of the transition state and the stability of the carbenium ion formed in the cleavage process. This causes the cleavage of the C-C bonds closer to the center of the n-alkane being energetically favored over cleavage of terminal bonds, while the transition entropy decreases as the resulting transition state becomes more symmetric. These differences in the kinetic parameters suggest that the carbonium ion like transition state is not as closely related to the products formed as frequently stated and suggests a surprisingly high configurational space compared to the reactants adsorbed in the zeolite channel. While the majority of Brønsted acid sites show identical turnover rates for protolytic cracking, a fraction of these sites, which is equivalent to the concentration of sites exchangeable with Co^{2+}, is not (or at least drastically less) active for protolytic cracking. As the acid strength of all sites determined by the stability of basic molecules is

equivalent, this is attributed to a perturbation of the transiently formed carbonium ion by the nearby positive charge of the second Brønsted acid site.

2.1 Introduction

Brønsted acid catalyzed cracking of hydrocarbons is one of the most important individual reactions in the conversion of fossil hydrocarbon resources. This has led to an impressive body of research and a wealth of information hardly matched by another type of energy related reaction. Two pathways of the cleavage of carbon-carbon bonds have been identified for alkanes and alkenes with carbonium and carbenium ions being the species in the transition state for these two groups of molecules [1-5]. At very low densities of reactants both pathways occur monomolecularly, while at higher temperature the pathways may be linked by hydride transfer and secondary products form by dimerization of olefins and repeated cracking [6-8].

The protolytic cracking of alkanes has found recent interest [9-12] and these results strongly emphasized the role of the transition entropy rationalizing the differences in rates primarily upon the extrapolated thermodynamic data of the ground states of the sorbed reactants, compared to earlier studies [13-15]. Recent theoretical studies suggest that such extrapolation are indeed feasible and that the thermodynamic data do not change markedly in the temperature interval between 80°C (at which most of the sorption studies have been performed) and the typical reaction temperature of 500°C [16]. It should be noted, however, that the measurements are very sensitive and deviations of less than 10 % of the measured adsorption enthalpies would lead to significant deviations in the entropic values of the molecules in the sorbed state [17-19].

The principal mechanism of protolytic cracking of alkanes, as originally proposed by Dessau and Haag [20], is widely accepted as the dominating reaction pathway for the Brønsted acid site catalyzed routes to cleave alkanes in the absence of hydride transfer [14, 21-24], i.e., at high temperatures and low reactant pressures. In Brønsted-acidic, microporous materials such as zeolites, the reaction is preceded by physisorption of the reactants in the micropores [15, 25], an exothermic process (approximately 12 kJ·mol^{-1}

per carbon atom for the MFI structure) that significantly reduces both the translational and rotational components of the partition function, as well as the configurational space of the sorbed molecule [16]. The resulting enthalpy and entropy reflect the fit between the sorbed molecule and the pore. In consequence, both the enthalpy of the sorbed molecules and the entropy become more negative as the fit between the alkane and the zeolite pore improves [17]. Direct hydrogen bonding of the alkane is induced via polarization of the C-H bonds by the Brønsted acid site and is favored by 8-12 kJ·mol^{-1} over physisorption in the zeolite channel [18, 19]. Overall, this leads at ambient temperature to a marked preference of molecules to be more strongly adsorbed as their molecular weight increases and for zeolites to adsorb a particular molecule more strongly as the fit and, hence, the equilibrium constant of the adsorption increases [17]. It should be noted in passing that, of course, with increasing temperature, this trend weakens and even reverses [16].

Theory [13, 26] suggests that cracking proceeds via a penta-coordinated carbonium ions resembling the five coordinated carbonium ions proposed by Olah to exist in super acids [27]. The principal experimental findings from the protolytic cracking are in line with these observations [21, 28-29]. The carbonium ion decomposes at the five-coordinated carbon atom of the carbocation, generating dihydrogen or an alkane and a primary carbenium ion [20]. Literature has suggested that the generation of the carbonium ion occurs rather randomly [21, 23], leading to a statistical distribution of the products.

It has been established (for example for H-MFI) that the first order rate constant of protolytic cracking of *n*-alkanes increases exponentially with the size of the hydrocarbon [14, 25, 30-32]. While originally this had been implicitly associated with variations in the surface coverage [15, 33-34], Iglesia et al. have shown that entropy plays a significant, if not the dominating role for determining the variation of the rates. This had been associated with the difference between the entropy of the sorbed molecule and the entropy gain in the late transition state of protolytic cracking [9]. It is important to

emphasize that for high silica zeolites, i.e., those showing a constant strength of their Brønsted acid sites, the rate of cracking has been found to be strictly proportional to the concentration of protons [15, 35], indicating that each proton converts alkanes with an identical rate. Thus, one would expect a strict relation of the protolytic conversion of alkanes with the concentration of the Brønsted acid sites, the absolute values varying of course with the size of the alkane.

Gounder and Iglesia [10] have convincingly shown, however, that the rate of cracking depends subtly on the environment of the proton, with the consequence that even for zeolites with nearly equal sized pores and somewhat larger intersections marked differences in the intrinsic rates of protolytic cracking have been observed. The same authors also showed that for cracking of butane by H-MOR cleavage of the outer C-C bond was preferred in constrained environments, compared to the inner C-C bond. Both findings and their interpretations indicate that the transition state entropy significantly controls the overall reaction.

Assuming that interpretation is correct, the overall rates and the product distribution should be governed by the variations in entropy and enthalpy along the reaction pathway. We studied, therefore, cracking of light alkanes ranging from propane to hexane on one zeolite structure (MFI) with three different concentrations of acid sites. The experiments were designed to probe the dependence of transition enthalpy and entropy on the size of the hydrocarbon and the concentration of acid sites. Knowledge of the rates of individual pathways and, hence, activity and selectivity for alkane conversion in zeolites should open new possibilities for *de novo* design of zeolite catalysts and/or a better guided selection of catalysts from the body of known materials.

2.2 Methods

2.2.1 Catalyst treatment

The ammonium form of ZSM-5 with three different Si/Al ratios (CBV 3024E, CBV 5524G and CBV 8014) were obtained from the Zeolyst International in the ammonium form and were transformed into the acid form by calcination. Typically, the sample were treated in flowing synthetic air (2.5 ml·g^{-1}s^{-1}) by increasing the temperature to 773 K (1 K·min^{-1}) and holding it for 4 h. The resulting H-ZSM-5 powder was pelletized, crushed and sieved into particles of 180-250 μm (60-80 mesh). The BET surface areas of the materials were between 405 and 425 m^2 g^{-1}. The concentration of acid sites in the sample was quantified by IR spectra of adsorbed pyridine and temperature programmed desorption of ammonia. The average particle size distribution was determined by scanning electron microscopy. The phase purity of the samples was assessed by X-ray diffraction (Table 2-1).

Table 2-1 Elemental composition and structure characterization of the catalysts

Zeolite	Catalyst	Si/Al ratio[a]	Na/Al ratio[a]	Surface area[b] (m^{2}g^{-1})	Brønsted acidity[c] (μmol g^{-1})	Lewis acidity[c] (μmolg^{-1})
HMFI-1	CBV 3024E	15.3	0.017	405	807	144
HMFI-2	CBV5524G	27.0	0.029	425	511	91
HMFI-3	CBV 8014	38.7	0.043	425	265	55

[a]Determined from atomic absorption spectroscopy. [b]Surface area form BET measurement. [c] Concentration of Brønsted and Lewis acid sites in the samples determined from infrared spectroscopy of adsorbed pyridine.

2.2.2 Kinetic measurement of monomolecular alkane activation

Kinetic measurements of acid catalyzed alkane cracking and dehydrogenation were performed in a tubular quartz reactor with 6 mm inner diameter under differential conditions (< 2 % conversion). The catalyst samples (2 - 20 mg) were supported on a quartz frit and diluted by inert quartz pellets (180 - 250 μm). The temperature of the furnace was adjusted by a temperature controller with 18 segment programs (Eurotherm Series 2014). The catalyst bed temperature was monitored by a thermocouple mounted at the external surface of the quartz reactor.

Catalysts were activated in a mixture of 5 % O_2 in He flow (0.5 ml·s^{-1}) at 803 K (1 K·min^{-1}) for 2 h and then treated in pure He (0.5 ml·s^{-1}) for another 0.5 h before kinetic measurements. Propane (99.95 %) and *n*-butane (99.95 %) were supplied by Linde and Westfalen, respectively. Both gaseous reactants passed through an olefin trap loaded by activated zeolite H-Y (20 g), before they were mixed with He. In the case of *n*-pentane and *n*-hexane the liquid reactants were adjusted to the desired vapor pressure by controlling the temperature of the He-purged saturator. Reactant partial pressures were adjusted by mixing the reactant stream with He flow and remained around 0.03 bar. Olefin concentration in the resulting gas mixture was below the GC detection limit (i.e., < 1 ppm). Reactants and products were analyzed by a gas chromatograph (Agilent HP-5890) using Al_2O_3-KCl capillary column (50 m×0.32mm×0.53mm; Agilent) connected to a flame ionization detector (FID). The absence of bimolecular pathways was confirmed by the absence of hydrocarbons larger than the corresponding alkane reactant. The kinetic rates were based on alkanes as primary cracking products for *n*-pentane and *n*-hexane, because olefins undergo a wide variety of secondary reactions. The kinetic parameters were obtained from reaction rate measurement as a function of temperature (728 - 778 K). Transport limitation in the kinetic measurement was excluded by using Mears criteria.

**2.2.3 Kinetic models for monomolecular alkane cracking and dehydrogenation
   in the thermodynamically non-ideal zeolite system**

The transition state theory is applied to relate the measured kinetic parameters to thermodynamic states of the transition state, which is also extensively described elsewhere [9, 10, 12]. In the following, the rate expression for monomolecular cracking of alkane is derived based on the transition state theory in order to outline the formalism of entropy term.

We start the transition state formalism with the generalized reaction system. In an equilibrated system A+B $\rightleftharpoons$ P in which the reactants is in thermodynamic equilibrium among themselves, the rate of reaction is formulated as:

$$\vec{r} = \overleftarrow{r} = \gamma C_z \tag{2-1}$$

Where $\vec{r}$ is the rate of forward reaction, $\overleftarrow{r}$ is for back reaction, and C_z refers to the concentration of transition state species in equilibrium with reactants A and B, γ is equivalent to a frequency.

If the products are continually removed from the equilibrated system, the reaction becomes unidirectional A+B $\rightarrow$ P, the rate is also expressed by the forward reaction:

$$r = \vec{r} = \gamma C_z \tag{2-2}$$

Assuming that the system is in equilibrium, the transition state Z with the concentration C_z is also in equilibrium with the reactants A and B:

$$K_c^{\ddagger} = \frac{C_z}{C_A C_B} \tag{2-3}$$

According to the thermodynamic relation:

$$RT\ln K_c^{\ddagger} = -\Delta G^{0\ddagger} = -\Delta H^{0\ddagger} + T\Delta S^{0\ddagger} \tag{2-4}$$

Where R is the gas constant, $\Delta G^{0\ddagger}$ is the change in standard Gibbs free energy for the reaction while $\Delta H^{0\ddagger}$ and $\Delta S^{0\ddagger}$ are the change in standard enthalpy and entropy, respectively. In the expression the superscript $\ddagger$ denotes the species formed at the transition state.

Combining (2-3) and (2-4), (2-2) is transformed into:

$$r = \gamma \exp\left(\frac{\Delta S^{o\ddagger}}{R}\right) \exp\left(\frac{-\Delta H^{o\ddagger}}{RT}\right) C_A C_B \tag{2-5}$$

In the equation, the frequency γ relates to a universal frequency, which is independent of the nature of the relevant molecular system, and is equal to:

$$\gamma = \frac{kT}{h} \tag{2-6}$$

Where h is Planck's constant and k is Boltzmann's constant.

Therefore (2-5) can be expressed as:

$$r = \frac{kT}{h} \exp\left(\frac{\Delta S^{o\ddagger}}{R}\right) \exp\left(\frac{-\Delta H^{o\ddagger}}{RT}\right) C_A C_B \tag{2-7}$$

In a thermodynamically non-ideal system, such as the monomolecular reactions of alkanes on zeolite Brønsted acid sites, in which most of H^+ sites remains unoccupied during reactions [2,10], activity a has to be introduced to replace concentration C, thus:

$$K_c^{\ddagger} = \frac{a_Z}{a_A a_B} \tag{2-8}$$

For monomolecular cracking, alkanes adsorb from the gas phase A(g) on Brønsted acid sites (H^+Z^-) within the zeolite channels A(z) in a quasi-equilibrated step [10][39]. The pathways are depicted in Scheme 2-1.

1. $A(g) \rightleftharpoons A(z)$

2. $A(z) + H^+Z^- \rightleftharpoons \ddagger \rightarrow P$

Scheme 2-1 Reaction pathway for protolytic alkane activation on Brønsted acid sites within the zeolite (H^+Z^-)

Accounting for the thermodynamic activity of reactants, the transition state formalism of protolytic activation of alkanes on Brønsted acid sites becomes

$$r = \frac{kT}{h} \exp\left(\frac{\Delta S^{o\ddagger}}{R}\right) \exp\left(\frac{-\Delta H^{o\ddagger}}{RT}\right) \times \frac{\gamma_{H^+z} C_{H^+z} \gamma_{A_z} C_{A_z}}{\gamma_{\ddagger}} \tag{2-9}$$

Since both, alkane reactants A(z) and transition states species ‡ absorb on the same site in zeolites, activity coefficients for both species (γ_{A_z} and $\gamma_{\ddagger}$) must be identical. Besides, C_{H^+z} and γ_{H^+z} are approximately equal to unity due to the low occupancy of H$^+$ sites in monomolecular alkane activation. Thus, equation (2-9) can be simplified into:

$$r = \frac{kT}{h} \exp\left(\frac{\Delta S^{0\ddagger}}{R}\right) \exp\left(\frac{-\Delta H^{0\ddagger}}{RT}\right) \times C_{A_z} \qquad (2\text{-}10)$$

According to Langmuir adsorption theory the intra-zeolite concentration of adsorbed alkanes (C_{A_z}) becomes proportional to the partial pressure of alkanes in the gas phase (P_A) and the adsorption constant (K_A) at low coverage of the active sites:

$$C_{A_z} = K_A P_A \qquad (2\text{-}11)$$

Hence, equation (2-10) can be rewritten into:

$$r = k_{int} K_A P_A = \frac{kT}{h} \exp\left(\frac{\Delta S^{0\ddagger}}{R}\right) \exp\left(\frac{-\Delta H^{0\ddagger}}{RT}\right) \times K_A P_A \qquad (2\text{-}12)$$

In this context, the corresponding activation energies and entropies from the experiments can be directly related to intrinsic term by introduction of the adsorption parameters of alkane molecules on Brønsted acid sites according to (2-12):

$$Ea_{meas} = Ea_{int} + \Delta H_{ads} \qquad (2\text{-}13)$$

$$\Delta S_{meas} = \Delta S_{int} + \Delta S_{ads} \qquad (2\text{-}14)$$

$$\ln(A_{meas}) = \ln(A_{int}) + (\Delta S_{ads}/R) \qquad (2\text{-}15)$$

Where Ea$_{meas}$ and A$_{meas}$ (ΔS_{meas}) refer to measured activation barriers and pre-exponential factors, while E$_{int}$ and A$_{int}$ (ΔS_{int}) are their corresponding intrinsic terms with properties of adsorbed alkanes. Combing the equation (2-12) to (2-15) the measured entropy of activation can be defined as:

$$\Delta S_{meas} = R[\ln(A_{meas}) - \ln(k_B T/h)] \qquad (2\text{-}16)$$

In the transition state theory treatment the measured pre-exponential factor A_{meas} is strictly normalized by the number of Brønsted acid sites and the number of bonds available for each reaction.

2.3 Results and discussion

2.3.1 Monomolecular activation on H-ZSM-5 samples in the individual reaction pathways

In total, protolytic cracking under differential conditions has been investigated for propane to *n*-hexane with three H-ZSM-5 zeolites with increasing concentrations of aluminum in the lattice. Table 2-2 shows the measured rate constants k_{meas} of cracking and dehydrogenation for C_3 to C_6 paraffins at 777 K over H-ZSM-5 with Si/Al ratio of 25. The values for another two zeolites are given in the supporting information. The assessment of kinetic parameters for individual cracking pathways of all H-ZSM-5 samples based on the kinetic model is also compiled in the supporting information. The activation energies were derived from the temperature dependence of the rate constants (728 - 777K) and the corresponding activation entropies are obtained from the transition state treatment.

Table 2-2 Monomolecular cracking and dehydrogenation rate constants k_{meas} of C_3-C_6 paraffin at 777 K and measured activation energies (Ea_{meas}) and entropies (ΔS_{meas}) over H-ZSM-5 (Si/Al=25)

	$k_{meas}(\times 10^3 mol(molH^{+-1}s^{-1}bar^{-1}))$		$Ea_{meas}(kJ \cdot mol^{-1})$		$\Delta S_{meas}(J \cdot mol^{-1}K^{-1})$	
reactants	Cracking	Dehyd.	Cracking[a]	Dehyd[b].	Cracking[c]	Dehyd[d].
propane	6.0	3.2	152	100	-100	-173
n-butane	28.0	21.7	143	116	-98	-136
n-pentane	111.5	44.6	124	124	-115	-120
n-hexane	223.4	89.6	101	104	-135	-139

[a] Errors are $\pm$ 2 kJ mol^{-1}. [b] Errors are $\pm$ 5 kJ mol^{-1}. [c] Errors are $\pm$ 2 J mol^{-1}K^{-1}. [d] Errors are $\pm$ 3 J mol^{-1} K^{-1}.

The overall cracking rate constants increase with the carbon number of the reactants by a factor of up to 37, while the measured averaged activation energies decrease with increasing size of the reacting alkane. After subtracting the heat of adsorption of the reactant (determined by separate sorption experiments [16]), the intrinsic activation energies are nearly identical for all reactants (Table 2-3 to Table 2-5). In agreement with our previous papers we find that the intrinsic activation energy for protolytic cracking was approximately 200 kJ·mol^{-1} and was independent of the carbon number of the alkanes used [14]. This suggests that the average intrinsic barriers to cleave C-C bonds in alkanes do not change with the alkane size. However, these averaged barriers are weighted by means of individual reaction pathways and, consequently, the observed small fluctuations may not be related to the associated error bars.

In contrast to monomolecular cracking, the measured activation energies of dehydrogenation vary among these reactants, consistent with previous data [15, 29, 36-38]. The lower energy of activation compared to protolytic cracking is speculated to be due to a more confined (and secondary) carbenium ion formed in the dehydrogenation process. Furthermore, the measured activation entropies for protolytic dehydrogenation are consistently lower than for cracking. This difference between

cracking and dehydrogenation may indicate a later and looser transition state with larger configurational freedom for cracking, as we discuss below.

In order to facilitate the detailed discussion of the kinetic data, let us summarize first the results of previous quantum chemical calculations on protolytic cracking in terms of geometries of the transition state. These studies explored alkanes such as ethane [26, 40-41], propane [15, 42], *n*-butane [43, 44], isobutane [26], and *n*-hexane [43]. All results find the transition state to be based on non-classical three-centered C-C-H bond carbonium ions like species. These transition states species are stabilized by electrostatic interactions between the charged zeolite framework and the adsorbed reactant, but their configuration and charge distribution resembles those of free ions [45-46]. In this case the proton moves to the middle of the C-C bond of the molecule, which nearly instantly decomposes to a smaller alkane, while the rest of the molecule forms a primary carbenium ion like fragment, stabilized by the basic oxygen of the zeolitic lattice. Consequently, the energy level in the carbonium system is largely correlated to the magnitude of the stabilization of the carbenium ion produced upon the decomposition of the transition state species [45, 47]. The long range electrostatic interactions depend strongly on the structure and charge distribution of the local bonds of the transition state fragments [15, 26, 42, 48]. Such electrostatic stabilization by the zeolitic lattice depends markedly on the degree of ionicity of these transition state complexes [44]. The more ionic the transition state is, the less the activation barrier and the deprotonation ability of the Brønsted acid sites (E_{dep}) are correlated.
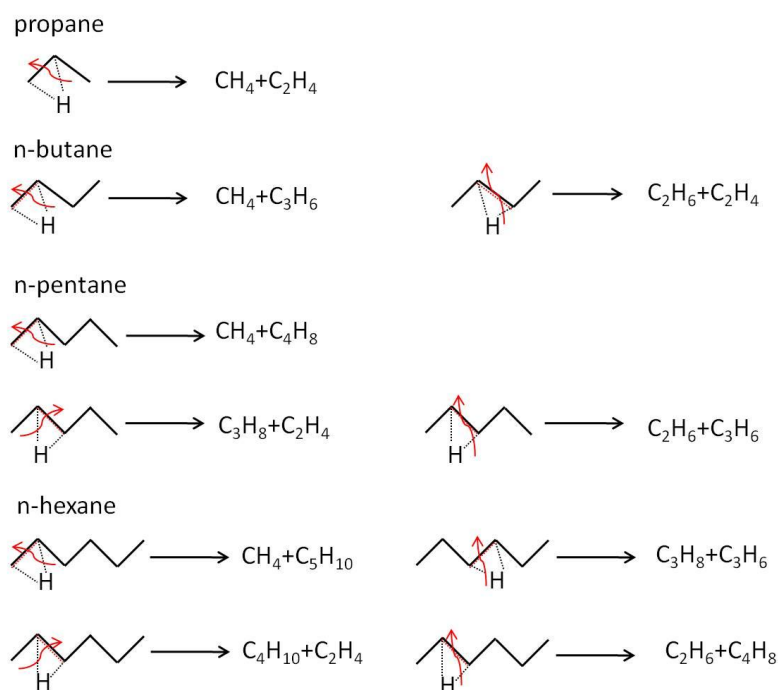
Table 2-3 Rate constants (k_{meas}) at 777K, activation energies (Ea) and entropies (ΔS) for monomolecular *n*-butane cracking in terms of different pathways over H-ZSM-5 (Si/Al=25)

	k_{meas} ($\times 10^3 mol(molH^{+-1}s^{-1}bar^{-1})$)	Ea_{meas}[a] ($kJ \cdot mol^{-1}$)	ΔS_{meas}[b] ($J \cdot mol^{-1}K^{-1}$)	Ea_{int} ($kJ \cdot mol^{-1}$)	ΔS_{int} ($J \cdot mol^{-1}K^{-1}$)
$C_1+C_3^=$	15.0	149	-96	201	8
$C_2+C_2^=$	13.0	137	-113	189	-9
Overall	28.0	143	-98	195	6

[a] Errors are $\pm$ 3 kJ mol^{-1}. [b] Errors are $\pm$ 3 J mol^{-1}K^{-1}.

Table 2-3 shows the activation energies and entropies of individual reaction pathways for monomolecular cracking of *n*-butane, estimated from the measured rate constant and the adsorption parameters by applying equations (2-12), (2-13) and (2-14). The cleavage of terminal bonds in n-butane (leading to CH_4 and C_3H_6) is 12 kJ·mol^{-1} higher in energy than cleavage of central bonds (leading to C_2H_6 and C_2H_4). This magnitude is consistent with the theoretical calculations for monomolecular cracking of *n*-butane by Collins and O'Malley (10 kJ·mol^{-1}) [43]. Given the same adsorption enthalpy of the reactant, the measured energy difference exemplifies the intrinsic differences between the two cracking pathways. The activation entropy of breaking the outer C-C bond is higher than that for cleaving the central bond, reflecting the differences in the geometry of transition state structure. As illustrated in Figure 2-1, the protonation of *n*-butane at different position results in two distinct transition states for these two routes. As the activation entropy is inversely proportional to constraints in the transition state, protonation of terminal bonds is concluded to lead to a less constrained transition state (i.e., one having larger vibrational and rotational freedom) or a transition state having a larger configurational space compared to that of inner C-C bonds. Conceptually, this difference could be related to the transition state (configurational entropy), or the larger mobility of methane formed in the cleavage of the transition state species. It should be noted at this point that this difference in the kinetic parameters for cracking seems to be inherent to the molecule and not necessarily related to constraints around

the catalytically active site [14], although the latter will play an important role as discussed below.

Figure 2-1 Individual pathways in monomolecular cracking of C_3-C_6 paraffins with proposed transition state

Let us analyze in the next step the individual cracking pathways of larger alkanes. The measured rate constants (k_{meas}) at 777K, activation energies and entropies of *n*-pentane cracking over the same sample are compiled in Table 2-4. As for *n*-butane, the cleavage of the terminal C-C bonds (leading to CH_4 and C_4H_8) is energetically more demanding than the cleavage of central C-C bonds (leading to C_2H_6 and C_3H_6 as well as to C_3H_8 and C_2H_4). It is important to emphasize that the route to C_3H_8 and C_2H_4 requires 8 kJ·mol^{-1} higher activation energy than the route to C_2H_6 and C_3H_6 although the proton cleaves the same C-C bond. If solely the initial approach of the proton would determine the overall barrier (early transition state) a difference among activation barriers for the protonation at the same C-C bond should not be observed. Thus, we conclude that the

transition state must resemble the configuration of products in the state of the cleavage of the C-C- bond, i.e., it is a relatively late transition state. For a late transition state, the stabilization of the resulting primary carbenium ion will play a significant role. As the larger carbenium ion is able to better delocalize the positive charge, its higher stability will lead to a lower barrier in line with the Polanyi relation [49].

Table 2-4 Rate constants (k_{meas}) at 777K, activation energies (Ea) and entropies (ΔS) for monomolecular *n*-pentane cracking in terms of different pathways over H-ZSM-5 (Si/Al=25)

	k_{meas} ($\times 10^3 mol(molH^{+-1}s^{-1}bar^{-1})$)	Ea_{meas}[a] ($kJ\cdot mol^{-1}$)	ΔS_{meas}[b] ($J\cdot mol^{-1}K^{-1}$)	Ea_{int} ($kJ\cdot mol^{-1}$)	ΔS_{int} ($J\cdot mol^{-1}K^{-1}$)
$C_1 + C_4^=$	28.8	135	-111	198	7
$C_2 + C_3^=$	64.2	118	-127	181	-9
$C_3 + C_2^=$	18.5	126	-128	189	-10
Overall	111.5	124	-115	187	3

[a] Errors are $\pm$ 4 J mol^{-1}. [b] Errors are $\pm$ 3 J mol^{-1}K^{-1}.

Like for *n*-pentane also for *n*-hexane two symmetric, equivalent C-C bonds exist, leading to $C_2H_6 + C_4H_8$ and to $C_2H_4 + C_4H_{10}$ and their rate constants (k_{meas}) at 777K, activation energies and entropies are compiled for the individual pathways with H-ZSM-5 (Si/Al=25) are compiled in Table 2-5. The energies of activation decrease in the order $CH_4 + C_5H_{10} > C_4H_{10} + C_2H_4 > C_2H_6 + C_4H_8 > C_3H_8 + C_3H_6$.

Table 2-5 Rate constants (k_{meas}) at 777K, activation energies (Ea) and entropies (ΔS) for monomolecular *n*-hexane cracking in terms of different pathways over H-ZSM-5 (Si/Al=25)

	K_{meas} (×10^{3}mol(molH^{+-1}s^{-1}bar^{-1}))	Ea_{meas} (kJ mol^{-1})	ΔS_{meas} (J mol^{-1}K^{-1})	Ea_{int} (kJ mol^{-1})	Δs_{int} (J mol^{-1}K^{-1})
C1+C5=	35.4	119	-127	211	11
C4+C2=	15.6	110	-146	202	-8
C2+C4=	100	98	-146	190	-8
C3+C3=	72.4	96	-151	188	-13
Overall	223.4	101	-135	193	3

[a] Errors are ± 3 kJ mol^{-1}. [b] Errors are ± 3 J mol^{-1}K^{-1}.

Also in this case it is observed that when cleaving the same C-C bond, the energy barrier of the reaction pathway, leading to the larger carbenium ion is favored. Furthermore, the activation energy to cleave the C-C bond decreases overall towards a central position, which is in line with the better polarizability of the C-H bonds (probed by ^{13}C MAS-NMR spectroscopy of alkanes [50, 51] and in agreement with previous experimental reports [15, 43]. As discussed above, also in this case the energy barriers for the cracking routes with protonation at the same position (leading to formation of C_4H_{10} + C_2H_4 as well as C_4H_8 + C_2H_6 for *n*-hexane cracking) are not equal. Despite cleaving the same C-C bond, the route to C_4H_{10} and C_2H_4 requires higher activation energy than the route to C_2H_6 and C_4H_8, while the similar activation entropies for these two pathways indicates the similarity between the two transition state structures.

Therefore, we conclude that in contrast to the marked dependence of the transition enthalpy on the products formed, the activation entropy only depends on the C-C bond cleaved, i.e., the activation entropy is predominantly influenced by the position of protonation at the transition state.

As the activation entropy for the reaction involving cleavage of the outer bonds is higher than that for corresponding cleavage of the inner bonds, we infer that this is related to the larger configurational space it may assume or to a less constrained transition state, which is in good agreement with the results reported for monomolecular cracking of *n*-butane.
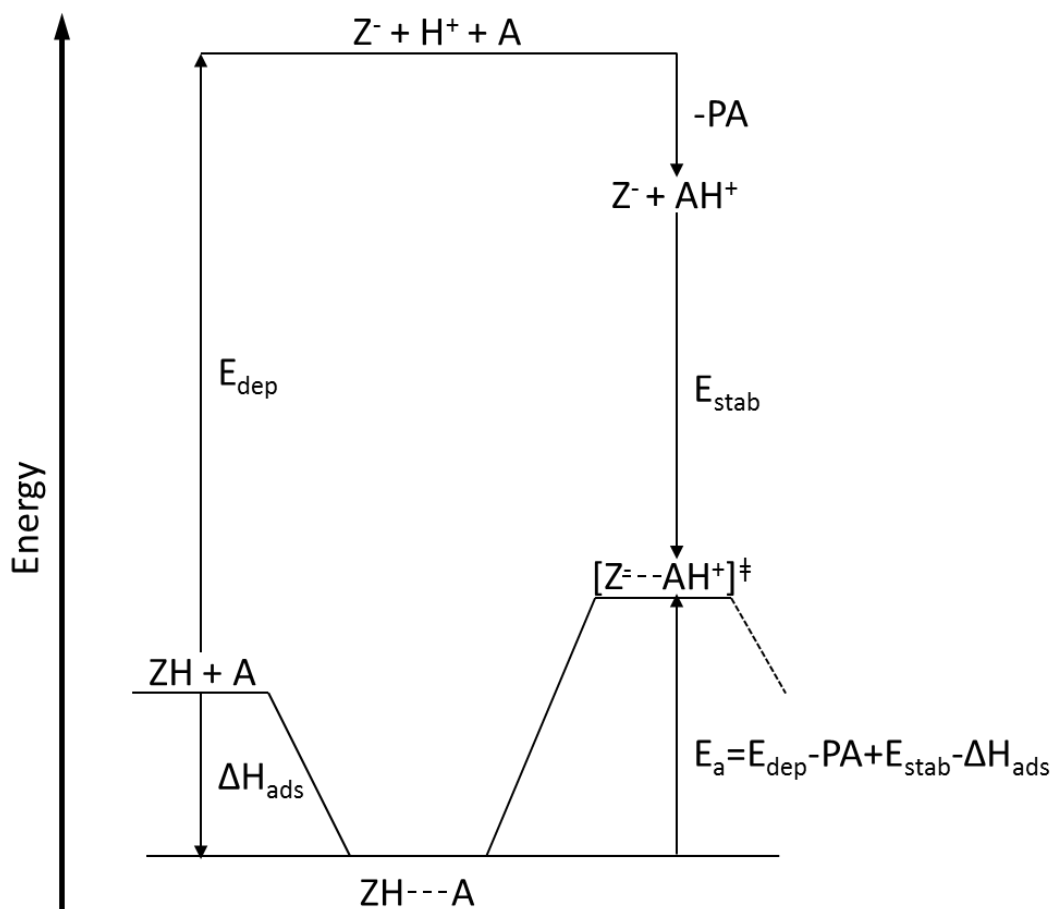
Scheme 2-2 Born-Haber thermochemical cycle for acid-catalysis reaction in zeolite (reproduced with modification from ref. [48]). The activation energy (Ea) for reaction on the Brønsted acid (ZH) depends on the deprotonation energy (E_{dep}), the proton affinity (PA) of gaseous reactant (A), the stabilization energy (E_{stab}) of TS species, and the adsorption enthalpy of reactant (ΔH_{ads}).

In the next step, we use thermochemical cycles to relate the activation barriers to the deprotonation energy of the Brønsted acid sites (E_{dep}), the adsorption enthalpies of reactants (ΔH_{ads}), the proton affinities (PA) of the gaseous reactants and transition state stabilization energies (E_{stab}). As shown in Scheme 2-2, alkanes physisorb from the gas phase to form an intermediate on a Brønsted acid site. The adsorbed alkanes are

transformed into carbonium ions-like species in the transition state, stabilized by the zeolitic framework via electrostatic interactions. From this, the energy barrier of the transition state is expressed as:

$$E_a = E_{dep} - PA + E_{stab} - \Delta H_{ads} \tag{2-17}$$

The deprotonation energy E_{dep} is defined as the energy difference between the protonated (ZH) and unprotonated (Z$^-$) zeolitic cluster [52-55]. The value, therefore, reflects the intrinsic property of the acid sites, and is independent of the reactants. High deprotonation energy indicates, for example, relatively low acid strength. The gas-phase proton affinity PA of a molecule A is defined as the enthalpy change upon the addition of the proton, , $A + H^+ \rightarrow AH^+$ and is used as a descriptor of the gas-phase basicity of A [42]. The stabilization energy E_{stab} reflects the interaction of the ion-pair in the cationic transition state with the anionic conjugate base of the framework cluster, predominately induced by the electrostatic stabilization [48]. The contributions to ΔH_{ads} result from the combination of charge induced hydrogen bonding between the acid site and the alkane (approximately 12 kJ·mol^{-1} for H-ZSM-5) and from the dispersion forces (approximately 10-12 kJ·mol^{-1} per carbon atom) reflecting the interaction between the absorbed reactants and the zeolite pore [50].

With respect to the different reaction pathways, for example in the monomolecular cracking of *n*-hexane, the differences in the activation barrier are then determined by the proton affinity PA at different C-C bonds and the stabilization energy of the ion-pair in the transition state. The deprotonation energy E_{dep} of the zeolite and the adsorption enthalpy ΔH_{ads} are identical for each reaction route in equation (2-17).

Theoretical estimates of C-C bond activation in alkanes indicate that protonating different C-C bonds in monomolecular alkane cracking requires different energy inputs, as the proton affinities of the C-C bonds increase monotonically from the terminal bonds to the central ones [56]. Thus, the measured activation enthalpies for cracking along different pathways reflect an intrinsic property of adsorbed reactants, as they are primarily determined by the proton affinities of different C-C bonds. However, for

identical C-C bonds, such as the cleavage of *n*-hexane to C_4H_{10} + C_2H_4 and to C_2H_6 + C_4H_8, the relative stability of the products, i.e., the carbenium ion like species formed in the rate determining step determines the difference in the activation energies. The higher intrinsic activation energy for the path to C_4H_{10} + C_2H_4 compared to that of C_2H_6 + C_4H_8 (Table 2-4), indicates that the higher stability of carbenium ion like species with the larger alkyl group induces lower activation barrier (see Figure 2-2).

This indicates that the single carbonium ion model (a penta-coordinated carbonium ion with a two-electron three covalent bonds) originally proposed is an over simplification, as such a transition state would not discriminate between different patterns of cleavage and the C-C and C-H bonds would be broken statistically as indeed postulated [20]. Thus, one would expect identical activation barriers for routes with protonation at the same position and similar transition entropies for all cracking routes of a given molecule. The differences observed strongly suggest that picture is incorrect leading us to postulate the discernible transition state structures depicted in Figure 2-2.

The relative stability of the two transition states addressing the same C-C bond must be caused by the differences in stabilization energies E_{stab} of zeolite channel. The variation in activation energy among such two cracking routes reflects, thus, the contribution from the electrostatic stabilization with the zeolite framework to the cationic fragments at the transition state. The increasing inductive effect (+I) of the alkyl fragments suggests that the higher availability of electrons at the carbon atom bonding to the zeolite lattice oxygen leads to a stronger and more covalent bond stabilizing the alkoxide (carbenium ions in the excited state). Indeed, the relative stabilities of *n*-alkyl carbenium ions increase with the carbon number (butenium>propenium>ethenium) [57]. Thus, the intrinsic activation barriers for reaction routes with protonation at the same C-C bond differ only by the relative stabilities of the nearly formed carbenium ions like fragments.

The marked influence of the final state (carbenium ion like species) in the rate determining step and the influence of the proton affinity indicate, therefore, an

interesting contribution of early and late transition state elements to the activation energy.
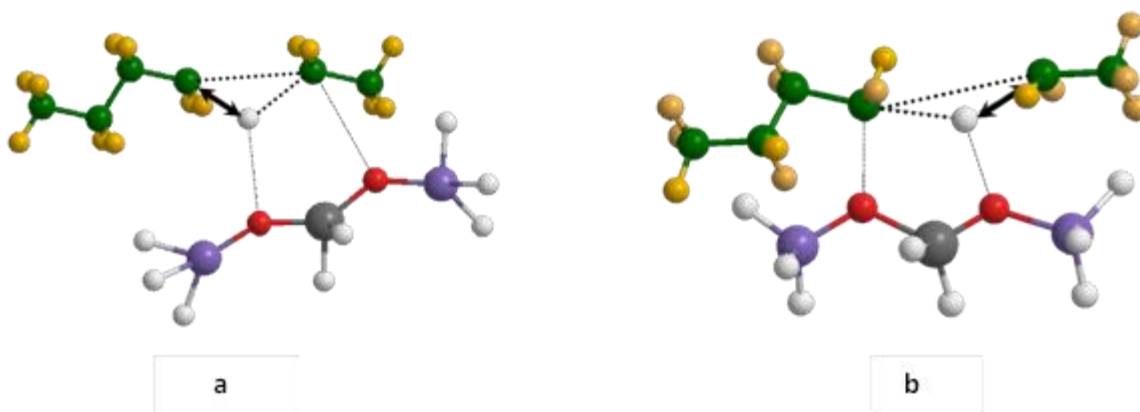
Figure 2-2 Schematic representation of the transition state structure for route to C_4H_{10} and C_2H_4 (a) and to C_2H_6 and C_4H_8 (b) in monomolecular cracking of *n*-hexane

It should be emphasized that the transition state complexes are not free, but strongly interact with zeolite framework via dispersion and electrostatic forces. Activation at the terminal C-C bonds generally shows larger and more positive entropies than activation at the central C-C bonds. The value is, for example, 16 $J \cdot mol^{-1} \cdot K^{-1}$ higher for the reaction pathway to $CH_4 + C_4H_8$ than that for the pathway to $C_2H_6 + C_3H_6$. This indicates that the more asymmetric the transition state is the higher the transition entropy. Given that the other changes from the ground to the transition are identical, we suggest that the larger configuration space of the more asymmetric transition state causes the relative entropy increase.

The partition functions of the two different reaction paths by the protonation at different positions, i.e., for example, for the routes to $C_2H_4+C_3H_8$ and to $CH_4+C_4H_8$, were calculated by using the harmonic approximation (see the appendix) and assuming that the adsorbate and transition state are rigid in space. The results indicate, regardless of formation of different butene isomers, cleavage at the terminal C-C bond leads

consistently to a higher value in partition function with a positive contribution to the entropic term. This trend is also in good agreement with the recent theoretical estimations for *n*-alkane cracking [58].
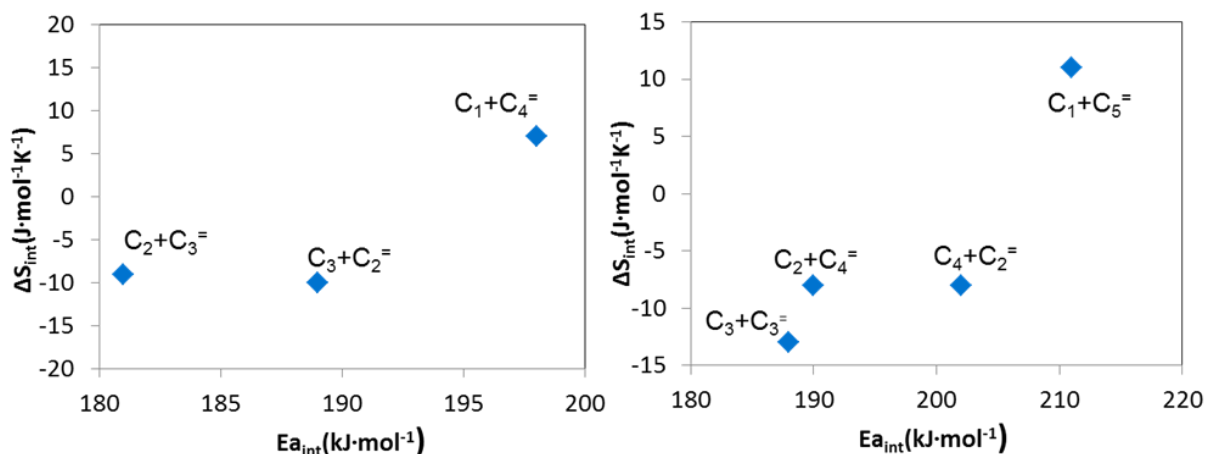
Figure 2-3. True transition state energy and entropy for individual pathways in monomolecular cracking of *n*-pentane and *n*-hexane

If we compare the variations in transition enthalpy and entropy for the individual cracking pathways, one notes in general that the higher entropy is accompanied by a higher transition enthalpy. This is concluded to be a fortuitous coincidence resulting from increasing proton affinity of this C-C bonds towards the center of the alkane (leading to a lower energy of activation) and the increasing asymmetry of the transition state towards the outer C-C bonds (leading to a higher transition entropy). The fact that this fortuitous relation is not observed for reactions involving the same C-C bond, but leading to two reaction products (in this case, the transition entropy is identical, while the enthalpy is lower for the reaction path with the larger carbenium ion formed, see discussion above) indicates that the transition entropy is not related to the stabilization of the products (and, thus, not to the transition enthalpy), but rather only to the configuration of the presumed transition state. This basically rules out that the reaction has an early transition state, as in this case a positive correlation between the activation

energy and the transition entropy is to be expected, as the strength of bonding of the reactants is likely to determine the activation energy.

2.3.2 Effects of Si to Al ratio in samples on kinetics of monomolecular C_3-C_6 paraffins cracking
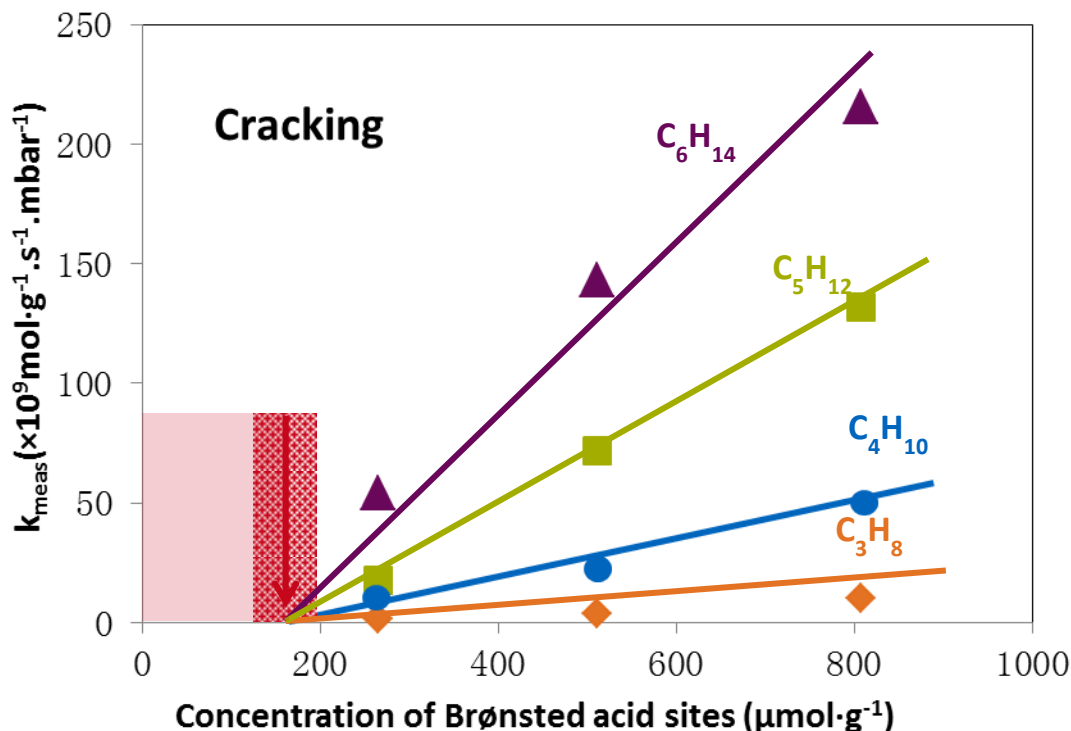
Figure 2-4 Rate constants in monomolecular cracking of C_3-C_6 paraffins upon variation of Si/Al ratio in samples

Figure 2-4 depicts dependence of the measured overall rate constants (k_{meas}) in monomolecular cracking of C_3-C_6 paraffins on the concentration of Brønsted acid sites (BAS) of the H-ZSM-5 samples. The rate constants and the concentration of Brønsted acid sites are linearly correlated for all alkanes. Higher concentrations of Brønsted acid sites lead to larger (catalyst weight normalized) rate constants indicating higher activities with increasing chain length of the alkane. As the rates appear to be

proportional to the concentration of Brønsted acid sites, we conclude that the turnover frequency is identical for all Brønsted acid sites. About 150 µmol·g^{-1} (± 40 µmol·g^{-1}) Brønsted acid sites appear, however, not to be catalytically active for all studied alkanes. This indicates that a small, but constant fraction of acid sites in all samples which is either unable to cleave alkanes protolytically, or that the rate catalyzed by these sites is at least one to two orders of magnitude smaller than that observed with the majority of Brønsted acid sites.

We would like to emphasize that all Brønsted acid sites were found to be of equal strength. Thus, the inactivity of some sites cannot be caused by the lower strength. Because the concentration of these sites is equivalent to the concentration of sites that can be exchanged by divalent cations (Figure 2-5), we relate the inability to crack tentatively to the presence of two neighboring Brønsted acid sites. We attribute the inactivity of such protons to the destabilizing effect of the nearby positive charge on the formation of the carbonium ions at the transition state.
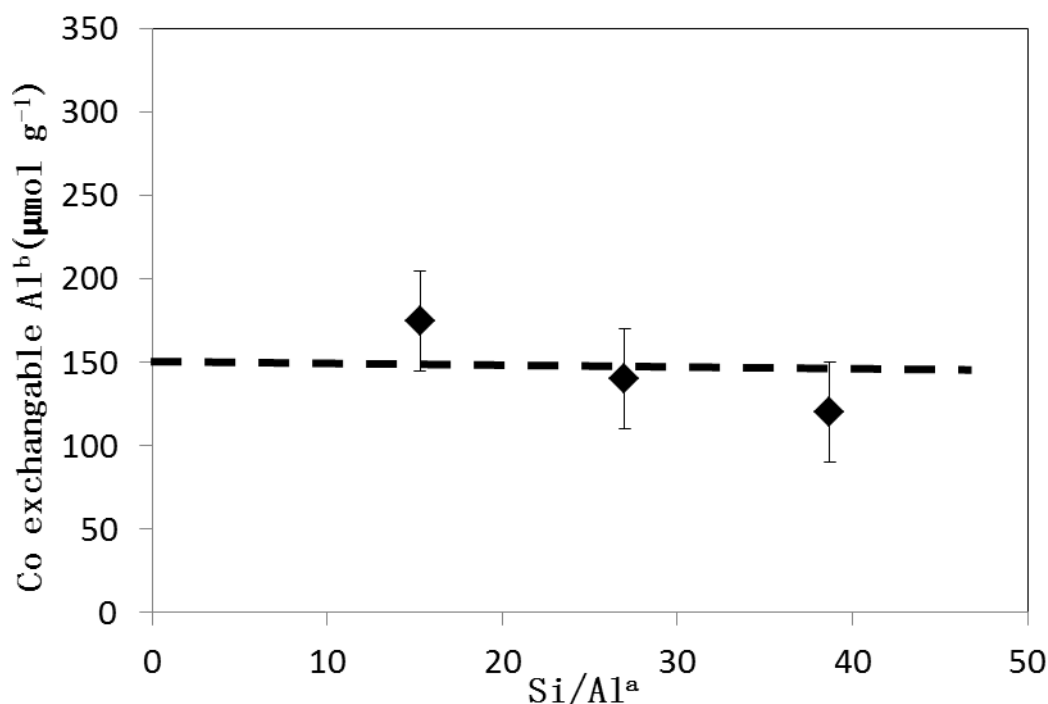
Figure 2-5 Co exchangeable Al concentration with variation of Si/Al ratios in the samples [a]Determined from AAS measurement. [b]Determined from AAS results of Co exchanged samples (methods from [52])

2.4 Conclusions

The rate of monomolecular cracking of C_3-C_6 paraffins on zeolites has been shown to depend strictly on the concentration of aluminum and in turn on the concentration of Brønsted acid sites, which all show identical acid strength. Only isolated Brønsted acid sites, however, are able to catalyze protolytic cleavage of C-C bonds in alkanes. The inability of neighboring Brønsted acid sites to catalyze alkane cracking is attributed to the destabilization of carbonium ion transition states by the second proton.

Cleavage of the C-C bonds closer to the center of the alkane molecules results in lower activation entropies and corresponding lower transition enthalpies than cleavage of the terminal bonds. This is related to a lower configuration space of the transition state, as well as to a more polarizable C-C bond compared to outer C-C bonds. For a given C-C bond, allowing the formation of two different product pairs, the route leading to the larger carbenium ion and, hence, the larger olefin is energetically favored, because the larger carbenium ion is able to better accommodate the positive charge. The results show that it is possible to understand individual reaction pathways in alkane cracking on the basis of the transition enthalpy and entropy. We have demonstrated here the relative importance of both thermodynamic quantities for the activity and selectivity of the zeolite-based catalyst. Understanding these kinetic details allows tailoring catalysts that show targeted activities and selectivities.

2.5 Appendix. Calculation of the partition function of transition state

For the calculation we used the harmonic approximation and assumed that absorbed and transition state species are rigid in space, therefore, only the vibrational contribution to the partition function has to be taken into account. Given a late carbonium-ion type transition state involved in the protolytic cracking, the vibrational quantities are equal to that of absorbed products. Here, we compare the partition function of transition states for the routes to $C_2H_4+C_3H_8$ and to $CH_4+C_4H_8$, for the latter one three different butene isomers are considered.

The vibrational partition function is given by the product of i-vibrational functions at different frequencies, by taking the zero point energies as reference:

$$q_{vib} = \prod_{i=1}^{f} \frac{e^{-\Theta_{vib,i}/2T}}{(1-e^{-\frac{\Theta_{vib,i}}{T}})} \equiv \prod_{i=1}^{f} \frac{1}{(1-e^{-\frac{\Theta_{vib,i}}{T}})} \tag{A1}$$

Where Θ_{vib} is defined by

$$\Theta_{vib} = \frac{h\nu}{k} \tag{A2}$$

and ν is the vibrational frequency in cm^{-1}.

Hence, based on the reported vibrational frequencies of different products [60, 61] the vibrational partition function at the reaction temperature can be obtained with respect to the transition states for the two routes, which are summarized in Table A1. It is shown that any of the values for the route to $CH_4+C_4H_8$ are much larger than that for the route to $C_2H_4+C_3H_8$, implying the more positive entropy change at the transition state for the former route. The findings are in good accordance with the trends from the experimental observations.

Table A1. Calculated value of vibrational partition function for cracking of n-pentane (T=777 K)

route	$CH_4+1-C_4H_8$	$CH_4+cis-2-C_4H_8$	$CH_4+trans-2-C_4H_8$	$C_2H_4+C_3H_8$
q_{vib}	688.7149	3201.044	1455.865	355.5254

2.6 References

1. Olah, G. A. *J. Am. Chem. SOC.* **1967**, *89,* 2227.

2. Olah, G. A. *J. Am. Chem. SOC.* **1977**, *99*, 4379.

3. Dejaife, P.; Vedrine, J. C.; Bollis, V.; Derouane, E. G. *J. Catal.* **1980**, *63***,** 331.

4. Dessau, R. M.; LaPierre, R. B. *J. Catal.* **1982**, *78,* 136.

5. Chang, C. D. *Catal. Rev.* Sci*. Eng.***1983***, 25*, 1.

6. Houriet, R.; Parisod, G.; Gaumann, T. *J. Am. Chem. Soc.* **1977**, *99*, 3599.

7. Riekert, L.; Zhou, J. *J. Catal.* **1992**, *137*, 437.

8. Zhao, Y.; Bamwenda, G. R.; Groten, W. A.; Wojciechowski, B. W. *J. Catal.* **1993**, *140*, 243.

9. Bhan, A.; Gounder, R.; Macht, J.; Iglesia, E. *J. Catal.* **2008**, *253*, 221.

10. Gounder, R.; Iglesia, E. *J. Am. Chem. Soc.* **2009**, *131*, 1958.

11. Gounder, R.; Iglesia, E. *Angew. Chem. Int. Ed.* **2010**, *49*, 808.

12. Gounder, R.; Iglesia, E. *Acc. Chem. Res.* **2012**, *45*, 229.

13. Lercher, J. A.; Van Santen, R. A.; Vinek, H. *Catal. Lett.* **1994**, *27*, 91.

14. Narbeshuber, T. F.; Vinek, H.; Lercher, J. A. *J. Catal.* **1995**, *157*, 388.

15. Xu, B.; Sievers, C.; Hong, S. B.; Prins, R.; van Bokhoven, J. A. *J. Catal.* **2006**, *244*, 163.

16. De Moor, B. A.; Reyniers, M. F.; Gobin, O. C.; Lercher, J. A.; Marin, G. B. *J. Phys. Chem. C.* **2011**, *115*, 1204.

17. Eder, F.; Lercher, J. A. *J. Phys. Chem. B.* **1997**, *101*, 1273.

18. Eder, F.; Lercher, J. A. *Zeolites.* **1997**, *18*, 75.

19. Eder, F.; Stockenhuber, M.; Lercher, J. A. *J. Phys. Chem. B.* **1997**, *101*, 5414.

20. Haag, W. O.; Dessau, R. M. *Proceedings of The Eighth International Congress On Catalysis*, **1984**, 305.

21. Krannila, H.; Haag, W. O.; Gates, B. C. *J. Catal.* **1992**, *135*, 115.

22. Kwak, B. S.; Sachtler, W. M. H. *J. Catal.* **1994**, *145*, 456.

23. Jentoft, F. C.; Gates, B. C. *Top. Catal.* **1997**, *4*, 1.

24. Cheung, T. -K.; Lange, F. C.; Gates, B. C. *J. Catal.* **1996**, *159*, 99.

25. Babitz, S. M.; Williams, B. A.; Miller, J. T.; Snurr, R. Q.; Haag, W. O.; Kung, H. H. *Appl. Catal. A.* **1999**, *179*, 71.

26. Kazansky, V. B.; Senchenya, I. N.; Frash, M.; Van Santen, R. A. *Catal. Lett.* **1994**, *27*, 345.

27. Olah, G. A.; Lukas, J. *J. Am. Chem. Soc.* **1967**, *89*, 4739.

28. Bandiera, J.; Ben Taarit, Y. *Appl. Catal.* **1990**, *62*, 309.

29. Kwak, B. S.; Sachtler, W. M. H.; Haag, W. O. *J. Catal.* **1994**, *149*, 465.

30. Haag, W. O. *Stud. Surf. Sci. Catal.* **1994**, *84*, 1375.

31. Kotrel, S.; Rosynek, M. P.; Lunsford, J. H. *J. Phys. Chem. B* **1999**, *103*, 818.

32. Ramachandran, C. E.; Williams, B. A.; Van Bokhoven, J. A.; Miller, J. T. *J. Catal.* **2005**, *233*, 100.

33. Van Bokhoven, J. A.; Williams, B. A.; Ji, W.; Koningsberger, D. C.; Kung, H. H.; Miller, J. T. *J. Catal.* **2004**, *224*, 50.

34. Xu, B.; Rotunno, F.; Bordiga, S.; Prins, R.; van Bokhoven, J. A. *J. Catal.* **2006**, *241*, 66.

35. Xu, B.; Bordiga, S.; Prins, R.; van Bokhoven, J. A. *Appl. Catal. A.* **2007**, *333*, 245.

36. Narbeshuber, T. F.; Brait, A.; Seshan, K.; Lercher, J. A. *J. Catal.* **1997**, *172*, 127.

37. Wang, X.; Carabineiro, H.; Lemos, M. A. N. D. A.; Ribiero, F. R. *J. Mol. Catal. A* **2004**, *216*, 131.

38. Bandiera, J.; Dufaux, M.; Ben Taarit, Y. *Appl. Catal. A.* **1997**, *148*, 283.

39. Madon, R. J.; Iglesia, E. *J. Mol. Catal. A* **2000**, *163*, 189.

40. Rigby, A. M.; Kramer, G. J.; van Santen, R. A. *J. Catal.* **1997**, *170*, 1.

41. Kazansky, V. B.; Frash, M. V.; van Santen R. A. *Appl. Catal. A.* **1996**, *146*, 225.

42. Zheng, X. B.; Blowers, P. *J. Phys. Chem. A.* **2005**, *109*, 10734.

43. Collins, S. J.; O'Malley, P. J. *J. Catal.* **1995**, *153*, 94.

44. Collins, S. J.; O'Malley, P. J. *Chem. Phys. Lett.* **1995**, *246*, 555.

45. Van Santen, R. A.; Kramer, G. J. *Chem. Rev.* **1995**, *95*, 637.

46. Blaszkowski, S. R.; van Santen, R. A. *Top. Catal.* **1997**, *4*, 145.

47. Collins, S. J.; O'Malley, P. J. *Top. Catal.* **1998**, *6*, 151.

48. Macht, J.; Carr, R. T.; Iglesia, E. *J. Catal.* **2009**, *264*, 54.

49. Polanyi, J. C. *Chem. Phys. Lett.* **1967**, *1*, 421.

50. Farneth, W. E.; Gorte, R. J. *Chem. Rev.* **1995**, *95*, 615.

51. Stepanov, A. G.; Sidelnikov, V.N.; Zamaraev, K. I. *Chem. Eur. J.* **1996**, *2*, 157.

52. Datka, J.; Boczar, M.; Rymarowicz, P. *J. Catal.* **1988**, *114*, 368.

53. Brand, H. V.; Curtiss, L. A.; Iton, L. E. *J. Phys. Chem.* **1993**, *97*, 12773.

54. Eichler, U.; Brandle, M.; Sauer, J. *J. Phys. Chem. B.* **1997**, *101*, 10035.

55. Sillar, K.; Burk, P. *J. Mol. Struct-Theochem.* **2002**, *589*, 281.

56. Hunter, K. C.; East, A. L. L. *J. Phys. Chem. A.* **2002**, *106*, 1346.

57. Nieminen, V.; Sierka, M.; Murzin, D. Y.; Sauer, J. *J. Catal.* **2005**, *231*, 393.

58. Swisher, J. A.; Hansen, N.; Maesen, T.; Keil, F. J.; Smit, B.; Bell, A. T. *J. Phys. Chem. C.* **2010**, *114*, 10229.

59. Dedecek, J.; Sklenak, S.; Li, C.; Wichterlova, B.; Gabova, V.; Brus, J.; Sierka, M.; Sauer, J. *J. Phys. Chem. C.* **2009**, *113*, 1447.

60. Shimanouchi, T. *Table of Molecular Vibrational Frequencies Consolidated Volume I*, **1972**, 1-160.

61. Schei, S. H. *Acta Chem. Scand. A.* **1984**, *38*, 377.

Chapter 3

Transition state consideration in protolytic cracking on steamed H-ZSM-5

The kinetic aspects of protolytic cracking of n-pentane at elevated temperature over H-ZSM-5, which were progressively dealuminated by steaming at 723 K for 1-20 h, were studied. The catalysts were characterized by different methods. ^{27}Al MAS NMR shows that increasing steaming duration leads to persistent loss in the framework Al with concomitant increase of extra-framework Al (EFAL). Additionally, infrared spectroscopic studies indicate an increase in Lewis acid sites with increasing EFAL at higher steaming duration. The measured cracking rates per active sites are promoted at the initial stage of steaming and decreased with steaming duration. Transition state theory is applied to assess the subtle variation in kinetic parameters of different cracking pathways. Changes in the catalytic activity are suggested to be predominantly controlled by the stabilities of transition state species involved. In general, the activation barrier for overall cracking decrease at the early stage of steaming and increase with the degree of dealumination. In lines with our previous findings cleavage of the terminal C-C bond is energetically less favored over cleavage of C-C bonds closer to the center of n-pentane on the parent material. The promotion effect of steaming on catalytic activity is speculated to be caused by the possible charge delocalization effects and corresponding stabilization of the transition state by the species with partially cleaved Al-O bonds, which were observed

from the characterization results. The elevated activation barrier with enhanced dealumination severity could be related to the formation of EFAL as Lewis acid site, which destabilizes the electron deficient cationic transition state.

.

3.1 Introduction

Mild dealumination of zeolites leads to enhancement in catalytic activity for a great number of acid-catalyzed reactions, such as paraffin cracking, isomerization and toluene disproportionation [1-5]. It has been demonstrated that the acid properties of resulting materials depend crucially on the methods being used. Mild steaming promotes more effectively catalytic activity, for example, for hydrocarbon cracking, than dealumination by chemical agents [6, 7].

Although a lot of work has been devoted to interpret the improvement of the catalytic activity by steaming, none of agreement has been reached by far. In general, the explanation for proved catalytic activity can be categorized into two views. One emphasizes the changes in the acidity of zeolites, while another concerns transportation and interaction of reactants within zeolitic channel. In terms of acidity model, for instance, many authors claim that the acid strength is increased by extra-framework Al (EFAL) via withdrawing the electron density of bridging oxide ion of Brønsted acid sites in the vicinity [7-9]. However, ^{1}H NMR [10] and infrared spectroscopic studies [10, 11] have failed in evidencing the increased Brønsted acid strength. Furthermore, some suggests that EFAL as Lewis acid sites could favor hydride transfer, in the case of paraffin cracking, which may increase the rate of olefin formation and consequently the overall cracking rate [12]. Nevertheless, some authors have pointed out the changes in acid strength induced by steaming is not significant to effect the catalytic activity. For example, van Bokhoven et al. propose the catalytic enhancement is due to the increased initial heat of adsorption and correspondingly higher surface coverage of reactants [13]. Another proposal demonstrates the hydrothermal treatment results in the formation of mesopores with larger external surface area, which reduce the diffusion limitation of bulky reactants [14, 15].

Recently, we have used transition state theory and Born-Haber thermochemical cycles to describe the contribution of activation enthalpy and entropy to reaction

selectivity in different pathways of protolytic cracking [16]. This approach allows us to sense the impact of zeolitic environment on the subtle changes in transition state entropy and enthalpy. It is shown that the stability of transition states involved are rigorously related to the proton affinity and the stabilization energy of the ion-pair formed at the transition state. Moreover, Gouder and Iglesia [17] report the strong influence of local structure of zeolites on the catalytic activity of monomolecular conversion of alkanes. Both findings show the crucial role of channel environments for the stability of transition states, which is in turn reflected in the activity for the acid catalyzed reaction.

In an attempt to address the questions we chose here *n*-pentane cracking as a specific reaction to probe H-ZSM-5 sample, where framework Al concentration was finely tuned by mild steaming to varying dealumination severity. Consequent changes in activation enthalpy and entropy for the individual cracking pathways reflect the role of dealumination in the stabilization of ion pairs formed in the acid-catalyzed monomolecular alkane conversions. Combining with Infrared spectroscopy and ^{27}Al MAS NMR we present the evidences for appearance of new species by steaming, with the catalytic consequences for the monomolecular conversion of *n*-pentane. The study illustrates the strong influence of transition state stability on activation barrier and reaction rate, which is essentially determined by the specific charge transfer within zeolitic lattice. Therefore, this approach should in turn allow us to probe the intrachannel environment and, predict the contributions from subtle changes in the channel geometry to tailor catalysts.

3.2 Methods

3.2.1 Catalysts preparation by steaming treatment

H-ZSM-5 zeolite (süd-chemie; Si/Al = 45; pellet size: 355 to 500 µm) was heated to 723 K with a heating ramp of 1 K min^{-1} under nitrogen flow in a quartz tube. Water was then pumped into the tube by a HPLC pump (Gilson 307) with a constant flow of 0.33 mol h^{-1} at 723 K. The duration of steaming varied from 1 h to 20 h to obtain different dealumination degrees.

3.2.2 Powder X-Ray diffraction (XRD)

The X-ray powder diffraction patterns of powder were measured using a Philips X'Pert Pro System operating with a Cu Kα1-radiation (0.154056 nm) at 40 kV / 40 mA. Measurements were performed on a spinner with a 1/4'' slit from 5° to 70° 2θ (0.00083°s^{-1}).

3.2.3 Infrared spectroscopy of adsorbed pyridine

IR spectra of self-supporting wafers (density 13-25 mg cm^{-2}) were collected using a Perkin Elmer 2000 spectrometer. All spectra were recorded in the region between 4000 and 800 cm^{-1} at a resolution of 2 cm^{-1}. After activation in vacuum (< 10^{-9} bar) for 1 h at 723 K (ramp in 1 K min^{-1}), the sample was cooled to 423 K and pyridine was adsorbed in small dosages until full saturation of the bridging OH group at 3606 cm^{-1} was observed. The system was then equilibrated for 0.5 h. All IR spectra were recorded at 423 K before adsorption of pyridine, during the adsorption of pyridine, and after outgassing (10^{-9} bar) at temperature of 523 K, 623 K and 723 K (holding at the maximum temperature for 0.5 h). The concentration of Brønsted and Lewis acid sites was estimated from the areas of the bands at 1565 – 1515 cm^{-1} and 1470 – 1435 cm^{-1} using the molar absorption coefficients of the bands of adsorbed pyridine, set equal to those determined for zeolites [18].

3.2.4 ^{27}Al MAS NMR

^{27}Al MAS NMR spectroscopic measurements of the zeolites were carried out using a Bruker Avance AMX-500 NMR-spectrometer with a magnetic field of 11.75 T. The samples were hydrated for at least 48 h in the atmosphere before measurements. The reference for the measurements was $Al(NO_3)_3 \cdot 9\ H_2O$ (δ = -0.543 ppm). The samples were packed in 4 mm ZrO_2 rotors and spun at 12 kHz. An excitation pulse with power level of 7 dB and a length of 0.6 μs was applied for NMR spectrum. The relaxation time was 250 ms, 2400 scans were recorded.

3.2.5 Kinetic measurement of *n*-pentane activation

Kinetic measurements of steady-state alkane cracking and dehydrogenation were performed in a tubular quartz reactor with 6 mm inner diameter under differential conditions (< 2% conversion). Catalyst samples (0.002-0.02g, 150-250 μm) were supported on a quartz frit and diluted by inert quartz pellets (180-250 μm). The temperature of the furnace was adjusted by temperature controller with 18 segment programs (Eurotherm Series 2014). Temperature of catalyst bed was monitored by a thermocouple mounted at the external surface of the quartz reactor.

Catalysts were activated in a mixture of 5 % O_2 in He flow (0.5 ml s^{-1}) at 803 K (with 1 K min^{-1}) for 2 h and then treated in a pure He flow before kinetic measurements. *n*-Pentane (≥ 99.0%) are supplied by Sigma-Aldrich. The partial pressure of *n*-pentane was adjusted around 0.03 bar by controlling He flow through the saturator in a cooling system (LAUDA RC 20). The gas mixture then passed through a trap loaded with activated H-Y zeolite (20 g) to maintain olefin concentration below the GC detection limit (i.e. <1 ppm). Reactants and products were analyzed by a gas chromatograph (Agilent HP-5890) using Al_2O_3-KCl capillary column (50 m × 0.32mm × 0.53mm; Agilent) connected to a flame ionization detector (FID). The absence of bimolecular pathways was verified by the absence of hydrocarbons larger than *n*-pentane. Kinetic data was

based on alkane molecules (*i.e.* methane, ethane and propane) as primary cracking products in order to evade impact of the secondary cracking of formed olefins. Activation energy and corresponding pre-exponential factors were determined from reaction rate measurement as a function of temperature (728-778 K). Transport limitation in the kinetic measurement was excluded by using Mears criteria.

3.3 Results

3.3.1 Catalysts characterization

Mild steaming does not change the integrity of crystallinity of the resulting zeolites. As shown in Figure 3-1, the X-ray diffraction (XRD) patterns of samples with different steaming duration are identical. The crystal structure of zeolites kept intact after steaming treatment.
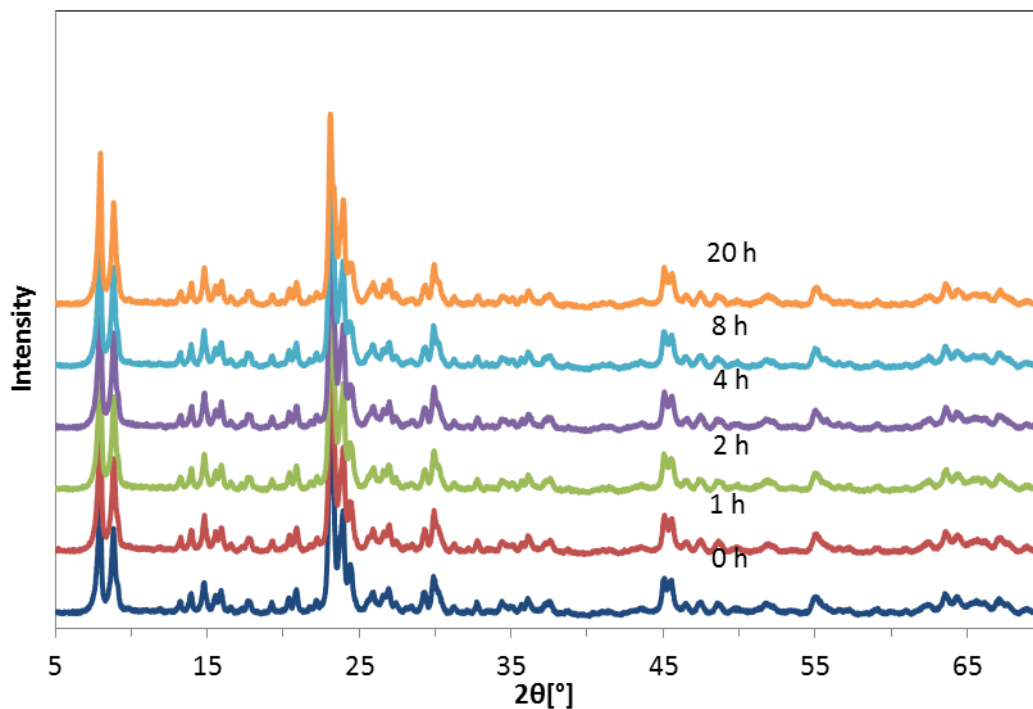
Figure 3-1 XRD patterns of H-ZSM-5 samples with different steaming durations. 0 h is for parent material

^{27}Al solid state MAS NMR spectroscopy was applied to examine the coordination state of Al species in the steaming-treated samples (Figure 3-2). The spectra show only one pronounced peak centered at a chemical shift of 54 ppm in the parent material, indicating all Al species are tetrahedrally coordinated. Nevertheless, a broad peak centered at ~0 ppm (octahedrally coordinated Al) becomes visible upon steaming and increases with steaming duration, while the peak at ~54 ppm decreases. The changes indicate some tetrahedral coordinated Al species transform stepwise into the octahedral coordination. Since the octahedrally coordinated Al atoms are usually present as EFAL [19, 20], we concluded that steaming treatment expels some tetrahedral Al out of the framework. With steaming duration a small broad peak at ~40 ppm is observed, which is attributed to in the distorted environment present (i) tetrahedral framework Al [21-23]; (ii) penta-coordinated [24-29], (iii) nonframework tetrahedral Al species [29-32] . The broadening of this peak could be owing to the significant quadrupolar interaction between those Al atoms upon steaming treatment. The additional broad signal at ~40 ppm indicates the tetrahedral framework Al can convert into tetrahedral or octahedral nonframework Al species via penta-coordinated hydrated Al species and partially attached Al with framework oxygen, which we will discuss more in detail in the following.
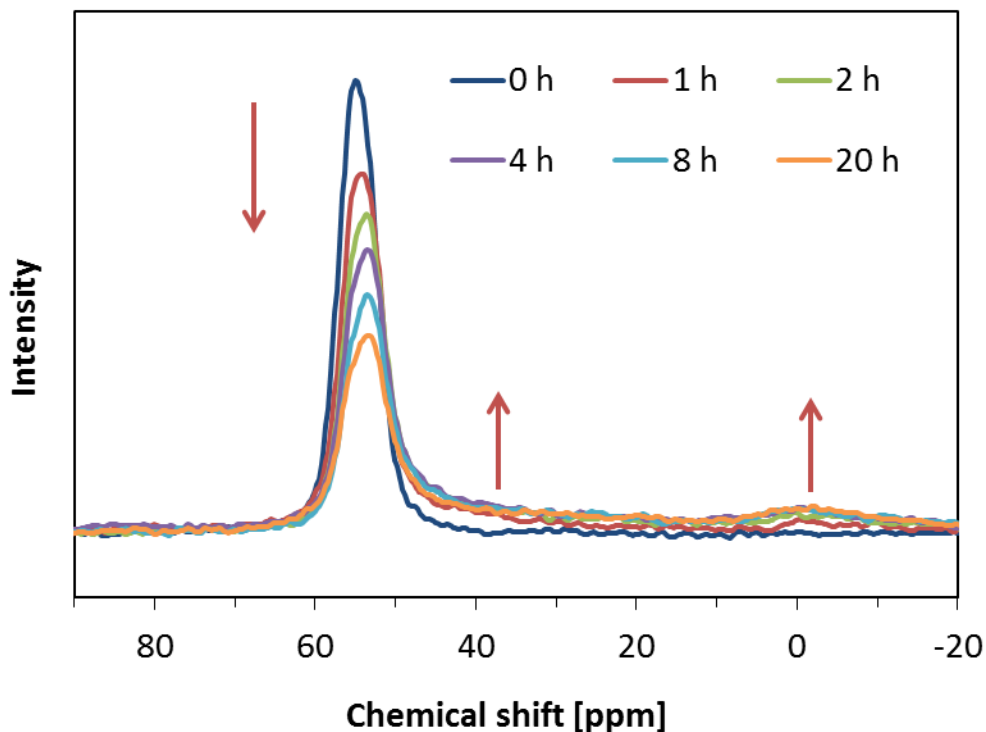
Figure 3-2 ^{27}Al MAS NMR spectra of H-ZSM-5 with different steaming duration

Numbers of Brønsted and Lewis acid sites in the steamed H-ZSM-5 samples were determined by IR spectroscopy of adsorbed pyridine (Figure 3-3). It is clear that Brønsted acid sites decreased dramatically at the first 10 h of steaming and the change became much equable with further treatment, indicating the loss of bridging hydroxyl group in the framework Al at the earlier stage of steaming. Comparatively, the Lewis acid sites increased to a certain extent upon steaming treatment. This trend was in agreement with the increase of octahedrally coordinated Al species at ∼0 ppm (Figure 3-2). Therefore, Lewis acidity is created upon dealumination in steaming due to the appearance of EFAL [33-35].
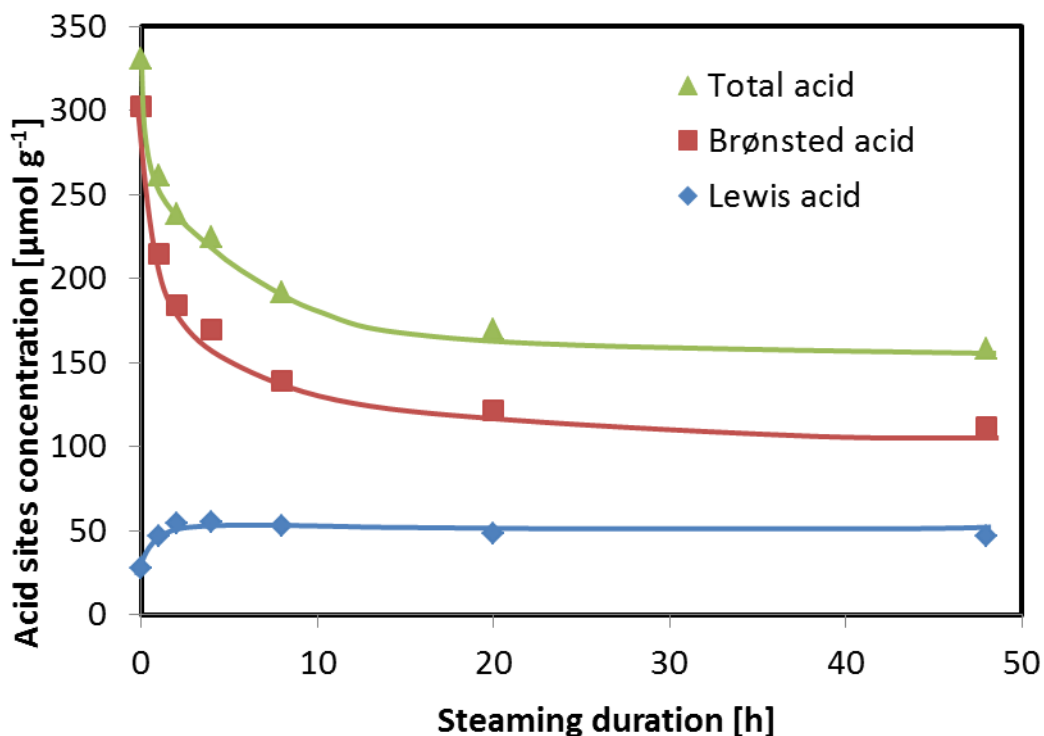
Figure 3-3 Acid sites concentration of H-ZSM-5 samples with different duration by Pyridine IR (outgassed at 423 K)

Infrared spectra of the parent H-ZSM-5 and dealuminated H-ZSM-5 with varying steaming duration are shown in Figure 3-4 for the hydroxyl region. All of the samples exhibit two major bands at 3742 cm^{-1} and 3605 cm^{-1}, assigned to OH stretching vibrations of terminal silanol group (Si-OH) and bridging hydroxyl groups (Si-OH-Al) in the lattice, respectively. The latter one accounts for the strong Brønsted acidity in H-form zeolites. Therefore, the intensity of the 3605 cm^{-1} band significantly decreased at the beginning of steaming, in line with the decrease in the number of Brønsted acid sites measured by pyridine adsorption (Figure 3-3). Upon steaming a slight shift to a higher wave number was observed, implying unequal contributions of Brønsted acid sites at different Al sitting in the zeolite framework [37]. The Al species at the higher wave number seems to be easier removed from the framework. A broad absorption band in the range of 3200-3500 cm^{-1} was observed in the steamed samples, which could be

assigned to the internal Si-OH groups owning to defect of the lattice [37, 38]. Several bands between 3630 and 3720 cm^{-1} become clearly visible after steaming. The band at 3665 cm^{-1} could be attributed to the extra lattice Al ions in an octahedral coordination [39]. In addition, a small band at 3700 cm^{-1} appeared in the steamed sample for 1 and 2 h and then disappeared with further steaming duration. Although the attribution of bands is still a matter of disputation in the literature, many authors assigned it to the OH group at the Al ions partially attached to the lattice [37, 39-40]. These loosely bound Al species could also be responsible for the broad band at ~40 ppm from ^{27}Al MAS NMR spectroscopy arising at the initial stage of steaming (Figure 3-2.)
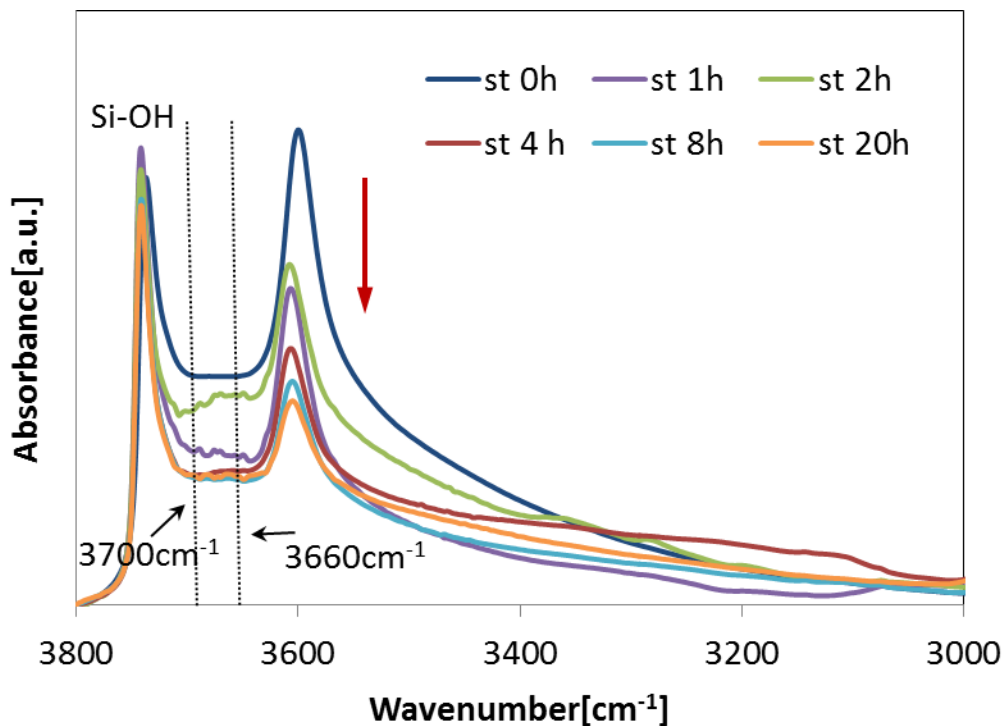
Figure 3-4 IR spectra of H-ZSM-5 samples with different steaming duration

3.3.2 Kinetic measurement

Applying Brønsted acidity of the samples quantified from the infrared spectroscopy of adsorbed pyridine we are able to compare catalytic activity of the H-ZSM-5 zeolites with varying dealumination severity. Figure 3-5 shows the rate constants of *n*-pentane cracking (777 K) as a function of steaming duration for the parent and steamed samples. The activity of steamed H-ZSM-5 first increases and then decreases with steaming duration, reaching a maximum for the sample steamed to 2 h, which is 30 % higher than activity of the parent sample.

Since the rate constants are strictly normalized to concentration of the Brønsted acid sites (Figure 3-3), the trend in the plot strictly describes changes in the intrinsic catalytic properties of the active sites upon mild steaming of the parent materials. As reported in the previous studies, contributions of activation enthalpy and entropy can be defined by the transition state theory, thus, bridging reaction activity and the local catalytic environment for solid acid catalyzed reaction in zeolites [16, 17]. In the context, we will discuss how catalytic activities are critically related to the changes in local structure via the assessment of kinetic parameters for monomolecular cracking of *n*-pentane based on the transition state theory.
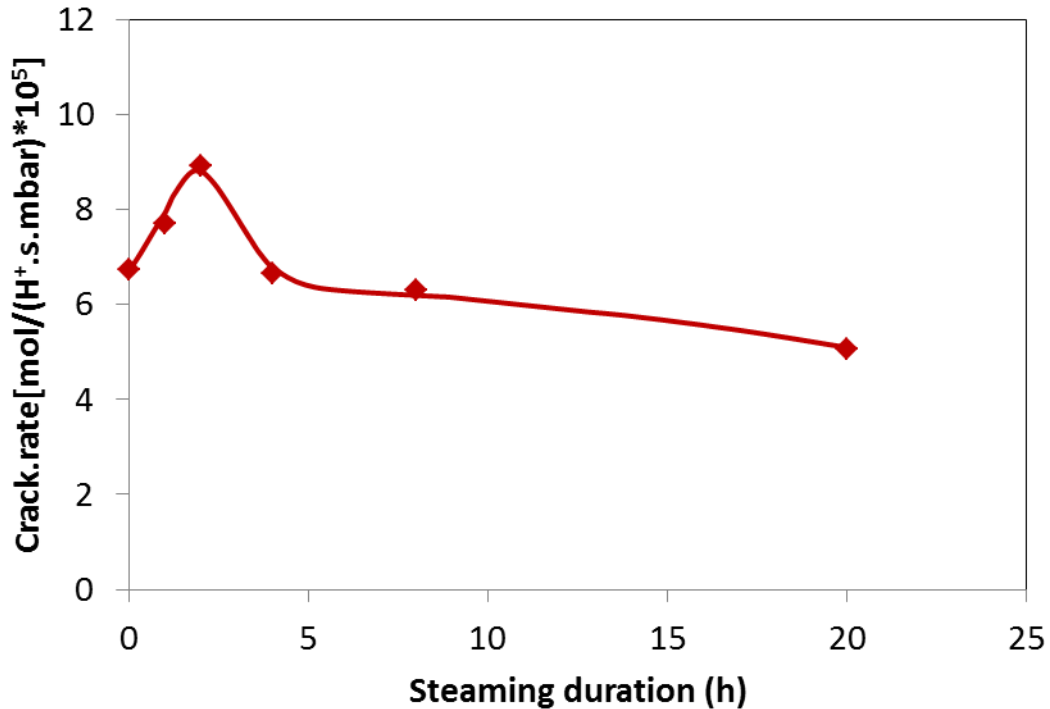
Figure 3-5 Catalytic Activity of H-ZSM-5 with different Steaming Duration in *n*-Pentane Cracking

3.4 Discussions

3.4.1 Transition state consideration of monomolecular *n*-pentane activation

Due to the specific topology of zeolite structure, molecules can be confined within zeolitic channels, which present a thermodynamically non-ideal environment. The confinement effects of zeolitic channels therefore resemble the solvation of catalytic complexes in the homogenous system, in which ligands react with the catalysts via chemical interactions [41, 42]. In the case of monomolecular cracking, alkane adsorb on the Brønsted acid sites (H^+Z^-), which keep in quasi-equilibrium with fluid phase A(g). By

monomolecular rearrangement the adsorbed alkane molecules transform into transition state species (†), which eventually leads to formation of cracking products (P) (Scheme 3-1).

1. $A(g) \leftrightarrow A(z)$

2. $A(z) + H^+Z^- \leftrightarrow \dagger \rightarrow P$
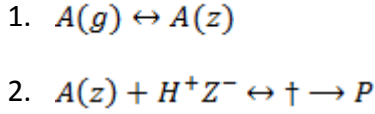
Scheme 3-1. Reaction scenario for protolytic cracking of alkane activated by Brønsted acids (H^+Z^-) of zeolites

Using transition state theory for thermodynamically non-ideal systems, typically for monomolecular cracking of alkanes in zeolites, as discussed in great detail elsewhere [16, 17], rate formulism becomes proportional to the concentration of adsorbed alkanes within zeolite channel (C_{Az}):

$$r = \frac{k_B T}{h} \exp\left(\frac{\Delta S^{\circ\dagger}}{R_g}\right) \times \exp\left(\frac{-\Delta H^{\circ\dagger}}{R_g T}\right) C_{Az} \tag{3-1}$$

Under reaction conditions adsorption of alkanes onto Brønsted acid sites rigorously follows Langmuir model, therefore, the concentrations of adsorbed alkanes (C_{AZ}) are proportional to partial pressure in the gas phase (P_A) and the adsorption constants (K_A):

$$r = k_{int} K_A P_A \tag{3-2}$$

With:

$$k_{int} = \frac{k_B T}{h} \exp\left(\frac{\Delta S^{\circ\dagger}}{R_g}\right) \times \exp\left(\frac{-\Delta H^{\circ\dagger}}{R_g T}\right) = A_{int} e^{(-\Delta H^{\circ\dagger}/R_g T)} \tag{3-3}$$

Temperature dependence of the equilibrium constant (K_A) is given by:

$$K = e^{-\Delta G_{ads}/RT} = e^{(-\Delta H_{ads}/RT)} e^{(\Delta S_{ads}/R)} \tag{3-4}$$

Combining equations (3-2), (3-3) and (3-4) the measured activation energy (E_{meas}) and pre-exponential factors (A_{meas}) are obtained:

$$E_{meas} = E_{int} + \Delta H_{ads} = \Delta H^{\circ\dagger} + \Delta H_{ads} \tag{3-5}$$

$$\ln(A_{meas}) = \ln(A_{int}) + (\Delta S_{ads}/R) \qquad (3\text{-}6)$$

$$\Delta S_{meas} = \Delta S_{int} + \Delta S_{ads} = \Delta S^{o\dagger} + \Delta S_{ads} \qquad (3\text{-}7)$$

Here, ΔH_{ads} is the adsorption enthalpy, which can be experimentally determined, from the temperature dependence of the Henry coefficients [43, 44], calorimetry [45, 46] etc. The adsorption enthalpy is a rigorous descriptor for van der Waals stabilization interaction of alkanes with framework oxygen, i.e. stronger interaction leads to more negative adsorption enthalpies [45-47]. In contrast, adsorption entropy ΔS_{ads} is not experimentally measured but indirectly calculated from the Henry coefficient [43, 44] or from the Langmuir equilibrium coefficient [45-46, 48], which reflects the confinement effect of adsorbed species within zeolite channels.

Table 3-1 Measured activation energies for monomolecular cracking and dehydrogenation of *n*-pentane over steamed H-ZSM-5

Steaming Duration (h)	0	0,25	0,5	1	2	4	8	20
Ea$_{app}$crack.^{a} (kJ mol^{-1})	133	125	127	126	133	135	136	143
Ea$_{app}$DH^{b} (kJ mol^{-1})	98	107	96	90	83	88	78	84

^{a} Errors are ± 2 kJ mol^{-1}. ^{b} Errors are ± 5 kJ mol^{-1}.

The measured activation energies for monomolecular *n*-pentane cracking and dehydrogenation over H-ZSM-5 samples with varying steaming duration are shown in Table 3-1. Activation energies for cracking decreases at the initial stage of steaming and then increases gradually with further duration, with even a higher value for sample steamed to 20 h over that for the parent material. Furthermore, changes in measured activation energies for cracking are on the contrary with the trend of rate constant, implying that activation barrier could play a vital role for the variations in catalytic activity by steaming. However, the measured activation energies for monomolecular

dehydrogenation scatter for the samples with different steaming duration, which is consistent with previous reports for dehydrogenation energies that vary largely for propane among various different H-ZSM-5 studies [49-53].

Table 3-2. Comparison of kinetic parameters for individual cracking pathways in monomolecular *n*-pentane conversion over steamed H-ZSM-5

Steaming Duration (h)	0	0,25	0,5	1	2	4	8	20
$Ea_{app}(C_1+C_4^=)^a$ $(kJ\,mol^{-1})$	146	134	137	136	145	146	147	157
$Ea_{app}(C_2+C_3^=)^b$ $(kJ\,mol^{-1})$	128	121	122	122	129	131	132	138
$Ea_{app}(C_3+C_2^=)^c$ $(kJ\,mol^{-1})$	130	126	127	126	128	130	129	125
Delta $S_{int}(C_1+C_4^=)^d$ $(J\,mol^{-1}K^{-1})$	15	6	10	8	17	22	5	17
Delta $S_{int}(C_2+C_3^=)^e$ $(J\,mol^{-1}K^{-1})$	0	-5	-4	-6	2	7	-4	3
Delta $S_{int}(C_3+C_2^=)^f$ $(J\,mol^{-1}K^{-1})$	-7	-10	-9	-12	-12	-5	-16	-29

[a] Errors are ± 2 kJ mol^{-1}. [b] Errors are ± 1 kJ mol^{-1}. [c] Errors are ± 2 kJ mol^{-1} [d] Errors are ± 4 J mol^{-1}K^{-1}. [e] Errors are ± 2 J mol^{-1} K^{-1}. [f] Errors are ± 3 J mol^{-1}K^{-1}.

To probe how the variations in local catalytic environments of the different steamed samples could critically influence the transition state entropies and enthalpies on protolytic cracking, we determined activation energies and calculated intrinsic activation entropies for the individual cracking routes of *n*-pentane (Table. 3-2).

In line with our recent findings, on the parent materials cleavage of the C-C bonds closer to the center is energetically more favored over cleavage of the terminal bonds, while the activation entropy decreases with degree of symmetry of the transition state species [16]. The results implies that the carbonium ion as transition state in protolytic cracking resembles the products formed, therefore, the stability of transition state is

closely related to the nearly formed carbenium ion like species upon cleavage of C-C bonds. In this context, comparing these kinetic parameters for the different cracking pathways provides an opportunity to sense the subtle changes of transition state species due to the local structure of catalysts. It is shown, measured activation barriers for the route to CH_4 + C_4H_8, C_2H_6 + C_3H_6 decrease first and then increase with steaming duration, while activation energies are least influenced for the route to C_3H_8 + C_2H_4.

Next, we use the Born-Haber thermochemical cycle to qualitatively interpret the individual contribution of the thermodynamic factors to the reaction energy, which is determined by the acid properties and ion-pair stabilization at transition state [16, 17, 54-57]. Upon protonation of the adsorbed reactants, the formed cationic transition states in protolytic cracking are stabilized by Brønsted acid sites via electrostatic interactions. In a Born-Haber cycle, measured activation barrier (E_{meas}) is directly related to deprotonation energy of the zeolites (E_{dep}), gas phase proton affinity of the reactant (PA) and stabilization energy of the ion-pair (E_{stab}):

$$E_{meas} = E_{dep} - PA + E_{stab} \tag{4-8}$$

$$E_{int} = E_{dep} - PA + E_{stab} - \Delta H_{ads} \tag{4-9}$$

Deprotonation energy (E_{dep}) is a probe-independent value, reflecting energy requirement to separate a proton form the zeolite cluster to non-interacting distances. Thus, the magnitude of E_{dep} is a rigorous descriptor for Brønsted acid strength [47, 48]. Lack of evidence for the enhancement in Brønsted acidity upon steaming [10, 11], we surmise that the changes in E_{dep} are not significant by the treatment. Proton affinities (PA) define the energy difference by protonating a neutral molecule in the gas phase. Theoretical estimation indicates PA decreases monotonically from the central C-C bonds to the terminal C-C bonds for a given alkane [49]. As a result, PA value of C-C bonds for a given cracking route keeps invariable by steaming. Ion-pair stabilization energy (E_{stab}) depends strictly on the interaction energy of the transition state, mainly induced by the electrostatic stabilization with the relevant conjugate base of the framework cluster [57].

To which extent the ion pairs at the transition state are stabilized by the zeolite framework are not only related to the ion-pair formed but also to the channel size and structure [61-63]. For mildly steamed samples any variations in E_{stab} are driven by the change of local catalytic environment in the zeolitic framework. In contrast, adsorption enthalpies (ΔH_{ads}) of alkanes reflect primarily van der Waals interactions between absorbed reactants and framework oxygen [45-47]. Here, we assume that mild steaming dealumination can hardly influence ΔH_{ads} value for: (1) the measured activation barriers within different cracking pathways are not equally changed on the steamed zeolites to different severity of dealumination, especially for the path to C_3H_8 + C_2H_4, one observed least changes (5 kJ mol^{-1}) in the measured activation energy; (2) the initial ΔH_{ads} of propane adsorbed on the steamed samples exhibits almost a constant value (38-39 kJ mol^{-1}). Moreover, activation entropies for the individual cracking routes, reflecting the confinement effects of transition states within zeolitic channel, are weakly affected (Table 2). Hence, we conclude that the enhanced activity due to mild steaming predominately depends on the stabilization effect of local environment, reflected in the term of E_{stab} in equation (4-9). Combining with the experimental observations in infrared studies and ^{27}Al MAS NMR, we conclude that some new species arising at the initial steaming stage are responsible for the changes in E_{stab}.

3.4.2 Catalytic implication of local structure in steamed H-ZSM-5
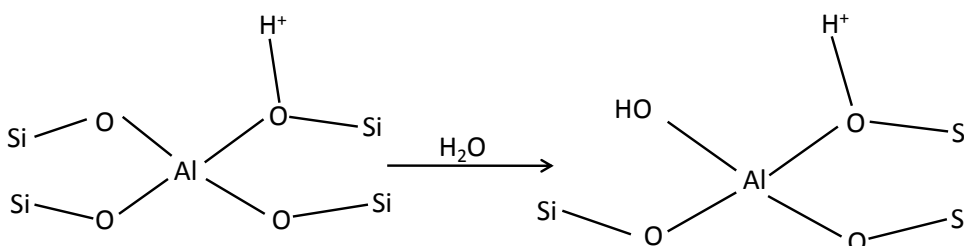
Scheme 3-1 Partially hydroxylation of framework Al during steaming adapted from ref. [51]

At the initial stage of steaming dealumination caused by the procedure is negligible, At the initial stage of steaming, we observed a small band at 3700 cm^{-1} in the infrared spectroscopy for the steamed sample of 1 and 2 h, which can be attributed to Al ions partially attached in the framework [39], and the broad signal at ~40 ppm, most likely also assigned to the loosely bound Al species as we have discussed above. For example, Al-OH group can replace Si-O-Al in the framework by partially hydroxylation, leading to a defect site with OH group exposing to the zeolite channel (Scheme 3-1). It is well known that the negative charge of zeolites is delocalized over the entire framework oxygen ions by so-called solvation effect of zeolitic channel [65]. Correspondingly, the charge of cationic transition states or intermediates such as hydrocarbons can be redistributed and stabilized via interactions with framework oxygen in the vicinal position. Therefore, the stability of the transition state is sensitively related to the local structure around the species adsorbed at Al sites [66]. Given such a defect site (Scheme 3-1) in the proximity of cationic transition state species, the positive charge is redistributed over the defect site. The higher polarity of OH group over that of the original Si-O-Al may alleviate electron deficiency of carbocationic transition state, resulting in stabilization of these species.
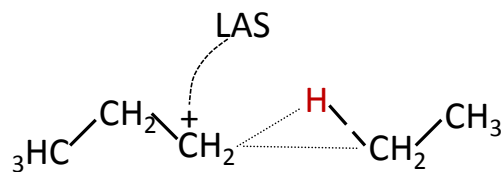
Scheme 3-2 Transition state species of protolytic pentane cracking in pathway of ethane and propylene

With the increase of steaming duration, the partially hydrolyzed framework Al ions are eventually expelled from the framework, which are normally regarded as Lewis acid sites, as observed in the infrared studies (Figure 3-3). For the late transition state of protolytic cracking, carbenium like species (the part forming the olefin) are nearly formed. And stabilization energies of ion-pair in the zeolite are largely related to the

relative stability of these nearly formed carbenium like species [16]. On the premise that a Lewis site within the lattice is in the vicinity of transition state species, the positive charge can be delocalized, in part, destabilized by the electron-deficient Lewis acid sites. However, the measured activation barrier for the route to $C_3H_8 + C_2H_4$ is least influenced by more severe steam dealumination (Table 3-2). Therefore, we conclude that energy barriers to form the transition state species are leveled via the inductive effect of Lewis acid sites according to the relative stabilities butylium > propylium > ethylium.

3.5 Conclusions

With increasing steaming duration under constant partial pressure of steam at 723 K, mild steaming leads to the persistent loss of Brønsted acidity of H-ZSM-5 zeolites with concurrent increase in the number of EFAL. Accordingly, concentration of Lewis acid sites increase according to the infrared spectroscopy of adsorbed pyridine. Turnover rate per H^+ site of *n*-pentane cracking strongly depends on the dealumination severity of the samples. Cracking activity is initially promoted and then goes through a maximum, which is 30 % higher than that of the parent material. Further dealumination results in a gradual loss of catalytic activity.

The changes in cracking activity are predominantly controlled by the activation barrier, which is in turn reflected in the stabilization energy of the ion-pair formed in the transition state based on Born-Haber thermochemical cycles. Activation enthalpies for protolytic cracking decrease first and then increase with steaming duration. However, the barrier for path to $C_3H_8 + C_2H_4$ is relatively insensitive to the treatment. The differences for individual cracking pathways indicate the strong dependence of activation enthalpies on the local catalytic environment of transition state. The positive charge of cationic transition state is delocalized by framework and thus strongly influenced by the local variation in zeolite structure. Partially hydrolyzed Al species in the vicinity increase the negative charge density of local Al sites, leading to more

stabilized transition state. Nevertheless, electron deficiency of Lewis acid sites results in destabilization effect of the vicinal transition state species. The findings in this contribution show the strong impact of local structure of zeolites on the reactivities of acid catalysis, providing more fundamental understanding of catalytic details via the transition state theory. The approach opens not only the opportunity to predict the catalytic consequence of zeolite, but also allows us to select and tailor the catalysts with targeted activities and selectivities.

3.6 References

1. Beaumont, R. *J. Catal.* **1973**, *30*, 288.

2. DeCanio, S. J.; Sohn, J. R.; Fritz, P. O.; Lunsford, J. H. *J. Catal.* **1986**, *101*, 132.

3. Sohn, J. R.; DeCanio, S. J.; Fritz, P. O.; Lunsford, J. H. *J. Phys. Chem.* **1986**, *90*, 4847.

4. Denayer, J. F.; Baron, G. V.; Souverijns, W.; Martens, J. A.; Jacobs, P. A. *Ind. Eng. Chem. Res.* **1997**, *3242*, 36.

5. Segawa, K.; Shimura, T. *Appl. Catal. A.* **2000**, *194*, 309.

6. Beyerlkein, R. A.; McVicker, G. B.; Yacullo, L. N.; Zemiak, J. J. *J. Phys. Chem.* **1988**, *92*, 1967.

7. Lonyi, F.; Lunsford, J. H. *J. Catal.* **1992**, *136*, 566.

8. Lukyanov, D. B. *Zeolites.* **1991**, *11*, 325.

9. Fritz, P. O.; Lunsford, J. H. *J. Catal.* **1989**, *118*, 85.

10. Brunner, E.; Ernst, H.; Freude, D.; Hunger, M.; Krause, C. B.; Prager, D.; Reschetilowski, W.; Schwieger, W.; Bergk, K. H. *Zeolites* **1989**, *282*, 9.

11. Topsoe, N. Y.; Joensen, F.; Derouane, E. G. *J. Catal.* **1988**, *404*, 110.

12. Chen, F. R.; Fripiat, J. J. *J. Phys. Chem.* **1993**, 97, 5796.

13. Van Bokhoven, J. A.; Tromp, M.; Koningsberger, D. C.; Miller, J. T.; Pieterse, J. A. Z. *J. Catal.* **2001**, *202*, 129.

14. Lynch, J.; Raatz, F.; Dufresne, P. *Zeolites* **1987**, *33*, 7.

15. Kung, H. H.; Williams, B. A.; Babitz, S. M.; Miller, J. T.; Haag, W. O.; Snurr, R. Q. *Top. Catal.* **2000**, *10*, 59.

16. Lin, L.; Ember, E.; Lercher, J. A. submitted, **2012**.

17. Gounder, R.; Iglesia, E. *J. Am. Chem. Soc.* **2009**, *131*, 1958.

18. Emeis, C. A. *J. Catal.* **1993**, *141*, 347.

19. Sanz, J.; Fornes, V.; Corma, A. *J. Chem. Soc. Faraday Trans.* **1988**, *84*, 1988.

20. Van Bokhoven, J. A.; Roest, A. L.; Koningsberger, D. C.; Miller, J. T.; Nachtegaal, G. H.; Kentgens, A. P. M. *J. Phys. Chem. B* **2000**, *104*, 6743.

21. Freude, D.; Brunner, E.; Pfeifer, H.; Prager, D.; Jerschkewitz, H.-G.; Lohse, U.; Oehlmann, G. *Chem. Phys. Lett.* **1987**, *139*, 325.

22. Koningsberger, D. C.; Miller, J. T. *Studies in Surface Science and Catalysis;* Elsevier Science BV: New York, **1996**; Vol. 101, p 841.

23. Yan, Z.; Ma, D.; Zhuang, J.; Liu, X.; Liu, X.; Han, X.; Bao, X.; Chang, F.; Xu, L.; Liu, Z. *J. Mol. Catal. A* **2003**, *194*, 153.

24. Triantafillidis, C. S.; Vlessidis, A. G.; Nalbandian, L.; Evmiridis, N. P. *Microporous Mesoporous Mater.* **2001**, *47*, 369.

25. Engelhardt, G.; Michel, D. *High-Resolution Solid-State NMR of Silicates and Zeolites;* Wiley: New York, **1987**; Chapter V.3.4.

26. Rocha, J.; Klinowski, J. *J. Chem. Soc., Chem. Commun.* **1991**, 1121.

27. Yang, X.; Truitt, R. E. *Zeolites* **1996**, *16*, 249.

28. Chen, T. H.; Wouters, B. H.; Grobet, P. J. *Eur. J. Inorg. Chem.* **2000**, *2*, 281.

29. Zhuang, J.; Ma, D.; Yang, G.; Yan, Y.; Liu, X.; Liu, X.; Han, X.; Bao, X.; Xie, P.; Liu, Z. *J. Catal.* **2004**, *228*, 234.

30. Menezes, S. M. C.; Camorim, V. L.; Lam, Y. L.; San Gil, R. A. S.; Bailly, A.; Amoureux, J. P. *Appl. Catal. A* **2001***, 207*, 367.

31. Beyerlein, R. A.; Choi-Feng, C.; Hall, J. B.; Huggins, B. J.; Ray, G. J. *Top. Catal.* **1997**, *4*, 27.

32. Chen, J. X.; Chen, T. H.; Guan, N. J.; Wang, J. Z. *Catal. Today* **2004**, *93*, 627

33. Severino, A.; Esculcas, A.; Rocha, J.; Vital, J.; Lobo, L. S. *Applied Catalysis, A.* **1996**, *142*, 255.

34. Matrin, A.; Wolf, U.; Kosslick, H.; Tuan, V. A. *React. Kinet. Catal. L.* **1993**, *51*, 19.

35. Li, S. H.; Zheng, A. M.; Su, Y. C.; Zhang, H. L.; Chen, L.; Yang, J.; Ye, C. H.; Deng, F. *J. Am. Chem. Soc.* **2007**, *129*, 11161.

36. Zholobenko, V. L.; Makarova, M. A.; Dwyer, J. *J. Phys. Chem.* **1993**, *5962*, 97.

37. Kiricsi, I.; Flego, C.; Pazzuconi, G.; Parker, W. O.; Millini, R.; Perego, C.; Bellussi, G. *J. Phys. Chem.* **1994**, *98*, 4627.

38. Kunkeler, P. J.; Zuurdeeg, B. J.; van der Waal, J. C.; van Bokhoven, J. A.; Koningsberger, D. C.; van Bekkum, H. *J. Catal.* **1998**, *180*, 234.

39. Kumar, S.; Sinha, A. K.; Hegde, S. G.; Sivasanker, S. *J. Mol. Catal. A: Chem.* **2000**, *154*, 115.

40. Maache, M.;Janin, A.; Lavalley, J. C.; Joly J. F.; Benazzi, E. *Zeolites*, **1993**, *13*, 419.

41. Gutmann, V. *The Donor–Acceptor Approach to Molecular.* Plenum Press: New York, **1978**.

42. Collman, J. P.; Hegedus, L. S.; Norton, J. R.; Finke, R. G. *Principles and Applications of Organotransition Metal Chemistry.* University Science Books Press: Mill Valley, **1987**.

43. Denayer, J. F.; Baron, G. V.; Martens, J. A.; Jacobs, P. A. *J. Phys. Chem. B* **1998**, *102*, 3077.

44. Denayer, J. F.; Souverijns, W.; Jacobs, P. A.; Martens, J. A.; Baron, G. V. *J. Phys. Chem. B* **1998**, *102*, 4588.

45. Eder, F.; Stockenhuber, M.; Lercher, J. A. *J. Phys. Chem. B* **1997**, *101*, 5414.

46. Eder, F.; Lercher, J. A. *Zeolites* **1997**, *18*, 75.

47. Eder, F.; Lercher, J. A. *J. Phys. Chem. B* **1997**, *101*, 1273.

48. Zhu, W.; Kapteijn, F.; Moulijn, J. A. *Phys. Chem. Chem. Phys.* **2000**, *2*, 1989.

49. Narbeshuber, T. F.; Vinek, H.; Lercher, J. A. *J. Catal.* **1995**, *157*, 388.

50. Narbeshuber, T. F.; Brait, A.; Seshan, K.; Lercher, J. A. *J. Catal.* **1997**, *172*, 127.

51. Wang, X.; Carabineiro, H.; Lemos, F.; Lemos, M. A. N. D. A.; Ribiero, F. R. *J. Mol. Catal. A.* **2004**, *216*, 131.

52. Bandiera, J.; Dufaux, M.; Ben Taarit, Y. *Appl. Catal., A.* **1997**, *148*, 283.

53. Xu, B.; Sievers, C.; Hong, S. B.; Prins, R.; van Bokhoven, J. A. *J. Catal.* **2006**, *244*, 163.

54. Aronson, M.T.; Gorte, R. J.; Farneth, W. E. *J. Catal.* **1986**, *98*, 434.

55. Farneth, W. E.; Gorte, R. J. *Chem. Rev.* **1995**, *95*, 615.

56. Gorte, R. J. *Catal. Lett.* **1999**, *62*, 1.

57. Macht, J.; Janik, M. J.; Neurock, M.; Iglesia, E. *J. Am. Chem. Soc.* **2008**, *130*, 10369.

58. Brändle, M.; Sauer, J. *J. Am. Chem. Soc.* **1998**, *120*, 1556.

59. Koppel, I.A.; Burk, P.; Koppel, I.; Leito, I.; Sonoda, T.; Mishima, M. *J. Am. Chem. Soc.* **2000**, *122*, 5114.

60. Hunter, K. C.; East, A. L. L. *J. Phys. Chem. A.* **2002**, *106*, 1346.

61. van Santen, R. A.; Kramer, G. J. *Chem. Rev.* **1995**, *95*, 637.

62. Rigby, A. M.; Kramer, G. J.; van Santen, R. A. *J. Catal.* **1997**, *170*, 1.

63. Zygmunt, S. A.; Curtiss, L. A.; Zapol, P.; Iton, L. E. *J. Phys. Chem. B* **2004**, *104*, 1944.

64. Roberge, D. M.; Hausmann, H.; Holderich, W. F. *Phys. Chem. Chem. Phys.* **2002**, *4*, 3128.

65. Gates, B. C. *Catalytic Chemistry*. Wiley: New York, **1992**.

    Kazansky, V. *Acc. Chem. Res.* **1991**, *24*, 379.

Chapter 4

Mechanistic consequence of reaction intermediates in acid-catalysis by zeolites: kinetic studies of 1-pentene cracking

The mechanism of 1-pentene activation on Brønsted acid catalysts is addressed by kinetic analysis of the elementary steps via steady-state treatment in terms of the stability of transition state and intermediates. Mechanistic interpretations of the measured reaction rate and equilibrium constants are applied to sense activation barriers for individual reaction routes and relate them to the relative stability of reaction intermediates involved. Cleavage reactions proceed via β-scission in two different pathways: direct cracking and oligomerization-cracking. It is for the first time experimentally supported two reaction intermediates for monomolecular cleavage of C=C bond are present in the energy profile, i.e. physisorbed π-complexes and carbenium cations. The proposed reaction scenario consists of several consecutive steps: the formation of stable physisorbed intermediates, followed by protonation of those absorbed species, subsequent formation of carbenium ions and eventual cracking into smaller fragments. Reaction activity is directly related to the greater stability of physisorbed π-complex via hydrogen bond with zeolitic cluster

than that of carbenium ion intermediates. This is in agreement with recent theoretical estimations, revealing energy difference between those intermediates is mainly dominated by electrostatic stabilization and steric constrain inhibition in the zeolite framework. Difference in the experimental activation barrier for monomolecular cracking at varying surface coverage can rigorously reflect discrepancy in potential energy surface of the reaction intermediates. The carbenium cations, which are stabilized within the framework by electrostatic interaction, are present as a true reaction intermediate for monomolecular cracking. Turnover rates for bimolecular routes are driven by both formation rate of dimers and subsequent breakage of those surface moieties in kinetically relevant steps. Catalyst deactivation is depressed by introducing H_2 into the reaction system, which is speculated to encumber adsorption of some less reactive carbenium ions as precursors of carbonaceous deposits.

4.1 Introduction

The acid catalyzed alkene transformation over zeolites has drawn much attention, since it takes part in many important petrochemical reactions, for instance, from catalytic cracking to catalytic oligomerization of light olefins. These reactions are widely present in several vital fuel-related processes such as MTG and MTO for converting methanol to gasoline and olefins, and MOGD for converting mobile or light olefin to gasoline and distillate [1, 2]. In general, acid catalysis of alkene transformation involves different reactions such as isomerization, hydride transfer, oligomerization and cracking [3]. It is widely accepted that the active centers for these reactions are Brønsted acid sites on the catalyst surface which protonates C=C double bonds to form carbenium ions like species [4-7]. At present, Y and ZSM-5 zeolites are two of the most employed catalysts in fuel industries, which find extensive individual applications due to different catalytic performance in the products selectivity, overall conversion and degree of catalyst decay [8-11]. 10-Ring consisting ZSM-5 is attractive for reactions with alkene as feedstock owning to the better deactivation resistance. Narrow pores in the framework of ZSM-5 disfavor the formation of bulky coke precursors inside zeolitic channels [12]. In addition, relative low density of acidity also accounts for slower deactivation compared to several zeolites [13].

The cracking mechanism of alkenes over solid acid catalysts has been established over years, which relates to a "β-cracking" ionic reaction. In the initiation step alkenes adsorb on the acid sites to form adsorption complexes which are further protonated to tri-coordinated carbenium ions like species. However, it is not clear yet whether the nature of transition state as relative "free" carboncations or covalent bonded to the framework [14]. Subsequent fission of a C-C bond in the β-position leads to formation of a free olefin and a smaller carbenium ion like specie, which could desorb from the acid site. In spite of simplicity in mechanistic formalism for cracking of pure olefin, few literatures have provided direct kinetic assessment for the reaction because of difficulty

in quantification of the reactions. The carbenium ions like species by protonation of olefin are immediately available for other reactions like isomerization, oligomerization, hydride transfer etc. Besides, cracking of heavier alkenes at elevated temperature is experimentally challenged due to high reaction rates [15-17].

In contrast to protolytic cracking of alkane, which has been investigated extensively in recent decades [18-23], quantification of the elementary processes is difficult for cracking of pure olefins. Due to the complexity of the reaction network it is tough to sort out the rate-determining step and attribute the measured activation barrier to a specific kinetic steps. Also, acquisition of intrinsic activation barrier is encumbered by experimental determination of adsorption enthalpy of olefin on zeolites, owning to inevitable reactions even at nearly room temperature. To address the question for a basic mechanistic understanding we focus in this work on cracking of 1-pentene on H-ZSM-5 samples at elevated temperature because: (i) pentene is relatively simple and also a potential example for mechanistic insight into C=C cracking in larger alkenes, (ii) ZSM-5 is featured with its catalytic stability in hydrocarbon interconversion, (iii) high temperature favors cracking reaction and suppresses polymerization and coke formation. The kinetic results are rigorously obtained based on the zero-conversion extrapolation to exclude implication of secondary reactions. Effort is made in this contribution to offer a fundamental understanding of carbenium-ions cracking mechanism concerning the possible elementary steps based on detailed kinetic studies of the individual pathways involved in the reaction network.

4.2 Experimental

4.2.1 Catalysts preparation and characterization

Three ZSM-5 samples with different Si to Al ratio (CBV 3024E, CBV 5524G and CBV 8014) are purchased from Zeolyst Internatial in ammonium form. The powder of

samples were treated in flowing air (2.5 $cm^3g^{-1}s^{-1}$) by heating to 773 K in 1 K·min^{-1} and holding for 4 h to obtain H-ZSM-5, which were pelleted, crushed and sieve to 150-250 μm particles for kinetic measurements. Structural integrity of the calcined samples was examined by X-ray powder diffraction using a *Philips X'Pert Pro System.* Surface areas were measured by N_2 physisorption by a PMI automated BET-sorptometer. Acid sites concentration in the samples was measured on a Perkin-Elmer 2000 spectrometer with a resolution of 4 cm^{-1}. A spectrum was recorded after evacuation of physisorbed pyridine after stabilization of the temperature at 423 K.

4.2.2 1-Pentene conversion on H-ZSM-5

1-Pentene conversion was performed in a packed-bed quartz reactor with 6 mm inner diameter. H-ZSM-5 catalysts (0.0005-0.003 g, 150-250 μm) were diluted with inert quartz pellets (acid-washed) to prevent temperature gradients and turbulent flow through the bed. All transfer lines were heated at 423 K to evade condensation of the reactant. Flow rates of He (Westfalen AG, 99.996 %) and H_2 (Westfalen AG, 99.999 %) were controlled by mass controllers (Brooks 5850 series). The temperature of the furnace was adjusted by a temperature controller with 18 segment programs (Eurotherm Series 2014). Catalyst bed temperature was monitored by a thermocouple mounted at the external surface of the quartz reactor. 1-Pentene (Sigma-Aldrich, 99.5 % analytic standard) was kept in a saturator and cooled by a temperature-controlled cooling system (LAUDA RC 20), which was carried out by additional He flow. The mixture of reactants and He was diluted by a second stream of He. By varying the temperature in saturator the partial pressure of reactants was adjusted and maintained below 2 kPa to minimize bimolecular reactions and catalyst decay. In the case of reaction in presence of hydrogen an additional He flow was introduced to balance the total flow. Initial rate constants and selectivities were obtained by extrapolation to zero bed residence time. All the kinetic data in the study were based on the initial rate constants.

Catalysts were activated in a pure He flow (0.5 cm^3 s^{-1}) at 803 K (1 K·min^{-1}) for 2 h before kinetic measurements. The reaction temperature was varied between 728 and 778 K and reactor bed residence time was adjusted by varying the amount of catalyst. The reactants and products were separated by capillary gas chromatography (Agilent Hewlett-Packard 5890) with Al$_2$O$_3$-KCl capillary column (50 m × 0.32mm × 0.53mm; Agilent) and detected by flame ionization.

4.3 Results

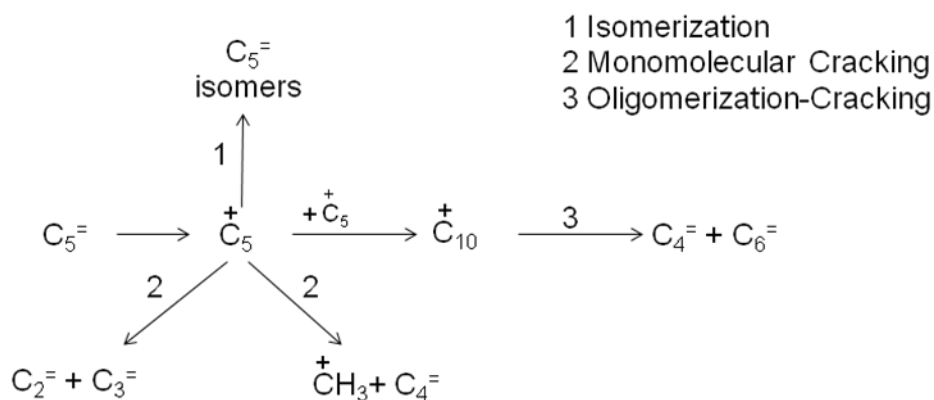### 4.3.1 Reaction pathways in activation of 1-pentene

Figure 4-1 shows the product selectivity in 1-pentene conversion with variation of temperature on H-ZSM-5 (Si/Al = 40) at 1.5 kPa 1-pentene excluding the contribution from isomerization, which occurs very rapidly and is considered to reach a quasi-equilibrium of isomer mixtures on the surface of catalysts [24, 25]. The main products consist of ethylene and propylene, which are from β-scission of C$_5^+$ carbocation upon protonation of pentene by Brønsted acid sites. Selectivity of propylene remains higher than ethylene at variation of the temperatures, implying the excessive propylene is most likely from secondary cracking of hexene. The formation of butylene and hexene originates from oligomerization-cracking reaction of pentene. This bimolecular pathway involves two step reactions: oligomerization and subsequent cracking of the formed C$_{10}^+$ carbocation, both of which are kinetically relevant for the overall conversion. However, no decene is found under GC detect limit in the products, implying decene plays as a stable reaction intermediate. Alkanes like methane, ethane, propane, hexane are formed via hydride transfer reactions between their corresponding carbenium ions and olefins, most probably from the most abundant pentene [26, 27]. In addition, measurable amount of cyclopentene and cyclohexene are resulted from pentenyl and

hexenyl cations via cyclization and subsequent elimination of a proton. The proposed reaction pathways are shown in Scheme 4-1.
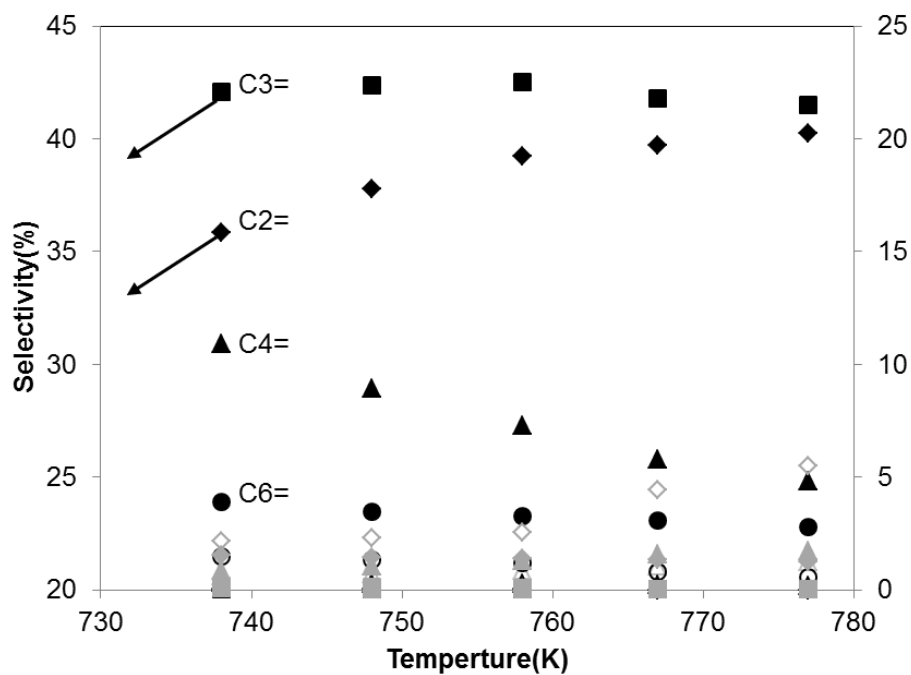
Figure 4-1 Products selectivity with variation of temperature ($\blacklozenge$ $C_2^=$, $\blacksquare$ $C_3^=$, $\blacktriangle$ $C_4^=$, $\bullet$ $C_6^=$, $\blacklozenge$ i-C_5, $\blacksquare$cyclohexene, $\blacktriangle$ n-C_6, $\bullet$ C_2, $\diamond$ cyclopentene, $\square$ C_3, $\triangle$ n-C_5, $\bigcirc$ neo-C_5, $\diamond$ others, $\square$ C_6 isomers, $\triangle$ C_1) (1.5 kpa 1-pentene, He in balance)

• Main pathways
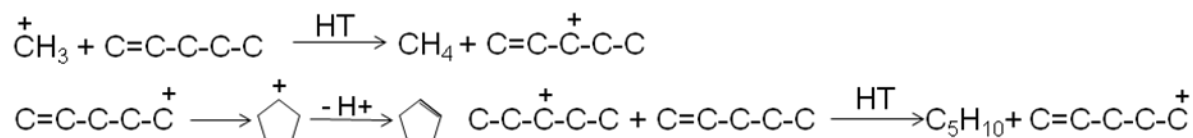
Scheme 4-1 Reaction pathways for 1-pentene conversion on H-ZSM-5

Conversion excluding the contribution from isomerization of pentene increases linearly with contact time (Figure 4-2), suggesting cracking rate keeps invariable up to the maximal conversion under reaction conditions. The observation is consistent with formation rate plot at varying contact time (Figure 4-3). In Figure 4-3 the initial formation rates of products from direct cracking of pentenyl cation as well as oligomerization-cracking are obtained by extrapolation to zero contact time. Obviously, the initial rate in monomolecular cracking exceeds that of oligomerization-cracking (leading to formation of butylene and hexene) more than one order of magnitude. Nearly constant formation rate in direct cracking also implies that cracking of C_5^+ carbocation is much slower than isomerization of those cations, which cannot limit the cracking rate consequently. Although the formation rate of butylene is higher than that of hexene at higher contact time, the initial rates remain nearly the same by extrapolation, indicating both of them are from the same reaction at zero conversion.

Nevertheless, with higher conversion at longer contact time some of hexenes likely take part in secondary cracking, leading to production of propylene. Indeed, slightly higher selectivity of propylene is expected than that of ethylene at longer contact time. Figure 4-4 shows selectivity of cracking products as a function of conversion, based on which the initial selectivity of cracking products can be obtained. The initial selectivity of products from direct cracking is approximately 42 %, while the Initial selectivity of products from oligomerization-cracking is lower than 5 %, with decrease in the selectivity of hexene with increasing contact time due to secondary cracking.
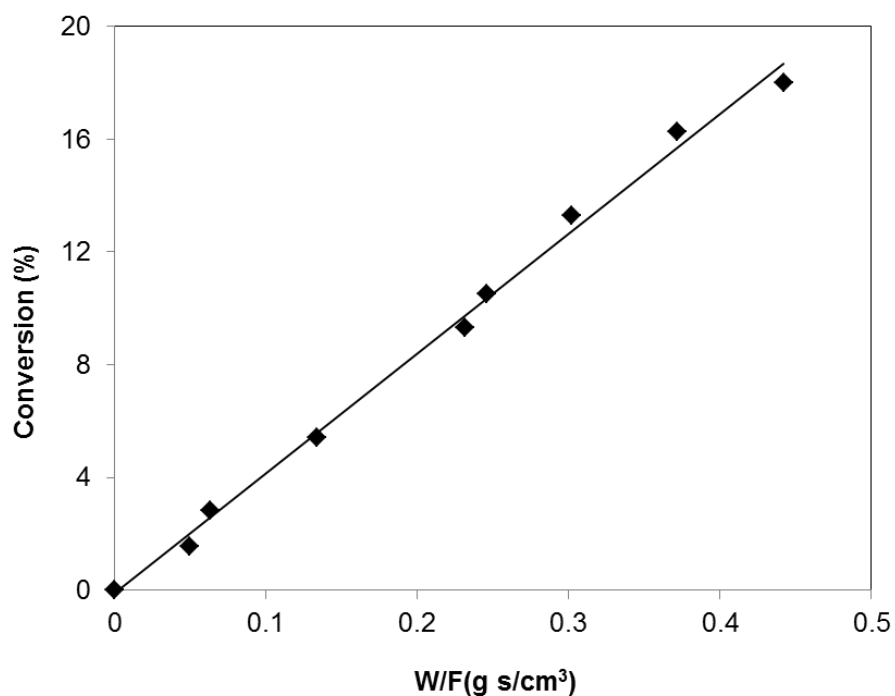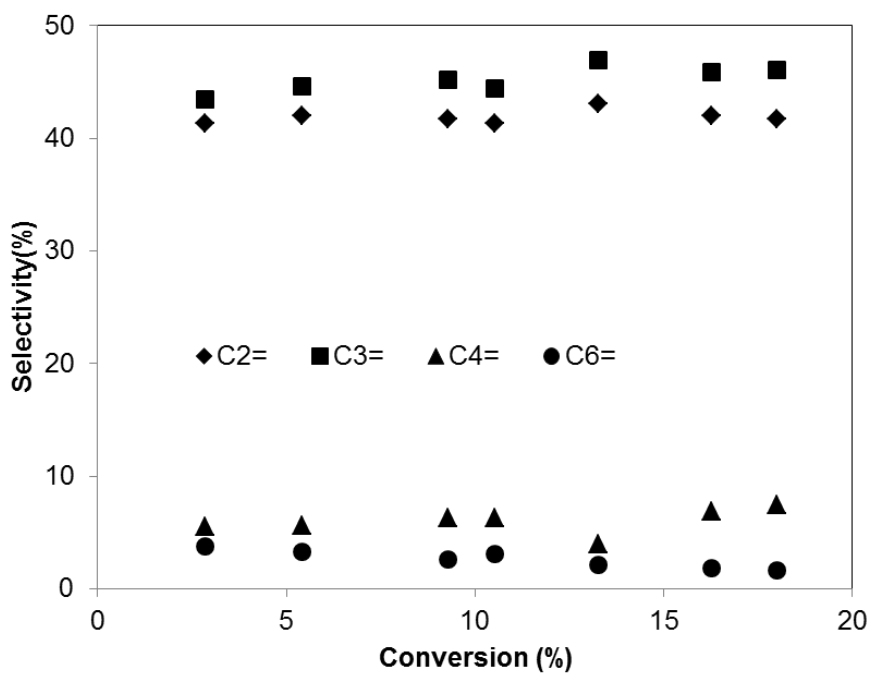

Figure 4-2 Dependence of cracking conversion on bed residence time (1.5 kpa 1-pentene, He in balance)
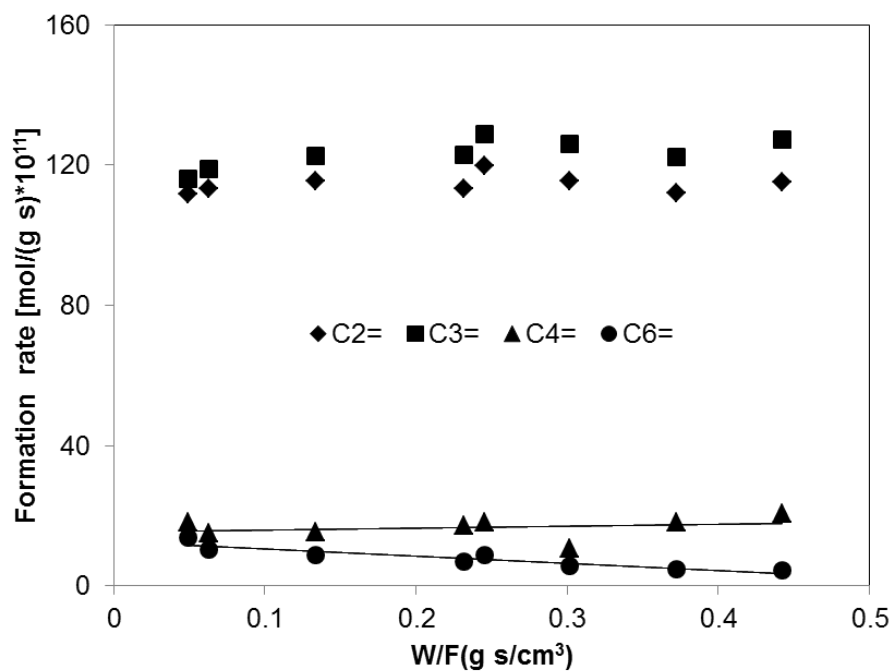
Figure 4-3 Determination of initial rate by extrapolation to zero conversion (1.5 kpa 1-pentene, He in balance)

Figure 4-4 Selectivity of main products with variation of conversion (1.5 kpa 1-pentene, He in balance)

4.3.2 Kinetic studies of monomolecular and oligomerization-cracking

Temperature dependence of the initial rate for monomolecular cracking at different partial pressure is shown in Figure 4-5. It is worth noting that the rate change represents true kinetic effects at high temperature without corruption of catalyst deactivation, since all the rate data are obtained from steady-state measurement. According to the Arrhenius plot, the measured activation energy increases despite decrease in the partial pressure of 1-pentene from 1.7 kPa to 0.7 kPa. Further kinetic assessment illustrates that the reaction order is close to 1 at 0.7 kPa of 1-pentene while it approaches zero order at 1.7 kPa (Table 1). Nevertheless, the measured activation energy decreases from 83 kJ·mol^{-1} to 60 kJ·mol^{-1}. Obviously, the classical relation between measured activation energy Ea$_{meas}$ and intrinsic activation energy Ea$_{int}$ cannot account for this kinetic behavior.

$$E_{a_{meas}} = E_{a_{int}} + \Delta H_{ads}\,(1 - \theta) \qquad (4\text{-}1)$$
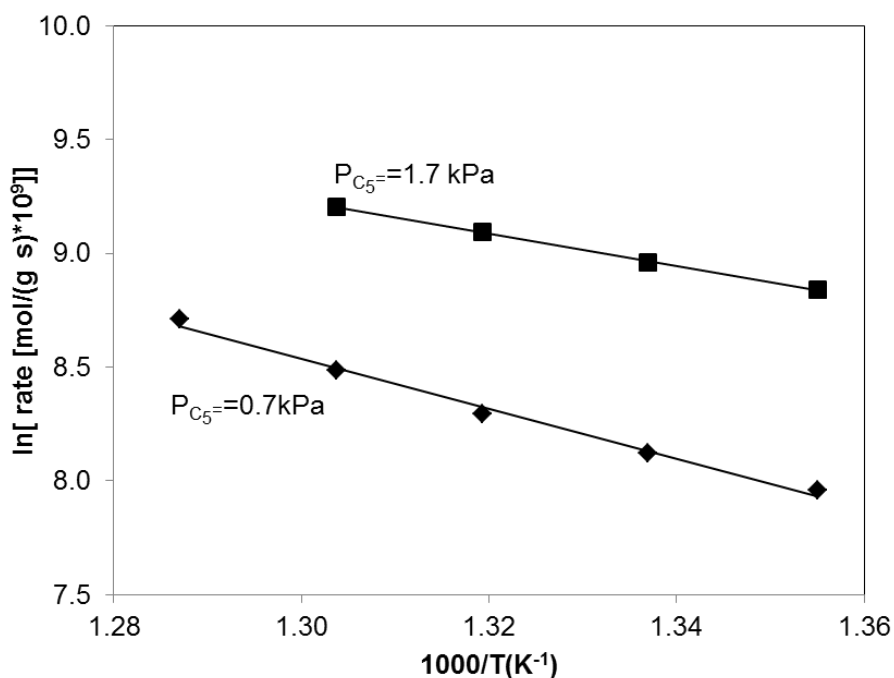
Figure 4-5 Arrhenius plot for monomolecular cracking under different partial pressure of 1-Pentene (based on the formation rate of propylene)

Table 4-1 Kinetic parameters for monomolecular cracking under different partial pressure of 1-Pentene

| $P_{C_5=}$ (kPa)	Reaction order	Ea_{meas} (kJ·mol)
0.72	0.96	83
1.73	0.06	60

In the expression the measured activation energy is directly related to the intrinsic activation energy by introducing heat of adsorption of reactants on the surface ΔH_{ads} and surface coverage θ [28, 29]. By reference, the adsorption heat of reactants ΔH_{ads} has always negative contribution due to the exothermal nature. Therefore, the measured activation energy at the high partial pressure should exceed that at the low partial pressure because of higher coverage. Here, we conclude that the classical formalism is too simple to interpret the difference in the activation barrier of monomolecular cracking at different partial pressure. The observation led us to investigate dependence of individual rate parameters for their elementary steps on temperature, which is discussed in next part of the work.

In comparison, the initial rate of oligomerization-cracking with variation of temperature is shown in Figure 4-6. It is noticed that the rate decreases with increase of temperature up to around 770 K but increases abruptly with further elevation of the temperature. The rate dependence on temperature reflects a complex kinetic behavior which cannot be expressed by a simple power-law analysis. Hence, oligomerization-cracking pathway could consist of several sequent elementary steps, each of which involves several adsorbed species. Thus, the overall rate expression has to be formulated into a combination of individual rate constants k_{app} and equilibrium constant K from the elementary steps.
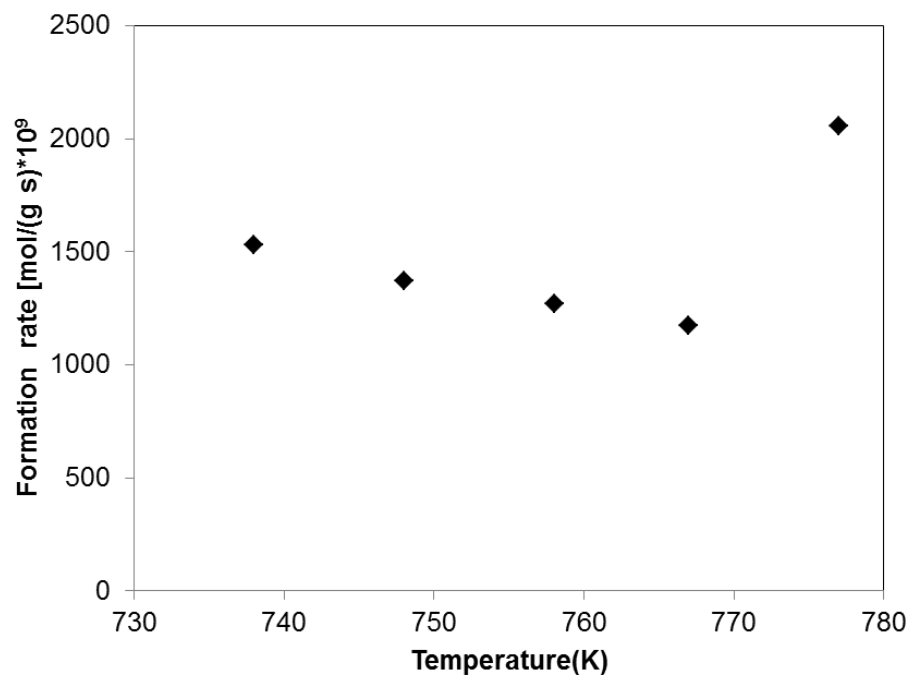
Figure 4-6 Initial rate of oligomerization-cracking with variation of temperature (1.5 kpa 1-pentene, He in balance) (based on the formation rate of butylene)

4.3.3 Catalyst decay

It is well known that catalyst deactivation plays a significant role in many important industrial reactions such as catalytic cracking, isomerization, alkylation [30, 31]. In these reactions catalyst decay proceeds via the formation of carbenium species that can propagate further to inhibit the acid sites. In this respect, knowledge of catalyst deactivation becomes necessary to estimate effect on the kinetics and design stable catalysts.
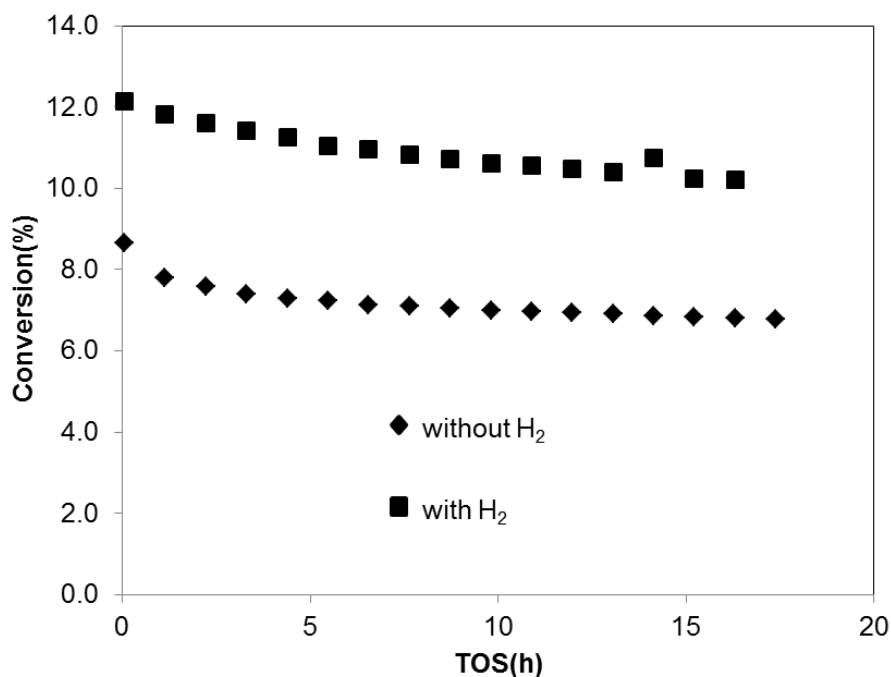
Figure 4-7 Comparison of deactivation behavior under different conditions (1.5 kpa 1-pentene, He in balance, 767 K)

As shown in Figure 4-7, cracking conversion as a function of time on stream is compared under different conditions. In both cases catalysts undergo two stages: deactivation and subsequent steady state. In absence of hydrogen catalyst loses 25 % activity within 5 hours and reaches the steady stage. In contrast catalysts become more stable irrespective of loss of 16 % activity within 5 hours with hydrogen. It seems that hydrogen disfavors formation of carbonaceous deposits and consequently depresses catalysts decay. However, the increase in the partial pressure of hydrogen does not improve resistance of catalyst to deactivation. Figure 4-8 shows deactivation behavior of the catalysts under different partial pressure of hydrogen. Up to 94 % of hydrogen in total flow all the curves show very similar trend at the deactivation stage.
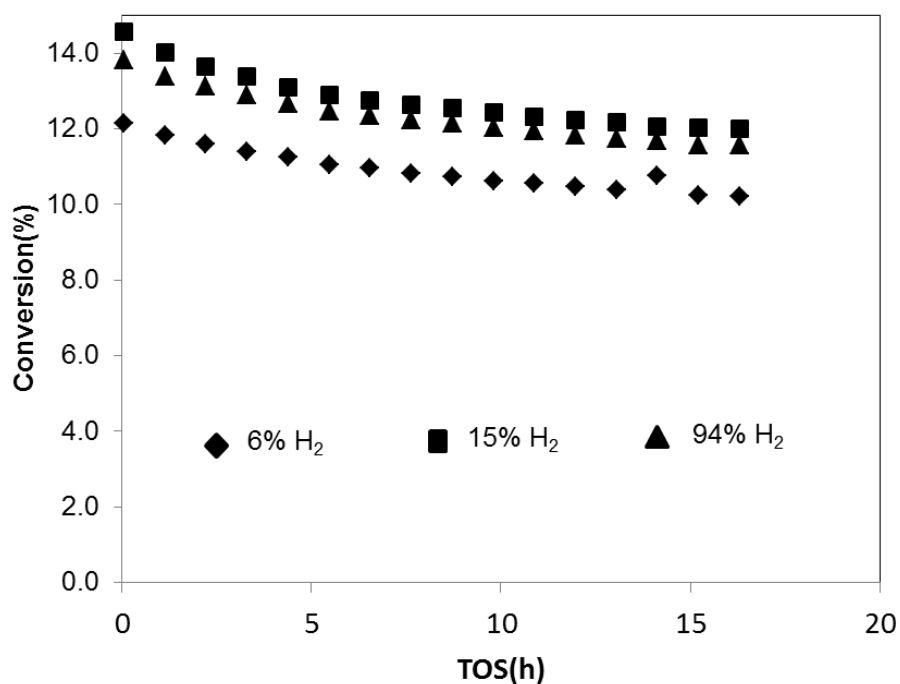
Figure 4-8 Comparison of deactivation behavior under different H_2 partial pressure (1.5 kpa 1-pentene, He in balance, 767K)

4.4 Discussion

4.4.1 Mechanistic implications for kinetics in monomolecular cracking

As discoursed before, the experimental conflicting with the classical relation between the measured and intrinsic activation energy under different partial pressure of reactants led us to consider separation of the overall reaction scenario into individual elementary steps, i.e., adsorption of reactants, followed by protonation of adsorbed species and subsequent β-scission into smaller fragments.

It has been widely accepted the mechanism of catalysis in solid acids, such as zeolite resembles that of homogeneous reaction in superacid. In general, protonation of olefins by Brønsted acid sites leads to the formation of adsorbed carbenium ions, which could

be involved in the catalytic cracking, isomerization and alkylation. However, experiments failed to verify the free carbenium cations on the surface of acidic zeolites except for alkyl-substituted cyclopentenyl and indanyl cations [32, 33]. It was proposed by Kazansky that the free carbenium cations most probably exist as transition states instead of stable intermediates in acid-catalyzed reactions over acidic zeolites [34, 35]. Contrastively, alkoxy species were confirmed as the intermediate species in acid-catalyzed reactions on zeolites by various ^{13}C-NMR MAS spectroscopic studies [36-39]. These alkoxy species are stabilized via covalent bonds between zeolite O atoms and C atoms. In accord with experimental observations, quantum-chemical studies also showed protonation of olefins by Brønsted acid sites results in formation of covalently bonded alkoxide intemediates via ionic transition states with similar geometry and electronic structure to that of classical carbenium ions [40-42].

Protonation of olefins initiating various acid-catalyzed reactions proceeds via a mechanism consisting of several elementary steps. At first olefins adsorb on Brønsted acid sites to form weakly hydrogen-bonded complexes (π complex). Subsequently, acidic protons from zeolitic framework are transferred to olefins to form alkoxide for small olefins such as ethylene and propylene via a carbenium ion-like specie as the transition state [43, 44]. Comparatively it was theoretically supposed that the carbenium ion pair may be present as a real reaction intermediate for bulkier and more basic olefins (e.g., isobutylene) [14, 45, 46]. As shown in Scheme 4-2, the ion pair, π-complex and alkoxy species could transform into each other. Furthermore, quantum chemical calculation reveals the stability of those carbenium ion intermediates is strongly influenced by electrostatic stabilization or steric destabilization via interaction with zeolite framework.
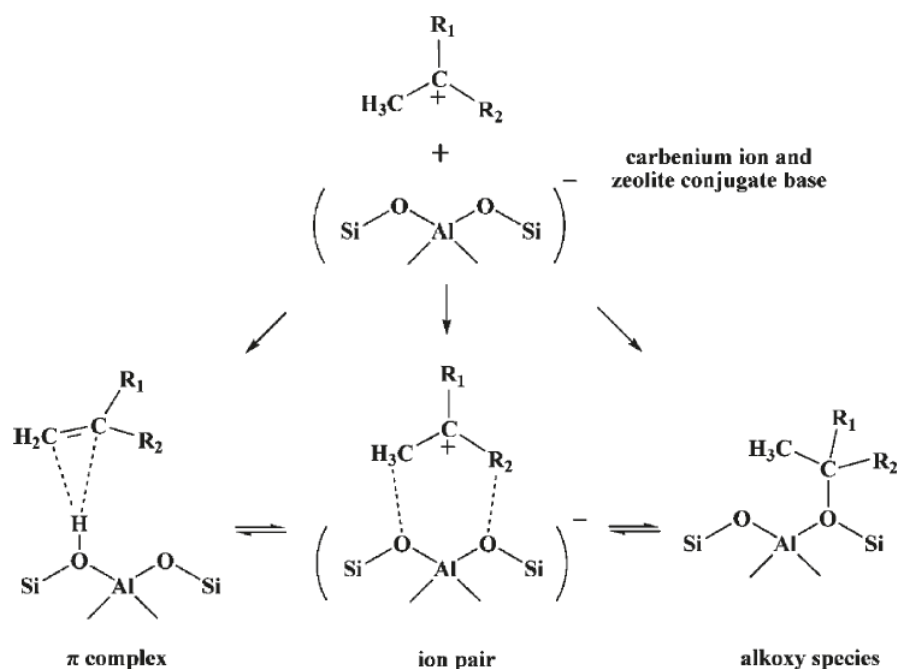
Scheme 4-2 Transformation of carbenium ions in zeolites adapted from ref.[49]

Here, the mechanism of monomolecular olefin cracking in elementary nature is proposed in Table 4-2 with pentene as illustration. In the reaction sequence the first step refers to the rapid physisorption of olefins on Brønsted acid sites to form π complexes, which is presumed to be quasi-equilibrated. In the following step the physisorbed complexes are converted into alkoxy like species, which are stabilized by the framework with carbenium ions as the transition state. However, it is still unclear whether the nature of the reaction intermediates would be ionic or covalent. Finally, the alkoxy like species are irreversibly cleaved at β-position into smaller olefins, specific as ethylene and propylene.

Table 4-2 Elementary steps for monomolecular cracking

$C_5^=$ activation and monomolecular cracking	
1. $* + C_5^=(g) \rightleftharpoons C_5^=*$	(quasiequilibrated)
2. $C_5^=* \rightleftharpoons C_5^=(c)$	(quasiequilibrated)
3. $C_5^=(c) \longrightarrow C_2^= + C_3^=$	

$C_5^=*$ denotes physisorbed pentene (π-complex) on active sites
$C_5^=(c)$ denotes chemisorbed or alkoxide like species.

Therefore, an overall rate expression can be obtained by using pseudo-steady-state approximation for all absorbed species and supposition of quasi-equilibrium for some of the reaction steps. In the following, K_i, k_i represent the equilibrium and rate constants in i-step respectively. Concentration of physisorbed pentene $[C_5^=*]$ can be related to the partial pressure $P_{C5}^=$ (equation (4-2)):

$$[C_5^=*] = K_1 P_{C5}^=[*] \tag{4-2}$$

Under the premise of quasi-equilibration in step 2 with elimination of $[C_5^=*]$, it is derived:

$$[C_5^=(c)] = K_2 [C_5^=*] = K_2 K_1 P_{C5}^=[*] \tag{4-3}$$

Considering a site balance on the catalysts surface for all active sites [L]:

$$[*] + [C_5^=*] + [C_5^=(c)] = [*] + K_1 P_{C5}^=[*] + K_2 K_1 P_{C5}^=[*] = [L] \tag{4-4}$$

From equation (4-4) we can obtain the undetectable concentration of available active sites:

$$[*] = \frac{[L]}{1 + K_1 P_{C5=} + K_2 K_1 P_{C5=}} \tag{4-5}$$

Hence the reaction rate is determined by the cracking rate of alkoxy like species in step 3:

$$r = k_3[C_5^=(c)] = k_3 K_2 K_1 P_{C_5^=}[*] = k_3 \frac{K_2 K_1 P_{C_5^=}[L]}{1 + K_1 P_{C_5^=} + K_2 K_1 P_{C_5^=}} \tag{4-6}$$

On one hand, under the condition of high partial pressure of pentene, $K_1 P_{C5}^=$ and $K_2 K_1 P_{C5}^=$ in the denominator term of equation (4-6) are larger than 1 and $K_1\ P_{C5}^=$ in other terms can be cancelled, giving a rate equation in the form (equation (4-7)):

$$r = k_3 \frac{K_2[L]}{1 + K_2} \tag{4-7}$$

Since the rate equation (4-7) does not contain the term of partial pressure anymore, reaction then becomes zero order which is consistent with our experimental results up to 1.5 kPa of 1-pentene. Under the condition rate expression is determined by both rate constant k_3 and equilibrium constant K_2. For this rate expression, the overall rate constant is dependent of the relative composition of reaction intermediates under reaction conditions. Given higher fraction of alkoxide like species $C_5^=(c)$ than physisorbed $C_5^=*$, then K_2 becomes larger than 1 which results in (equation (4-8)):

$$r = k_3[L] \tag{4-8}$$

We note that only rate constant k_3 appears in equation (4-8), the apparent rate constant k_{app} has to be equal to k_3 correspondingly.

$$k_{app} = k_3 \tag{4-9}$$

Therefore, the apparent activation energy is merely related to activation barrier in step 3, i.e. cracking of chemisorbed reaction intermediates (equation (4-10)).

$$E_{a,app} = E_{a,3} \tag{4-10}$$

On the contrary, provided more abundant physisorbed species $C_5^=*$ than chemisorbed $C_5^=(c)$, K_2 is then smaller than 1, K_2 in the denominator term of equation (4-7) can be cancelled:

$$r = k_3 K_2[L] \tag{4-11}$$

Here step 2 and 3 are kinetically relevant steps in the overall sequence in Table 4-2 with rate and equilibrium constants k_3 and K_2 present in the apparent rate constant (k_{app}):

$$k_{app} = A_{app}e^{-E_{app}/RT} \tag{4-12}$$

$$k_{app} = k_3K_2[L] \tag{4-13}$$

$$k_3 = A_3e^{-E_{a,3}/RT} \tag{4-14}$$

$$K_2 = \frac{A_{a,2}}{A_{d,2}}e^{\Delta Q_1/RT} = \frac{A_{a,2}}{A_{d,2}}e^{-\Delta H_1/RT} \tag{4-15}$$

By plotting lnk_{app} against the reciprocal temperature the apparent activation energy can be obtained in the Arrhenius plot as equation (4-7). The apparent activation energy is dominated by both the adsorption enthalpy in adsorption step 2 and the activation energy in step 3:

$$lnk_{app} = ln_{A_{app}} - \frac{E_{a,app}}{RT}$$

$$= ln\frac{A_{a,2}}{A_{d,2}} + lnA_3 + ln[L] - (\frac{\Delta H_2 + E_{a,3}}{RT}) \tag{4-16}$$

$$E_{a,app} = E_{a,3} + \Delta H_2 \tag{4-17}$$

On the other hand, under the condition of low partial of pentene $K_1P_{C5}^=$ and $K_2K_1P_{C5}^=$ in the denominator of equation (4-7) can be neglected, which results in simplification of rate expression into equation (4-18):

$$r = k_3K_2K_1P_{C_5^=}[L] \tag{4-18}$$

This expression represents a first-order pentene dependency which is in agreement with the experimental results under the low partial pressure of pentene (Table 4-1). Accordingly, apparent rate constant (k_{app}) is then determined by rate and equilibrium constant in step 1, 2, 3 (equation (4-19)).

$$k_{app} = k_3K_2K_1[L] \tag{4-19}$$

Comparably, we can derive that the apparent activation energy depends now on activation energy in step 3 and also adsorption heats in step 1 and 2 (equation (4-20)).

$$E_{a,app} = E_{a,3} + \Delta H_1 + \Delta H_2 \tag{4-20}$$

From our experimental results the measured activation energy at the first order of monomolecular cracking is about 80 kJ·mol^{-1}, while it decreases to about 60 kJ·mol^{-1} at the zero order under higher pressure of reactants (Table 4-1). Since the formulism of

apparent rate constant for the first order is unique according to derived rate equation above (equation (4-20)), one of two cases (equation (4-8) and equation (4-11)) for the zero order has to be excluded. Comparing equation (4-20) and equation (4-17), higher apparent activation energy in equation (4-20) leads to the conclusion that ΔH_1 has a positive value of about 20 kJ·mol^{-1}, which is not possible because adsorption heat has always negative contribution to the overall energy profile. Consequently, the apparent activation energy under higher pressure of reactants has to be equal to activation barrier for step 3 (equation (4-8)), and the positive value of about 20 kJ·mol^{-1} is from comprehensive contribution of the term $\Delta H_1+\Delta H_2$ in equation (4-20). In other words, absolute formation heat of chemisorbed species ΔH_2 is 20 kJ·mol^{-1} higher than adsorption heat ΔH_1, suggesting that the alkoxy like species as reaction intermediates are less stable than the π-complexes via physisorption.

The conclusions led us to rationalize the potential energy profile and transition state during monomolecular cracking of pentene. Before reaching the transition state of cracking, it has to overcome a free carbenium like specie energy barrier along reaction coordinate. At present, the experimental efforts to acquire adsorption heat of olefin over Brønsted acid sites of zeolites are in vain due to the rapid isomerization at an approximate room temperature, and merely a few theoretical studies are available [47, 48]. In addition, the clear structure for the chemisorbed intermediates cannot be obtained; it could be of ionic or covalent character (Scheme 4-2). Indeed, recent theoretical investigation reveals that π-complexes are more stable than the corresponding alkoxy species for many carbenium ions in zeolites [49], which is consistent with our experimental results. In this sense it could be possible to assess experimentally the stability of reaction intermediates and energies involved for acid-catalyzed activation of alkenes, which influence the reaction mechanism in reverse.

4.4.2 Temperature dependence of the reaction rate in oligomerization-cracking

As shown in Figure 4-6 the initial rate for oligomerization-cracking decreases firstly with the temperature and undergoes an inflexion point at higher temperature. The unusual temperature effect can be also rationalized by analysis of elementary steps to assign specific temperature dependencies. The proposed elementary steps for this pathway are summarized in Table 4-3. To simplify the formalism of rate expression without loss of validity only one adsorption intermediate $C_{5=}*$ is taken into account. In analogy with monomolecular cracking the rate of oligomerization-cracking can be given by measurable quantities and rate constants from the individual elementary steps (equation (A. 4-7) in the Appendix A),

$$r = \frac{k_2 k_3}{k_{-2}+k_3} \cdot \frac{K_1^2 P_{C_5=}{}^2 [L]^2}{1+2K_1 P_{C_5^{=}}+K_1{}^2 P_{C_5^{=}}{}^2} \tag{4-21}$$

Note that the reaction rate is determined by multiple factors in this rate expression, implying reaction rate can be dominated by different elementary reaction at varying temperature range. For instance, rate constant k_3 of step 3 can be neglected in the denominator term of equation (4-20) when the rate constant k_{-2} for back reaction of step 2 is much larger than k_3. Hence reaction rate is governed by k_2 in the numerator term, i.e. reaction rate of oligomerization from two adsorbed pentene molecules. Since oligomerization is more favored at lower temperature than cracking [50], the overall rate of oligomerization-cracking could be enhanced at lower temperature, which is consistent with our experimental observation (Figure 4-6). With increase of temperature the rate constant k_3 could play a role in the rate expression, leading to an abrupt increase in the overall rate of oligomerization-cracking as appearance of inflexion point in Figure 4-6.

Table 4-3 Elementary steps for oligomerization-cracking

$C_5^=$ oligomerization-cracking

1.	$C_5^= + \ * \rightleftharpoons C_5^{=*}$	(quasiequilibrated)
2.	$2C_5^{=*} \rightleftharpoons C_{10}^{+**}$	
3.	$C_{10}^{+**} \longrightarrow C_4^{+*} + C_6^{+*}$	

$C_5^{=*}$ denotes adsorbed and protonated pentene on active sites.
C_{10}^{+*} denotes C_{10}^{+} intermediates on active sites

4.4.3 Catalysts deactivation behavior

In agreement with the previous studies, the catalysts undergo a rapid initial decay period in the activity and then reach a steady state. However, it remains still in debate which process is responsible for catalyst deactivation. Currently, it is widely accepted that the loss of catalytic activity during deactivation is attributed to the formation of carbonaceous deposits [30, 31]. It was argued that some less reactive carbenium ions accumulated on the active sites take part in side reactions in the complex process, which results in the deposition of carbonaceous components [30]. Furthermore, assuming an exponential deactivation function in terms of conversion (y) with time-on-stream (t) at the initial deactivation period, from the experimental observation for cracking of cumene on Y zeolite [51],

$$\frac{y_t}{y_0} = exp(-k_D t) \tag{4-22}$$

We can obtain the deactivation coefficient k_D for the two cases in Figure 4-8 by fitting of the experimental data, which show a two-fold higher k_D (0.037) for decay behavior in absence of hydrogen than that in presence of hydrogen (0.017). However, k_D keeps nearly unchanged with further increase in partial pressure of hydrogen (Figure 4-

9). Since the value of k_D denotes the degree of deactivation rate, it is speculated that hydrogen disfavors formation of coke deposits, possibly by inhibition of adsorption of the less reactive carbenium ions on the active sites. In addition, the absolute amount of those less reactive carbenium ions are limited, hence excessive hydrogen cannot further improve catalysts deactivation.

4.5 Conclusions

Initial kinetic data based on steady state treatment were applied to elucidate the mechanistic understanding for β-scission type cracking during activation of 1-pentene on H-ZSM-5 catalysts. Two different pathways can account for production of smaller olefins: monomolecular and oligomerization-cracking. For monomolecular activation of C=C bond two reaction intermediates are involved to account for proceedings in the catalytic cycles. By derivation of the rate expression from the proposed sequence of elementary steps the potential energy profile can be obtained, implying the difference in the activation barrier with variation of reactant coverage is attributed to relative stability of the two reaction intermediates. It is for the first time from experimental data evidenced the π-complex intermediates exhibit a higher energy level than alkoxy like intermediates, which is consistent with recent ab initio density functional theoretical calculations. Moreover, the free carbenium ions like species are regarded as the transition state for transformation from π-complex to alkoxy like species. Kinetic relevant steps for oligomerization-cracking are more complicated in the formalism of rate expression by pseudo-steady-state treatment. Oligomerization is speculated to dominate reaction rate at lower temperature while cracking of C_{10}^+ species could play an important role in kinetics at elevated temperature. Catalysts undergo a deactivation period and then reach to a steady state. The loss of catalytic activity is due to formation of carbonaceous components with some less reactive carbenium ions as precursors.

Hydrogen could inhibit the adsorption of those carbenium precursors, which alleviate the formation of carbonaceous deposits.

4.6 Appendix Derivation of rete expression for oligomerization-cracking

The kinetic relevant steps for oligomerization-cracking are listed in Table 4-3, where step 2 is considered as reversible. According to pseudo-steady-state assumption each step proceeds at equal rates, overall rate is given by

$$r = r_3 = k_3[C_{10}^{+**}]$$ (A. 4-1)

where rate constants k_i, and k_{-i} are used for forward and reverse reaction of elementary steps (i) in Table 4-3, K_i stands for equilibrium constant. To solve number of active sites [*], the site balance over the total number of sites [L] is given by the sum of intermediates, here C_{10}^{+**} is ignored because of undetectable amount of C_{10} products under GC detect limit.

$$[L] = [*] + [C_5^{=*}]$$ (A. 4-2)

Since step 1 is regarded as quasi-equilibrated, $[C_5^{=*}]$ can be expressed into,

$$[C_5^{=*}] = K_1[*]P_{C_5^=}$$ (A. 4-3)

Therefore, we obtain available active sites [*] on the catalysts surface,

$$[*] = \frac{[L]}{1 + K_1 P_{C_5^=}}$$ (A. 4-4)

The rates for step 2 and 3 are expressed in terms of their individual relevant species,

$$r_2 = k_2[C_5^{=*}]^2 - k_{-2}[C_{10}^{+**}]$$ (A. 4-5)

Applying the pseudo-steady-state assumption overall rate is equal to rate for each elementary step, which leads to solvation of $[C_{10}^+**]$ in terms of measurable partial pressure of pentene $P_{C_5^=}$ from equation (A. 4-1) and (A. 4-5),

$$[C_{10}^{+**}] = \frac{k_2[C_5^{=*}]^2}{k_{-2} + k_3} = \frac{k_2}{k_{-2} + k_3} \cdot \frac{K_1^2 P_{C_5^=}^2 [L]^2}{(1 + K_1 P_{C_5^=})^2}$$ (A. 4-6)

The overall rate for oligomerization-cracking can be eventually given by,

$$r = k_3[C_{10}^{+**}] = \frac{k_2 k_3}{k_{-2} + k_3} \cdot \frac{K_1^2 P_{C_5^=}^2 [L]^2}{1 + 2K_1 P_{C_5^=} + K_1^2 P_{C_5^=}^2}$$ (A. 4-7)

4.7 References

1. Tabak, S. A.; Krambeck, F. J.; Garwood, W. E. *J. AlCHE.* **1986**, 32, 1526.

2. Garwood, W. E.; Caesar, P. D.; Brennan, J. A. *150. Patent* United States of America, **1979**, 4.

3. Voge, H. H.; Emmett, P. H. *Catalysis—Hydrocarbon Catalysis.* Reinhold Publishing Corp.: New York, **1958**.

4. Gayer, F. H. *Ind. Eng. Chem.* **1933**, 25, 1122.

5. Greensfelder, B. S. *Ind. Eng. Chem.* **1949**, 41, 1122.

6. Thomas, C. L. *Ind. Eng. Chem.* **1949**, 41, 2564.

7. Kissin, Y. V. *Catal. Rev.* **2001**, 43, 85.

8. Wojciechowski, B. W.; Corma, A. *Catalytic Cracking: Catalysis, Chemistry and Kinetics.* Marcel Dekker Inc.: New York, **1986**.

9. Venuto, P. B. *Micropo. Mater.* **1994**, 2, 297.

10. Van Bekkum, H.; Kouwenhoven, H. W. *Stud. Surf. Sci. Catal.* **1988**, 41, 45.

11. Haag, W. O.; Chen, N. Y. *Catalytic Design, Progress and Perspectives.* Wiley Publishing Corp.: New York, **1987**.

12. Van den Berg, J. P.; Wolthuizen, J. P.; van Hooff, J. H. C. *J. Catal.* **1983**, 80, 139.

13. Guisnet, M.; Magnoux, P. Zeolites Microporous Solids: Synthesis,Structure and Reactivity. Kluwer Academic Publischers.: Dordrecht, **1992**.

14. Boronat, M.; Viruela, P. M.; Corma, A. *J. Am. Chem. Soc.* **2004**, *1*26, 3300.

15. Haag, W. O.; Lago, R. M.; Rodewald, P. G. *J. Mol. Catal.* **1982**, 17, 161.

16. Dejaife, P.; Vedrine, J. C.; Bollis, V.; Derouane, E.G. *J. Catal.* **1980**, 63, 331.

17. Dessau, R. M.; Lapierr, R. B. *J. Catal.* **1982**, 78, 136.

18. Krannila, H.; Haag, W. O.; Gates, B. C. *J. Catal.* **1992**, 135, 115.

19. Lercher, J. A.; van Santen, R. A.; Vinek, H. *Catal. Lett.* **1994**, 27, 91.

20. Narbeshuber, T. F.; Vinek, H.; Lercher, J. A. *J. Catal.* **1995**, 157, 388.

21. Van Bokhoven, J. A.; Williams, B. A.; Koningsberger, D. C.; Kung, H. H.; Miller, J. T. *J. Catal.* **2004**, 224, 50.

22. Bhan, A.; Gounder, R.; Macht, J.; Iglesia, E. *J. Catal.* **2008**, 253, 221.

23. Lin, L.; Ember, E.; Lercher, J. A. **2012**, Submitted for publication.

24. Stepanov, A.G.; Arzumanov, S.S.; Luzgin, M.V.; Ernst, H.; Freude, D. *J. Catal.* **2005**, 229, 243.

25. Sassi, A.; Wildman, M. A.; Haw, J. F. *J. Phys. Chem. B.* **2002**, 106, 8768.

26. Sievers, C.; Onda, A.; Guzman, A.; Otillinger, K. S.; Olindo, R.; Lercher, J. A. *J. Phys. Chem. C.* **2007**, 111, 210.

27. Sanchez-Castillo, M. A.; Agarwal, N.; Bartsch, A.; Cortright, R. D.; Madon, R. J.; Dumesic, J. A. *J. Catal.* **2003**, 218, 88.

28. Hinshelwood, C. N. *The Kinetics of Chemical Change.* Oxford Univ. Press.: London, **1940**.

29. Eley, D. D. *Nature.* **1962**, 194, 1076.

30. Wojciechowski, B. W. *Catal. Rev.* **1998**, 40, 209.

31. Sievers, C.; Zuazo, I.; Guzman, A.; Olindo, R.; Syska, H.; Lercher, J. A. *J. Catal.* **2007**, 246, 315.

32. Olive, F. G.; Munson, E. J.; Haw, J. F. *J. Phys. Chem.* **1992**, 96, 8106.

33. Xu, T.; Haw, J. F. *J. Am. Chem. Soc.* **1994**, 116, 10188.

34. Kazansky, V. B. *Acc. Chem. Res.* **1991**, 24, 379.

35. Kazansky, V. B. *Catal. Today.* **1999**, 51, 419.

36. Aronson, M.T.; Gorte, R.J.; Farneth, W.E.; White, D. *J. Am. Chem. Soc.* **1989**, 111, 840.

37. Haw, J. F.; Richardson, B. R.; Oshiro, I. S.; Lazo, N. D.; Speed, J. A. *J. Am. Chem. Soc.* **1989**, 111, 2052.

38. Malkin, V. G.; Chesnokov, V. V.; Paukshtis, E. A.; Zhidomirov, G. M. *J. Am. Chem. Soc.* **1990**, 112, 666.

39. Lazo, N. D.; Richardson, B. R.; Schettler, P. D.; White, J. L.; Munson, E. J.; Haw, J. F. *J. Phys. Chem.* **1991**, 95, 9420.

40. Kazansky, V. B.; Senchenya, I. N. *J. Catal.* **1989**, 119, 108.

41. Viruela, P.; Zicovich-Wilson, C.M.; Corma, A. *J. Phys. Chem.* **1993**, 97, 13713.

42. Van Santen, R. A. *Catal. Today.* **1997**, 38, 377.

43. Rozanska, X.; Demuth, T.; Hutschka, F.; Hafner, J.; van Santen, R. A. *J. Phys. Chem. B.* **2002**, 106, 3248.

44. Bhan, A.; Joshi, Y. V.; Delgass, W. N.; Thomson, K. T. *J. Phys. Chem. B.* **2003**, 107, 10476.

45. Tuma, C.; Sauer, J. *Angew. Chem. Int. Ed.* **2005**, 44, 4769.

46. Wang, W.; Hunger, M. *Acc. Chem. Res.* **2008**, 41, 895.

47. Dixit, L.; Rao, T. S. R. P. *J. Chem. Inf. Comp. Sci.* **1999**, 39, 218.

48. Benco, L.; Hafne, J.; Hutschka, F.; Toulhoat, H. *J. Phys. Chem. B.* **2003**, 107, 9756.

49. Fang, H.; Zheng, A.; Xu, J.; Li, S.; Chu, Y.; Chen, L.; Deng, F. *J. Phys. Chem. C.* **2011**, 115, 7429.

50. Nivarthy, G.S.; He, Y.J.; Seshan, K.; Lercher, J.A. *J. Catal.* **1998**, 176, 192.

51. Dumez, F. J.; Froment, G. F. *Ind. Eng. Chem. Process Des. Dev.* **1976**, 15, 291.

Chapter 5

Summary and conclusions

In this work we have investigated acid catalyzed activation of *n*-alkanes and *n*-alkenes by a serial of H-ZSM-5 samples. First of all, transition state theory and thermochemical cycles were applied to assess kinetic parameters for protolytic cracking of C_3-C_6 alkanes on H-ZSM-5 samples with different Si/Al ratios. The goal is to explore the transition state geometry and its role for product selectivities based on the well-established Haag-Dessau mechanism. Next, one parent H-ZSM-5 sample was chosen and subjected to mild steaming in varying degrees. Using protolytic cracking of pentane as a probe reaction and combining various methods of characterization, we present evidence for influence of the subtle change in zeolite framework on catalytic activity of those specifically modified materials. At last we turn our attention from carbonium to carbenium chemistry. Activation of 1-pentene at high temperature was studied concerning the kinetic and mechanistic consequences in the acid catalysis by zeolite. We address the role of reaction intermediates in kinetically relevant steps for the overall rate expression.

Kinetic assessment of C_3-C_6 alkanes cracking based on transition state theory and the thermochemical cycles provides the experimental evidence for the transition state structure in protolytic cracking. In general, breaking the C-C bonds closer to the center of the alkane molecules leads to lower activation entropies than that for breaking the terminal bonds, since the latter reaction route results in a spatially less constrained transition state. In spite of protonation at the same position, activation energies are found to be unequal for the different cracking paths. The finding led us consider the minor variation in the transition state for the two routes. Activation barriers are closely related to the relative stability of the transition state species. Therefore, it is concluded that the energy-demanding transition state for monomolecular cracking resembles the configuration of products, i.e. a late transition state. Furthermore, it is observed that selectivities to different cracking pathways are insensitive to the temperature variation, implying the loss in activation enthalpies is partially compensated by the gain in activation entropies. A nearly linear relation between the measured rate constants and

the concentration of Brønsted acid sites in the samples shows cracking activity is governed by the nature of alkanes and less affected by the samples. An offset in the coordinate indicates that not all of the Brønsted acid sites are active for monomolecular cracking of alkanes.

Increasing steaming duration leads to persistent loss of the Brønsted acidity with concurrent increase in the number of EFAL species. Accordingly, quantification from infrared spectroscopy shows the increase in the amount of Lewis acid sites, which is probably caused by presence of the EFAL species. Kinetic studies exhibit the catalytic activity for monomolecular cracking of *n*-pentane is promoted at the beginning of steaming and then gradually decreases with steaming severity. Moreover, we found activation enthalpies decreases to a minimum initially and then increases gradually with further steaming duration. Thus, we conclude variation in the catalytic activity is primarily dominated by the change in transition state structure. In combination with the characterization results we propose the promotion effect by mild steaming at the beginning of steaming is due to the appearance of partially hydroxylated Al species in the framework. Exposure of hydroxyl group to the channel could probably redistribute the electron density of the transition state species being formed nearby with concurrent change in the energy level. With further steaming severity those partially hydroxylated Al are eventually expelled to form the EFAL species, which are regarded as Lewis acid sites. Destabilization of the transition state by those EFAL species could account for the increase in activation enthalpies with the catalytic consequence in cracking activity.

Initial kinetic data based on steady state study were obtained for β-scission type cracking of 1-pentene on several H-ZSM-5 samples. Two different reaction paths account for production of smaller olefins: monomolecular and oligomerization-cracking. Since the simplified relation between the apparent and intrinsic activation energy cannot account for the difference in activation barrier with variation of reactant coverage, we postulate two reaction intermediates are involved in the monomolecular activation of C=C bonds in the catalytic cycles. Upon adsorption of olefins on the surface of catalysts π-complex intermediates are firstly formed, which can further transform

into the alkoxy like species. Therefore, from the proposed sequence of elementary steps we describe the energy profile during monomolecular cracking, showing a higher energy level of π-complex intermediates than that of alkoxy like intermediates. This finding is consistent with recent ab initio density functional theoretical calculations. Instead the free carbenium ions like species are regarded as the transition state for transformation from π-complex to alkoxy like species. Furthermore, pseudo-steady-state treatment shows a more complicated formalism of rate expression for the oligomerization-cracking. In this route oligomerization is speculated to dominate reaction rate at lower temperature, while cracking of formed C_{10}^{+} species could play a significant role in the expression of reaction rate at elevated temperature. Catalysts undergo a fast deactivation period at the incipient stage, followed by a steady state. The loss of catalytic activity could be attributed to the formation of carbonaceous components with less reactive carbenium ions as precursors. Hydrogen alleviates catalytic deactivation and formation of carbonaceous deposits probably by inhibiting the adsorption of those carbenium precursors.

Curriculum vitae

Lin Lin was born on December 27th 1982 in Yunnan, P. R. China. After finishing her education in a high school of her hometown in 2000, she began to study in Department of Materials Science and Engineering at Tongji University, Shanghai, China. In July 2005 she received her bachelor degree. Then she went on to study chemical engineering at Technische Universität München, Germany in October 2005. In March 2009 she started her Diplom thesis under the supervision of Prof. Johannes Lercher, entitled *"Hydroisomerization of alkane on sulfated ZrO_2"*. After accomplishing the Diplom degree in 2009, she joined the research group of Prof. Johannes Lercher and commenced on PhD study at the Chair of Technical Chemistry II at Technische Universität München, Germany. In the research she focus on the transformation of *n*-alkanes and *n*-alkenes over ZSM-5 catalysts at high temperature, aiming at understanding mechanistic details of carbonium as well as carbenium ions based cracking reaction.

List of publications

Lin Lin, Erika Ember, and Johannes A. Lercher "*Ehthalpic and entropic factors controlling the activity and the selectivity of alkane activation and cracking*", **2012**, submitted.

Lin Lin, Jie Zhu, Xuebing Li, Erika Ember, and Johannes A. Lercher "*Transition state consideration in protolytic cracking on steamed H-ZSM-5*", **2013**, in preparation.

Lin Lin, Stefan Schallmoser, Erika Ember, and Johannes A. Lercher "*Mechanistic consequence of reaction intermediates in acid-catalysis by zeolites: kinetic studies of 1-pentene cracking*", *J. Catal.* **2013**, in preparation.

Lin Lin, Erika Ember, and Johannes A. Lercher "*Protolytic alkane conversion in zeolites*", in preparation.

Lin Lin, Erika Ember, and Johannes A. Lercher "*Mono and bifunctional conversion of alkanes in zeolites*", in preparation.